Permeability Structure in Fractured Aquifers

by

Todd Halihan, B.A., M.S.

Dissertation

Presented to the Faculty of the Graduate School of

The University of Texas at Austin

in Partial Fulfillment

of the Requirements

for the Degree of

Doctor of Philosophy

The University of Texas at Austin

May, 2000

Permeability Structure in Fractured Aquifers

Approved by
Dissertation Committee:

John M. Sharp, Jr., Supervisor

Philip C. Bennett

Randall A. Marrett

Larry W. Lake

Peter G. Cook

Dedication

To my wife and all those who have been my teachers, formal or otherwise.

Acknowledgements

Thanks to Sue Hovorka and Robert Mace of the Texas Bureau of Economic Geology for providing access to their permeability database. Thank you to G. Ledder, G. Walker, J. Woods, and V. Zlotnik for their helpful discussions on dipole-flow tests. For all their assistance, thanks go to T. Fenstemaker, C. N. Hansen, R. Mace, K. Mohr, G. and S. Tsoflias, M. Uliana, C. Zahm, and a mob of other UT graduate students; K. Bradbury, M. Muldoon, and the staff of the Peninsular Agricultural Research Station; P. Cook, N. Robinson and the staff of CSIRO – Land and Water, South Australia; A. Love and the staff at PIRSA – Sustainable Resources; and C. Simmons and the Flinders group. Thanks to Jack and my committee for all of the assistance and advice, and to J. Famiglietti for capital. The Wisconsin dipole work was funded by the W.R. Muehlberger Field Geology Scholarship Fund. Funding for the Clare project was provided by CSIRO - Land and Water, PIRSA, and the Clare Valley Vineyards. Funding throughout this Ph.D. study was provided by a National Science Foundation Traineeship in Hydrology (NSF grant GER-9454098).

Chapter 2 is largely reprinted from Halihan, T., Mace, R.E. and Sharp, J.M., Jr., 2000, Flow in the San Antonio segment of the Edwards aquifer: matrix, fractures or conduits? The article is reprinted from: Groundwater flow and contaminant transport in carbonate aquifers, Sasowsky, Ira D. and Carol M. Wicks (eds) 90 5410 498 8, 2000, 25 cm, 208 pp., EUR 57.00 / US $60.00 / GBP 40. Please order from: A.A. Balkema, Old Post Road, Brookfield, Vermont 05036 (telephone: 802-276-3162; telefax: 802-276-3837; email: info@ashgate.com).

Permeability Structure in Fractured Aquifers

Publication No._____

Todd Halihan, Ph.D.

The University of Texas at Austin, 2000

Supervisor: John M. Sharp, Jr.

Understanding water movement through fractured and karstic aquifers is difficult, but it is important for those managing these resources. Determining which features contribute to flow in these aquifers is important because accurate predictions of flow and transport are most sensitive to variations in the permeability field. A continuum approach to these aquifers has led to two problems that are approached with two new techniques that quantify the permeability.

First, continuum hydraulics does not allow an understanding of which individual features in an aquifer provide flow. This permeability structure problem is manifested in scale dependent permeability (larger permeability values for larger scale tests). Interpretations of these aquifers are limited by ignoring small-scale data in addressing larger scale problems. The Edwards aquifer of central Texas was used to determine if data sets of matrix permeability, fracture

aperture, and conduit size from cores and outcrops can be effective utilized to interpret permeabilities measured at the small-, well-, and regional-scales. The results demonstrate that by quantifying permeability on the small-scale, larger scale interpretations of the aquifer are possible and have a stronger quantitative basis by utilizing geologic information from the aquifer.

The second problem is that standard hydraulic measurement techniques are optimized for porous media. This approach does not allow individual features and their connections with other features to be easily evaluated in these aquifers. Fractured carbonate aquifers in Wisconsin and Australia were evaluated using asymmetric dipole-flow tests to determine if the structure of permeability could be determined more effectively. Dipole-flow testing, analogous to resistivity dipole testing, is a relatively new technique that was developed from the use of recirculation wells in contaminant remediation. This asymmetric technique may overcome many of the problems inherent in other testing strategies. Asymmetric dipole-flow tests provided rapid testing and demonstrated the ability to quantify heterogeneities. The results demonstrate that boreholes can be connected in complex geometries with drawdown occurring above and below areas of pressure buildup.

Table of Contents

List of Tables

List of Figures

CHAPTER 1: Introduction

Permeability, or the ability of a medium to transmit fluids, is the most statistically sensitive physical groundwater parameter to estimate from field data. In nature, permeability has a range covering at least 17 orders of magnitude (Freeze and Cherry, 1979, p. 29; Neuzil, 1994). The variability in permeability is a key factor to understanding the transport of solutes in the subsurface (Rehfeldt, et al, 1989). Given the sensitivity of flow and transport equations to this parameter and the large range of possible values, accurate permeability data are critical for evaluating groundwater.

Field permeability data are commonly used in very complex modern groundwater models. Porous media models, such as SUTRA, can accommodate three-dimensional saturated and unsaturated flow for various fluids (Voss, 1984). Fracture models, such as FracMan/MAFIC and Frac3dvs can simulate the interactions of fractures and the matrix in which they are located (Dershowitz et al., 1993; Miller and Kleine, 1994; Therrien and Sudicky, 1996). Stochastic representations allow nearly any definable flow configuration to be modeled (Cacas et al., 1990). Even non-Darcian behavior has been incorporated into some flow models (Kohl and Hopkirk, 1995). Model outputs, however, are only as good as their input.

There are three problems existing with permeability data, even when these data are available and of high quality: scale effect, heterogeneity, well test

conceptual models. The scale effect has been discussed by many authors (Kiraly, 1975; Gelhar et al., 1985; Bhattacharya and Gupta, 1990; Molz et al., 1990; Clauser, 1992). Research shows that different methods of measuring permeability yield a range of results with order of magnitude differences. Permeability data collected from core or hand samples commonly yield the lowest values. Aquifer tests commonly yield higher values, while tracer tests yield some of the highest values (Quinlan et al., 1992). The value of permeability depends on the scale at which the data are obtained (Kiraly, 1975).

Another problem is heterogeneity on many scales in fractured and karstic aquifers. Pores range from microns to tens of meters (Ford and Williams, 1989). In these types of aquifers flow may be non-Darcian, thereby limiting the usefulness of many numerical models. Due to heterogeneous permeability, flow to a well may not be radial, but linear or spherical (Geier et al., 1995). In these aquifers, specific capacity well tests or standard drawdown tests may not yield useful information because of a lack of measurable drawdown (Hovorka et al., 1995). Pumping tests may require days or even weeks to yield appropriate results (Gernand and Heidtman, 1997). From the perspective of a representative elementary volume (Hubbert, 1956), the representative volume for a fractured or karstic aquifer may be the entire aquifer. Thus, smaller scale values of permeability will be controlled by individual fractures and conduits, with no single representative volume available for different portions of the aquifer.

Many available tests determine the permeability at only one location using only one scale. Zhang and Sudicky (1997) comment that "field data describing

spatial variations in the material properties are typically lacking." Other researchers indicate that there is a need for the ability to measure the permeability of aquifers at multiple locations to determine heterogeneity (Rehfeldt et al., 1989; Botha and Verwey, 1992). Numerical models are capable of high resolution, three-dimensional flow, but there are not field techniques generally available capable of gathering the three-dimensional heterogeneity data required.

With these difficulties, the selection of large-scale permeability used in models is difficult (Botha and Verwey, 1992). Well tests can have multiple interpretations, and each interpretation can generate an independent conceptual model of how the aquifer functions (Botha and Verwey, 1992). Some researchers doubt that laboratory scale permeability measurements are even useful (Bradbury and Muldoon, 1990). This ambiguity makes aquifer interpretation very difficult for practicing hydrogeologists (Williams, 1985).

Consequently, there are inherent difficulties in determining permeability. Techniques should be developed to gather adequate permeability data for fractured and karstic aquifers. The nature of the scale dependence of permeability should be investigated to determine the causes and diagnosis of the variability. Advanced testing techniques should be developed to measure the permeability tensor in the field. In addition, the determination of permeability should be made faster, cheaper, and more comprehensive.

The motivation to examine these issues is a result of studying a karst aquifer controlled by conduit diameter variations in a cave system in Missouri (Halihan and Wicks, 1998; Halihan et al., 1998). Even in a system dominated by

one large conduit, permeability variations from different scales needed to be evaluated to develop an appropriate quantitative conceptual model of springflow. This led to work on many scales to evaluate how to best characterize these aquifers.

On the small-scale, the physics of fracturing was investigated to determine how fracturing may affect the surface properties such as roughness, porosity, and permeability (Halihan, 1998; Lindsay, in preparation). Outcrop data from the Edwards aquifer, Texas was used to investigate how fracture and conduit data could be employed to 1) interpret permeability at multiple scales, 2) investigate recharge rates and mechanisms, and 3) evaluate flow and transport at leaky underground storage tank sites (Zahm, 1998; Sharp et al., 1998; Halihan et al., 1999a; Halihan, et al., 1999c). In the Clare Valley, South Australia, and Wagga Wagga, New South Wales, outcrop and creek data were incorporated to interpret the location of permeable regions, the direction of flow, and rates of transport in these complex aquifers (Cook et al., 1999; Halihan, 1999; Halihan et al., 1999b).

On the well scale, the work focused on employing hydraulic and geophysical techniques to understand flow in fractured aquifers. Ground penetrating radar (GPR) and resistivity techniques were used to interpret pumping tests, examine fracture aperture variability, and determine if hydraulically active fracture orientations could be determined using resistivity (Wilson et al., 2000a; Wilson et al., 2000b; Tsoflias et al., in review). Hydraulic techniques have focused on using a dipole-flow technique to evaluate fractured aquifer wells, and

using temperature and conductivity variations in an attempt to determine fracture locations and flow rates (Halihan, 1999; Love et al., 1999).

This dissertation addresses in detail some of the problems with permeability measurement and some solutions by evaluating permeability structure in fractured and karstic aquifers. First, Chapter 2 examines equilibrium models for integrating outcrop and laboratory permeability data to well- and regional-scale data. These models are developed and tested to determine if small-scale (outcrop and laboratory) data can be used to interpret flow at the well- and regional-scale in the Edwards aquifer of central Texas. Previous research has not attempted to combine the various regions of permeability with a quantitative, physical model. In fractured media, permeability data on the matrix and fractures can be obtained. In karstic media, data can also be collected on conduit sizes. Thus far, no models of which we are aware have tested the scale effect by incorporating these various data to determine if the scale effect may simply result from heterogeneity in the aquifer. A physical understanding of the causes of the scale effect would make quantifying permeability simpler. Aquifers could be accessed on many scales, and inconsistencies could be investigated by collecting appropriate data. This portion of the study tests if steady state modeling of permeability heterogeneities in a fractured, karstic aquifer can explain the scale effect.

Second, in Chapter 3, an asymmetric dipole flow test is developed and tested in Door County, Wisconsin as a multiscale heterogeneity profiling tool to detect the quantitative structure of permeability in a well in a fractured aquifer.

The asymmetric dipole flow technique has not been previously tested in the field, and the advantages of the technique for observing heterogeneities are presented in Chapter 3. Finally, in Chapter 4, the asymmetric dipole-flow test is applied to interpret connections between a well and piezometers in a complex fractured aquifer in the Clare Valley, South Australia. The combination of outcrop analysis and dipole-flow testing allows a better understanding of the structure of permeability on multiple scales in fractured aquifers.

CHAPTER 2: San Antonio segment of the Edwards aquifer: matrix, fractures, or conduits?

ABSTRACT

Understanding water movement through fractured karst aquifers is difficult, but it is important for proper management of these resources. Much of central Texas depends primarily on the fractured and karstified San Antonio segment of the Edwards aquifer. The problem of scale dependent permeability makes interpretations of the aquifer difficult by limiting our ability to effectively utilize small-scale data for larger scale problems. We used permeabilities measured at the small- (lab and outcrop), well-, and regional-scales to evaluate if small-scale data can be used to reproduce and interpret well- and regional-scale data. Small-scale data sets of matrix permeability, fracture aperture, and conduit size from cores and outcrops were utilized. Well-scale permeabilities were estimated from pump tests. Regional-scale permeabilities were estimated from numerical models. A modified layered aquifer model was used to calculate well- and regional-scale permeabilities from the small-scale data. Using an average regional hydraulic gradient to compute Reynolds numbers, the small-scale permeability data were used to predict the occurrence of non-linear laminar to turbulent flow. The results indicate that, in general, fractures control flow on the well-scale in the Edwards, and that many wells sample non-linear laminar to turbulent flow within the aquifer. The results also indicate that conduits are not the major contributors to well-scale permeability in the Edwards, but, if present,

control regional-scale permeabilities and have turbulent flow. Finally, the results indicate that pump tests would yield no meaurable drawdown in approximately 15% of wells due to either fractures or conduits.

INTRODUCTION

The ease with which water flows through an aquifer, quantified as permeability, can be difficult to determine. Permeability ranges over at least 17 orders of magnitude (Freeze and Cherry, 1979, p. 29; Neuzil, 1994). This variation in permeability is a key factor to understanding groundwater flow and solute transport in the subsurface (Rehfeldt et al., 1989).

In fractured karst aquifers, the difficulty in quantifying permeability is amplified by flow in fractured and dissolution zones. This is illustrated by the fact that measured permeability generally increases with scale in fractured karst aquifers (Kiraly, 1975). This is generally referred to as the scale effect. Permeability measurements in a karstic aquifer can vary by as much as nine orders of magnitude (Maclay and Land, 1988; Hovorka et al., 1995)(as shown in Figure 2.1).

In the San Antonio segment of the Edwards aquifer (hereafter referred to as the Edwards aquifer), quantifying permeability is important because of the increasing demands on the aquifer which require managers to understand how the aquifer functions so that it can be properly utilized and protected (Sharp and Banner, 1997). Fortunately, the Edwards aquifer has a large permeability database available over a range of scales from core samples to regional model estimates. Utilizing these data, this research addresses the question of what

controls flow in the Edwards aquifers: the matrix, the fractures, or the conduits. The question is not trivial, as workers in the Edwards aquifer have widely varying opinions of what is the appropriate conceptual model of the aquifer.

PREVIOUS WORK AND DEFINITIONS

Previous work has investigated the scale effect of permeability from field data and theoretical interpretations. In order to define scales in hydrology, different nomenclatures have evolved. The nomenclature used in this paper is similar to that of Bradbury and Muldoon (1990). Small scale refers to permeameter tests, fracture measurements, or conduit measurements that take place in the laboratory or outcrop and generally make a measurement over a volume of 0.01 m^3 to 10 m^3. This would correlate with the laboratory scale of Dagan (1986). Well scale refers to well or packer tests that occur on a scale of 100 – 1000 m^3, which is similar to the local scale of Dagan (1986). Finally, the regional scale refers to volumes of greater than 1000 m^3. Dagan (1986) uses the same term.

Kiraly (1975) first noticed the scale effect in karst aquifers of Switzerland, in which permeability continually increased from the small- to the regional-scale. He hypothesized that the increase from small- to well- scale was caused by fractures, and that the largest permeabilities on the regional-scale were caused by karstic conduits. Quinlan et al. (1992) compiled over 1800 dye traces from 25 countries, and concluded that average flow velocity values continually increased with scale. Extending the work of Brace (1984), Clauser (1992) noted that permeability increased approximately three orders of magnitude from the small-

scale to the well-scale in crystalline rocks. However, Clauser's data indicated that the permeability of fractured media measured on the well-scale would not continue to increase when measured on the regional-scale. Other authors have also suggested that if a sufficiently large volume of rock was selected, a single, representative value for permeability could be determined (Long et al., 1982; Odling, 1997). Rovey (1994) examined carbonate aquifer permeability with variogram models. He found that for fractured unkarstified carbonates, a range could be determined in which the permeability reached a constant value. But, for mature, well-developed karst aquifers, he suggested that permeability instead increased to "practical infinity."

Models of the scale effect depend on which theory is used. Does the value of permeability reach a constant value at an appropriate scale, or does it increase indefinitely? In fractured media, permeability data can be obtained on the matrix and fractures. In karstic media, data can also be collected on conduit sizes. Few, if any, models of which we are aware have tested the scale effect by incorporating these various data to determine which heterogeneities control the permeability of a fractured karst aquifer. A quantitative physical understanding of the scale effect makes quantifying permeability more robust, enabling the proper physical model to be used. An aquifer could be assessed on many scales, and inconsistencies could be investigated by collecting appropriate data.

Definitions for matrix, fractures, and conduits vary widely. For this paper, terminology was based upon observable hydrogeologic features in outcrops and caves. The terminology, which may provide a useful standard, is similar to that of

Atkinson (1985) (see also Ford and Williams, 1989, pp. 166-170); however, the terminology is based purely on the aquifer's geometric characteristics and not upon the potential or interpreted flow regime. In this paper, matrix refers to rock where no fractures visible to the unaided eye are present. Fracture refers to fractures that are visible to the unaided eye that are open, not filled by minerals. Conduit refers to dissolution features that extend for a range greater than that of the well-scale and are visible to the unaided eye. Dissolution feature refers to solutional features which are limited to meter-scale or smaller. For modeling, fractures are two-dimensional uniform slots and conduits are one-dimensional pipes.

SITE DESCRIPTION

Hydrostratigraphic relationships for the Edwards aquifer are given in Rose (1972), Maclay and Small (1986), Pavlicek et al. (1987), and Sharp and Banner (1997). The aquifer consists of Cretaceous limestones and dolomites that have undergone multiple periods of karstification. It is not well understood whether the high permeabilities observed in the aquifer are due to heterogeneities in the matrix, well-connected fractures, karstified conduits, or some combinations thereof. The aquifer supplies one of the highest naturally flowing wells in the world with a discharge of 1.58 $m^3 s^{-1}$ (25,000 gpm) (Swanson, 1991). It also has springs that discharge from fractures in the outcrop at combined average rates between 5 and 15 $m^3 s^{-1}$ (Sharp and Banner, 1997).

PERMEABILITY DATABASE

Permeability data are available for the Edwards aquifer on several scales (Figure 2.1). Small-scale data are available from core samples and measurements of fracture apertures and conduits in outcrop. Pumping test data evaluate the well-scale. Finally, three numerical models constructed for the Edwards aquifer provide estimates of regional-scale permeability. Permeability data collected on any scale have errors associated with those data, and we refer the reader to the data sources for discussions of errors.

In this study, the distributions of matrix permeability, fracture apertures, and conduit sizes were approximated as lognormal distributions. The distributions of fracture aperture and conduit sizes can also be modeled as power law distributions. By choosing lognormal distributions, the largest apertures and the largest conduits may not be represented in the analysis, resulting in a conservative estimate of the highest permeabilities.

Small-scale

Small-scale data for a fractured karst aquifer such as the Edwards aquifer are difficult to obtain. Representative samples of the matrix can be difficult to collect from cores. Fracture data can usually only be collected from the surface at outcrops or creek beds, or from caves and tunnels in the subsurface. Conduit data are yet more difficult to obtain due to the difficulty in determining the lengths of conduits that are smaller in diameter than a human body. For the Edwards aquifer, many small-scale data are available, but additional small-scale data are yet needed for quantifying flow at larger scales with a physical model.

Matrix

The matrix permeability data utilized for this study consist of 493 measurements from 0.025 m (1 inch) core plugs taken from various studies (Figure 2.1). 195 measurements are from Hovorka et al. (1993); an additional 195 measurements are from Hovorka et al. (1995); and the remaining 103 matrix permeability measurements are from unpublished measurements (Hovorka, personal communication). The matrix permeability appears to have a bottom truncation at a lower value of approximately 10^{-17} m^2. For this study, the matrix permeability was modeled as a lognormal distribution with a geometric mean of 1.3×10^{-15} m^2 (Figure 2.2). A value one standard deviation above the mean yielded a matrix permeability of 4.6×10^{-14} m^2, and a value of 3.7×10^{-17} m^2 resulted for one standard deviation below the mean.

Fractures

Fracture permeability was calculated from fracture apertures measured on three transects of roadcuts of the Edwards aquifer (Hovorka et al., 1998). A total of 776 fracture apertures were measured on 79 meters of outcrop (average fracture density = 10 m^{-1}) with a feeler gauge and a metal ruler, primarily in subvertical fractures (Figures 2.2 and 2.3). Intrinsic permeability was calculated from apertures using the cubic law (Lamb, 1932), which estimates the permeability of a fracture, k_f [L^2], as:

$$k_f = \frac{b^2}{12} \qquad (2.1)$$

where b is the fracture aperture [L]. The limit of the feeler gauge technique is apparent in the data set (Figure 2.3), with the data truncated below the 80th

percentile. Fracture apertures were assumed to follow a lognormal distribution (Figures 2.2 and 2.3). The geometric mean fracture aperture used was 0.0155 mm. This results in a geometric mean permeability of 2×10^{-11} m^2. A value one standard deviation above the mean yielded a fracture permeability of 2×10^{-9} m^2, and a value of 2×10^{-13} m^2 resulted for one standard deviation below the mean. It is not assumed that all fracture apertures measured at the outcrop were well connected, but it is assumed that the apertures of well-connected fractures follow the measured outcrop distribution. This assumes that connectivity of the fractures is scale independent.

The fracture distribution was tested for the validity of laminar Darcian flow. Reynolds numbers were calculated using the 0.11-0.42 m km^{-1} range of hydraulic gradients observed in the Edwards (McKinney and Watkins, 1993). A Reynolds number of 10 was used to represent the onset of non-linear laminar flow in the fractures (Lindquist, 1933; Scheidegger, 1974, pp. 152-187; Fetter, 1994, pp. 143-144). This occurred with apertures greater than 3.1-4.8 mm (Figure 2.3). Full turbulence was estimated at a Reynolds number of 2000 (Streeter, 1948). This occurred in fractures that ranged in aperture from 18-28 mm. From these calculations, it was estimated that the flow would be laminar for 99% of the fractures.

Conduits

Conduit permeability was calculated from the cross-sectional diameters of conduits measured at seven outcrops (Hovorka et al., 1995). They estimated the diameter of 2685 conduits (Figures 2.2 and 2.3) by tracing conduits from

photomosaics onto mylar sheets, and then scanning and interpreting these sheets using National Institutes of Health image processing software (Rasband, 1994). It cannot be expected that all of the conduits will maintain the same diameters along their entire length, but we assume that the extended conduits follow the measured distribution.

The permeability of the conduits was calculated from the Darcy-Weisbach equation assuming both laminar and smoothly turbulent flow. The laminar hydraulic conductivity of the conduits, K_l [L t^{-1}], was calculated using:

$$K_l = \frac{g}{\nu}\frac{d^2}{32} \tag{2.2}$$

where d is the hydraulic diameter [L], g is the gravitational constant [L t^{-2}], and ν is the kinematic viscosity [L^2 t^{-1}] (Gupta, 1989, pp. 549-551). The turbulent hydraulic conductivity (derived from Turcotte and Schubert, 1982, pp. 239-240; Halihan et al., 1998), K_t [L t^{-1}], was calculated for smoothly turbulent flow using the empirical relationship between friction factor and Reynolds number:

$$f = 0.3164 R_e^{-1/4} \tag{2.3}$$

where f [-, dimensionless] is the friction factor and R_e [-] is the Reynolds number. Substituting the definition for friction factor and Reynolds number yields an expression for the turbulent hydraulic conductivity of (Halihan and Wicks, 1998):

$$K_t = 4.706 \frac{g^{4/7}}{\nu^{1/7}} \left(\frac{d}{2}\right)^{5/7}. \tag{2.4}$$

Intrinsic permeability was calculated by dividing the hydraulic conductivities by g ν^{-1}. (Note: For non-Darcian flow, not only does the intrinsic permeability

formulation change, but the gradient is no longer linearly proportional to the flux. Equation (2.4) only accounts for conduit geometry and fluid properties.)

Reynolds numbers calculated using hydraulic gradients for the Edwards aquifer (0.11-0.42 m km^{-1}) indicate that flow would be turbulent ($R_e > 2000$) in conduits larger than 0.025-0.039 m. This includes 95-99% of the conduits (Figure 2.3). The conduit-size distribution was modeled with a lognormal distribution, with a geometric mean conduit having a hydraulic diameter of 0.087 meters. This yields a hydraulic diameter of 0.139 m for a value one standard deviation above the mean, and a value of 0.054 m for one standard deviation below. This yields a median laminar permeability of 2.4×10^{-4} m^2, and a median turbulent permeability of 1.4×10^{-6} m^2 (Figure 2.2).

The question arises using this conduit distribution as to whether the largest conduits have been included. The conduits may follow a power law or fractal distribution that would yield larger conduit diameters, and cave maps in the Edwards aquifer indicate meter scale conduits are common (Mace, in press; Veni, 1988). In order to test the effect of large conduits on permeability, we included both 1-meter and 10-meter conduits for analysis.

Well-scale

Well-scale data are abundant for the Edwards aquifer (Figure 2.1), but a major difficulty with some of the data is created by high permeabilities. A number of well tests in the aquifer recorded no measurable drawdown (Figure 2.4). These wells have been classified as zero drawdown wells (Hovorka et al.,

1995; Mace, in press). The other well tests that had measurable drawdown have been termed "normal" well tests for this study.

Normal well tests

Data on well permeability for 901 normal well tests in the Edwards aquifer (Figure 2.1) were utilized (Hovorka et al., 1995). The normal well tests were obtained throughout the aquifer, but the majority were in the confined portion. Some tests were standard pumping tests, but most were specific capacity tests. Permeability was estimated from the specific capacity data using an empirical relationship derived for the Edwards aquifer (Mace, 1997). The geometric mean permeability of the normal well tests was 8.64×10^{-12} m^2 with a value of 1.97×10^{-10} m^2 representing one standard deviation above the mean, and a value of 3.79×10^{-13} m^2 representing one standard deviation below.

Well test data also included information on aquifer thickness and the open interval (most well completions are open hole) for the well tests. These parameters were modeled as normal distributions for this study. The formation has an average thickness of 170 m with a standard deviation of 30 m. The open interval had an averaged length of 100 m with a standard deviation of 30 m. Although the deviation for the open interval approximates much of the data, it was used as an average comparison against the full formation thickness model, maintaining the same standard deviation.

Zero drawdown well tests

Approximately 15% of the well test data collected by Hovorka et al. (1995) had no measurable drawdown reported (Figures 2.1 and 2.4). If valid,

these 171 tests would yield an infinite permeability. Some researchers believe these tests are unusable or useless. Others claim that permeability may be at some "practical infinity" (e.g., Rovey, 1994). Specific capacity for these well tests was estimated by assuming a drawdown of 0.3 m (1 foot), which was considered the resolution of the test data collected by drillers (Hovorka et al., 1995; Mace, in press). The transmissivity was then estimated using an empirical relationship derived for the Edwards (Mace, 1997). The geometric mean permeability of the zero drawdown well tests was 5.42 x 10^{-11} m^2 with a value of 3.01 x 10^{-10} m^2 representing one standard deviation above the mean, and a value of 9.75 x 10^{-12} m^2 representing one standard deviation below the mean.

The uncertainty in these tests may limit the value of their data, but ignoring them adds bias. These data probably represent the highest permeabilities in the aquifer. Therefore, they must be considered. The average pumping rate for these well tests was 0.04 $m^3 s^{-1}$ (625 gpm) with the highest pump rate at 0.525 $m^3 s^{-1}$ (8337 gpm). The average borehole diameter for these tests was 0.23 m (9 inches) with the largest being 1.52 m (60 inches) (Hovorka et al., 1995).

Regional-scale

Regional estimates of permeability for the Edwards aquifer are limited to a few modeling studies (Figure 2.1) (Klemt et al., 1979; Maclay and Land, 1988; Thorkildsen and McElhaney, 1992). Klemt et al. (1979) used a number of values for transmissivity for their model of the aquifer, but the highest regional value used was 2.9 $m^2 s^{-1}$. Using a range of thickness equal to two standard deviations in formation thickness (i.e., 110 m to 230 m), the highest regional permeability

was calculated as 1 x 10^{-9} to 3 x 10^{-9} m^2. Maclay and Land (1988) use a slightly higher value for their highest transmissivity of 9.3 m^2 s^{-1}. Given the possible range of aquifer thickness, this equates to a regional permeability of 3 x 10^{-9} to 9 x 10^{-9} m^2. Finally, Thorkildsen and McElhaney (1992) use one of the smallest values for the high transmissivity area of their model. Their highest value was 1.4 m^2s^{-1}, equating to regional permeabilities of 5 x 10^{-10} to 1.5 x 10^{-9} m^2.

PERMEABILITY COMBINATION MODELS

To evaluate the effects of different high permeability heterogeneities on the scale effect in the Edwards aquifer, models were tested that combine the matrix permeability distribution with the fracture and conduit permeability distributions (Figure 2.5). These models are steady state and are modifications of equations for layered aquifers. In addition to the assumptions used for layered aquifers, four additional assumptions are necessary: 1) the matrix permeability, fracture apertures, and conduit diameters follow lognormal distributions; 2) the cubic law is valid for fractures and equations (2.2) and (2.3) are valid for laminar and turbulent flow in conduits; 3) the regions of high permeability do not strongly affect the matrix, and 4) the distributions of well-connected fracture apertures and conduit sizes are equivalent to the measured distributions of fracture apertures and conduit diameters.

Matrix + horizontal fractures

The effects of multiple fractures were examined to test the effect of fracture density on effective permeability. Effective permeability of matrix and fractures can be calculated using:

$$k_e = k_m - k_m\left(\frac{\sum b_f}{b_t}\right) + \left(\frac{\sum b_f^3}{12 b_t}\right) \qquad (2.5)$$

where k_e is the effective permeability [L^2], k_m is the matrix permeability [L^2], b_f is the fracture aperture [L], and b_t is the total thickness of the aquifer [L]. Equation (4) can be written in terms of the fracture permeability by substituting $(12k_f)^{1/2}$ for b_f, where k_f is the fracture permeability [L^2]. This is a modified form of permeability of a layered aquifer (Leonards, 1962; Fetter, 1994).

The k_e distribution was estimated from the distributions of k_m, b_f, and b_t using Monte Carlo simulations with 10,000 trials per simulation (Jensen et al., 1997, pp. 61-64). These simulations were performed using the distribution for the full aquifer thickness, and the open interval length for b_t. Each fracture was generated separately for the simulations. These simulations were performed for models of 1, 10, 50, and 100 horizontal fractures.

Matrix + horizontal conduit

The model for combining the matrix with the conduit permeability assumed a conduit would typically intersect a well horizontally. The effective permeability for the matrix and a conduit was calculated using:

$$k_e = k_m + (k_c - k_m)\left(\frac{d_c}{b_t}\right) \qquad (2.6)$$

where d_c is the hydraulic diameter of the conduit [L], and k_c is the laminar or turbulent permeability of the conduit [L^2]. This calculation is an average over the thickness of the aquifer (b_t), and is restricted laterally to a width equal to d_c. The k_e distribution was estimated from the distributions of k_m, k_c, d_c, and b_t using

Monte Carlo simulations. These simulations were performed with four different models: one laminar model with b_t as the total formation thickness and one with b_t as the open interval of the wells, and corresponding turbulent models.

The above conduit model is sufficient for investigating small- and well-scale effects because the flow regime near the conduit would be linear. However, on a regional basis, two questions remain unanswered: First, how would large diameter conduits (1-10 meters) observed in the Edwards affect the estimated regional model permeabilities (see Veni, 1988, for conduit examples)? Secondly, how does the averaging of low permeability areas adjacent to the conduit affect the calculated value? In order to answer these questions values for a 1 meter and a 10 meter diameter conduit were calculated using equation (2.5). In addition, permeabilities were calculated for a 10 km wide, 170 m thick region using the average well permeability for k_m to estimate the effect upon regional scale permeabilities.

RESULTS

The results indicate that large changes in the effective permeability are created by high permeability heterogeneities. The models generated for the aquifer result in permeabilities that have a range greater than the observed permeability data.

Matrix + horizontal fractures

For the multiple horizontal fracture model using the full aquifer thickness, large increases in permeability are evident over the matrix values. Whereas a single fracture increased effective permeability by only 2.3 times at the median,

100 fractures can increase the median effective permeability by over four and a half orders of magnitude (Figure 2.5). This would equate to an average connected fracture density of 1 fracture every 1.7 meters, with the majority of the fractures smaller than can be measured with a standard feeler gauge. Using the open interval of the wells instead of the full aquifer thickness had little effect on the value of k_e.

The best fit of the multiple horizontal fracture model to the well test data occurred with 50 fractures (average connected fracture density of 0.3 m^{-1}). At this density, the model fit approximately 80 percent of the well test data with an error in the median values of 8% (Figure 2.5). The model predicted higher values for the effective permeability below the 10th percentile and above the 90th percentile. This model fracture density is approximately 3% of the outcrop fracture density of 10 m^{-1}.

To determine the relative effects of the 50 horizontal fractures and the matrix on effective permeability, 20 trials of the model were examined. In the random trials, the matrix contributed less than 0.5% of the permeability in all but one case. The largest number of fractures contributing greater than 1% of the total effective permeability was 6 of 50 fractures, which occurred in 4 of the 20 trials analyzed. These four trials had an effective permeability range of 1.9×10^{-13} to 6.0×10^{-12} m^2. The largest fracture had an aperture of 1.77 mm contributing 46.2% of the permeability. The smallest number of fractures contributing greater than 1% of the permeability was 1 of 50, which occurred in 6 of the 20 trials. These six trials had an effective permeability range of 1.3×10^{-12} to 1.3×10^{-8} m^2

with the largest single fracture of 29.0 mm contributing 99.9% of the permeability. These limited tests indicate that flow occurs in a limited number of fractures for the model, and that some of these fractures flow under non-linear laminar ($10<R_e<2000$) to turbulent ($R_e>2000$) flow conditions.

Matrix + horizontal conduit

The laminar horizontal conduit model resulted in a predicted effective permeability increase of over 7 orders of magnitude compared to the matrix alone (Figure 2.5). This prediction is significantly above the calculated well test permeabilities and the regional permeabilities. The turbulent horizontal conduit model resulted in a predicted effective permeability increase of over 5 orders of magnitude. It is not expected that every well in the Edwards intersects a connected conduit of significant dimensions, so it is appropriate to compare the horizontal conduit model prediction either with the upper end of the well permeability distribution or with the regional values. The median value of the turbulent model is 20 times larger than the median well test value. However, these values are similar to some of the calculated values for the zero drawdown wells. The matrix and conduit model accommodating partial penetration using the open interval of the well for the total thickness is only 1.8 times higher than the model for the formation thickness.

The large conduit (1 and 10 meter) models yielded laminar permeabilities of 2×10^{-4} and 2×10^{-1} m^2 for the laminar model and 5×10^{-8} and 2×10^{-6} m^2 for the turbulent model, respectively. When averaged across a 10 km section of aquifer, the model yields laminar permeabilities of 1×10^{-8} and 1×10^{-4} m^2 and

turbulent permeabilities of 1 x 10^{-11} and 2 x 10^{-9} m^2, respectively. Thus, while a 1 meter conduit occupies only 0.00005% of the flow area in this estimate, it would contribute 99.94% of the flow under laminar conditions over a 10 km wide segment of aquifer.

DISCUSSION

When examining carbonate rock outcrops, fractures and karst conduits can commonly be observed. The permeability of these features can be estimated as easily as the matrix permeability (Figure 2.3). When examining permeabilities on the well- or regional-scale however, the location of permeable features is not simple to determine. For the Edwards aquifer, facies analysis indicates the presence of high permeability matrix in some locations (Hovorka et al., 1995). Lineament studies that delineate fracture traces by contouring lineaments per area instead of drawing discrete fracture traces indicate the Edwards aquifer is dominated by fracturing (Wermund et al., 1978). Up to 27 meter high (90 ft) bit drops observed in drilling wells, caliper tests that indicate large dissolution features, and live blind catfish discharged from wells all strongly indicate the presence of conduits (Longley, 1981; Thornhill et al., 1988; Poteet et al., 1992). So which heterogeneities control flow in the Edwards aquifer, and what additional data might be needed to improve our understanding of the aquifer?

Does the matrix control the Edwards' permeability?

In the Edwards aquifer, the matrix does not appear to contribute significantly to permeability at either the well-scale or regional-scale (Figure 2.6, Model A). From the permeability data, the average matrix can account for only

two measured well permeabilities and none of the regional values. Even if the entire aquifer was composed of the highest 1% of the matrix permeability (an unrealistic assumption), less than 38% of the well data could be explained. Additionally, if the matrix could explain the well- or regional-scale data, the contributions of the fractures and conduits would have to be negligible, which is not likely.

Do fractures control the Edwards' permeability?

For the Edwards aquifer, the fractures can explain all of the observed well permeability data (Figure 2.5; Figure 2.6, Model B or C). With a relatively simple model, fractures can be combined with the matrix to yield a match to the well permeability distribution. For individual wells, only a small number of fractures in the model contribute significantly to flow. This observation is made in many fractured systems (Dyke, 1995; Marrett, 1996). While fracture apertures are generally small, a few larger well-connected millimeter scale apertures can contribute a great deal to permeability in an aquifer.

The departures of the well test data at low permeabilities from the 50 horizontal fracture model can be explained by a number of factors (Figure 2.5). For example, these wells may not intersect many fractures. For economic reasons, some wells were only drilled until sufficient discharge was obtained. This could result in a decreased well test permeability because the majority of the permeability in the wells appears to be due to a small number of fractures.

The highest permeability well tests do not match the predicted fracture model well permeabilities above a value of approximately 10^{-9} m^2 (Figure 2.5).

This is likely due to the pumping limitation inherent in well tests. The limitation of well tests can be examined using the Thiem equation and examining the pumping rates required to obtain a given drawdown for different values of permeability (Thiem, 1906). For a permeability of 10^{-9} m^2, relative to a distance of 1000 meters, a well with a radius of 0.25 meters would require a pumping rate of 1.26 m^3 s^{-1} (20,000 gpm) to obtain a meter of drawdown in the Edwards aquifer. This flow rate is unreasonable to use for well testing. Therefore, few standard well tests or specific capacity tests can yield values above 10^{-9} m^2 for this aquifer. Above this value, permeabilities will appear "infinite" with these testing methods.

The fracture model requires a low intensity (3% of outcrop) of well-connected fractures to reproduce the well-scale permeabilities. This low fracture density indicates that *a priori* predictions of well-scale permeabilities using this technique would require information on fracture connectivity, roughness, channeling, and fracture length, but that the values are reasonable for the Edwards aquifer. The model also indicates that for many of the high flow wells of the Edwards aquifer, the formation flows under non-linear laminar ($10<R_e<2000$) to turbulent ($R_e>2000$) conditions.

Do conduits control the Edwards' permeability?

Conduits in the Edwards aquifer do not appear to contribute significantly to the average permeability in wells (Figure 2.5; Figure 2.6, Model D). Conduits would produce permeabilities above the observed values for the majority of the wells. This is not unexpected because there is a low probability of intersecting a

well-connected conduit in a karst aquifer. Quinlan and Ewers (1985) estimate this at 1 in 2600 for shallow karst in Kentucky. For the Edwards aquifer, which has both conduits produced by the normal carbonic acid reaction as in Kentucky and by mixing and/or oxidation of hydrogen sulfide, the distribution of conduits may be denser. However, it is unlikely that this probability will approach the 1 in 6 probability observed in the Edwards for the occurrence of a zero drawdown well.

The lack of continuous dendritic conduits draining the Edwards aquifer is observed at springs which discharge from fractures as opposed to conduits. The regional models also confirm this observation where regions of high permeability do not extend from the recharge to the discharge zone (Thorkildsen and McElhaney, 1992), however, these models may not have the resolution necessary to indicate conduit flow. Some research has indicated the presence of conduits associated with some springs, but it is difficult to determine the lateral extent of these conduits at depth. The presence of cave fish exiting wells, and the locations of high regional permeability do indicate that conduits control some areas of the Edwards aquifer.

Do fractures or conduits control high permeability wells?

A common debate among workers in the Edwards aquifer is whether the high permeabilities observed in many wells are due to fractures or conduits. This research suggests that most of the high yield wells are due to the numerous fractures that exist in the Edwards aquifer (Wermund et al., 1978). Alexander (1990) has found a correlation for this observation in the Barton Springs segment of the Edwards aquifer. It appears that the bit drops that are encountered during

drilling in the Edwards aquifer are usually laterally discontinuous dissolution features which are only hydraulically connected by fractures (Figure 2.6, Model C). The large amount of fracturing observed in the aquifer on many scales would support the hypothesis that the fractures control the well-scale permeability and portions of the regional-scale permeability.

If conduits contribute significantly to wells, it is unlikely that standard well tests or specific capacity tests could be used to obtain quantitative data about those wells because of minimal drawdowns (Figure 2.6, Model D). The large percentage and spatial distribution of zero drawdown wells also does not support conduit flow (Figure 2.4). Their pattern does not rule out a number of widely spaced conduits, but does not support the concept of a limited number of regionally significant conduits. The large percentage of zero drawdown wells, combined with the low probability of intercepting a conduit, makes it unlikely that conduits are the only contributors to high permeability wells; fractures must play a dominant role.

Fractures and conduits can both control flow through the Edwards aquifer. These models indicate that information on the fracture properties of the Edwards aquifer are needed to make *a priori* assessments of permeability for particular sites. The models also indicate that although dissolution features are often intercepted while drilling wells, the dissolution features are unlikely to be hydraulically continuous over long distances, and simply act to increase the effective radius of the well. In both cases, high permeability zones of the Edwards aquifer are flowing under non-Darcian conditions.

CONCLUSIONS

From the models used to test the scale effect for permeability in the Edwards aquifer, we conclude that:

1. Increasing permeability with scale is expected for a fractured karst aquifer. If the permeability did not increase, it would be difficult to explain how the fractures and conduits function unless they were entirely unconnected.

2. Well-scale permeability in the Edwards aquifer can be modeled as predominantly a function of fracture aperture distribution. Even when no measurable drawdown occurs during pumping tests, well permeability can be explained with fractures commonly observed in roadcuts. However, in these wells with no measurable drawdown, flow is likely non-Darcian.

3. Well-connected conduits do not appear to contribute significantly to well permeability for the average Edwards well. The probability of intersecting conduits by a large number of scattered wells is low, whereas fractures are much more abundant and can provide similar responses.

4. The Edwards aquifer has some finite high permeability for which the standard well test used in the Edwards is an insufficient method to estimate permeability in approximately 15% of the cases. The standard method is inadequate because of the high pumping rates required and discharge produced. Non-linear laminar ($10<R_e<2000$) to turbulent ($R_e>2000$) flow probably occurs in these wells.

5. Turbulent flow in conduits might influence regional flow in the Edwards aquifer. This is supported by modeling and demonstrated by wells that

have large bit drops and produce blind catfish from wells. This turbulent flow is localized within the conduits and would not affect many well-scale and small-scale measurements.

6. Small-scale data, particularly fracture apertures and conduit geometry, can be extrapolated to reproduce well- and regional-scale permeabilities. However, without sufficient density, connectivity, length, roughness, and channeling information, this is difficult to do *a priori*.

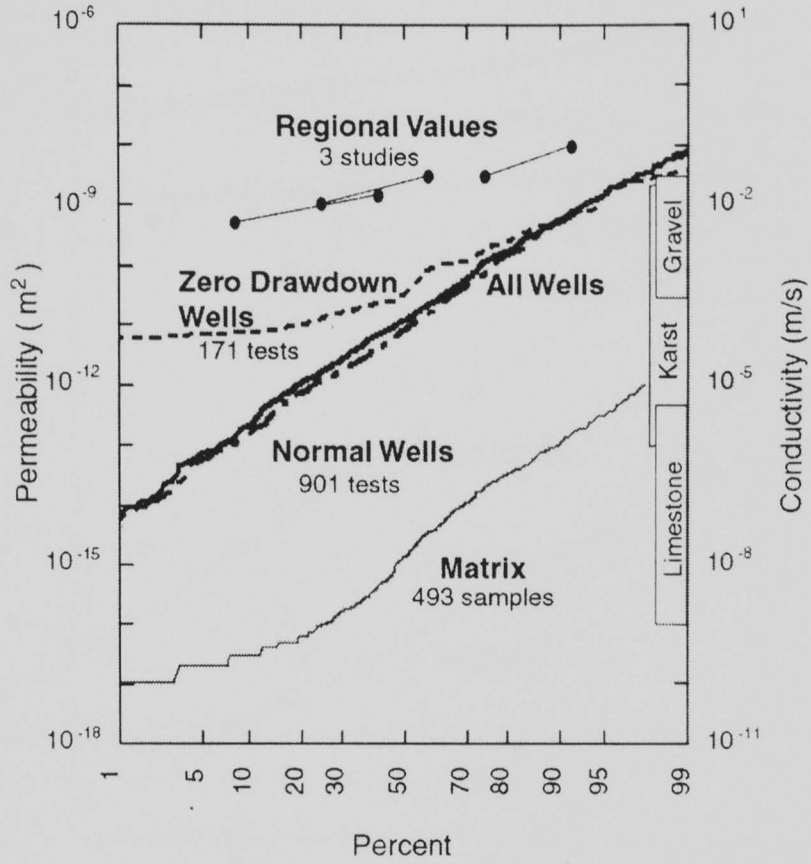

Figure 2.1: Permeability scale effect for the San Antonio segment of the Edwards aquifer.

Cumulative distribution function for permeability values measured from cores (Hovorka et al., 1993; Hovorka et al., 1995; Hovorka, personal communication), wells (Hovorka et al., 1995; Mace, 1997), and regional model (Klemt et al., 1979; Maclay and Land, 1988; Thorkildsen and McElhaney, 1992) data. Zero drawdown wells are wells in which no measurable drawdown occurred, but 0.3 m of drawdown (resolution of the test data collected by drillers) was assumed in order to calculate the permeability. Permeability values for 3 regional modeling studies were calculated using a range of thickness (110 m -230 m) to convert from transmissivity to permeability. Permeability ranges for limestone, karst, and gravel (Freeze and Cherry, 1979) are illustrated for comparison. The individual data points for matrix and well data are not indicated because the quantity of data available provides nearly continuous lines.

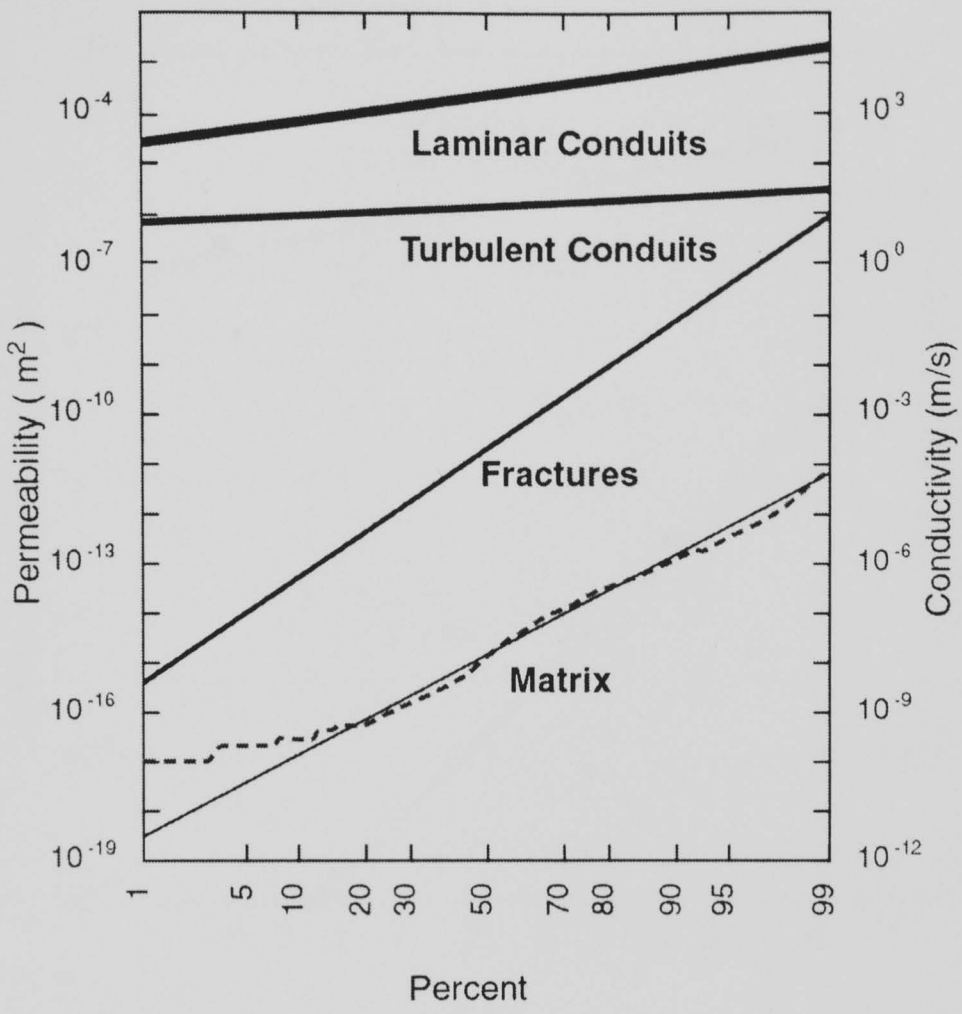

Figure 2.2: Small scale permeability information for the San Antonio segment of the Edwards aquifer.

Data for 493 matrix measurements (dashed line) illustrated along with lognormal model for matrix measurements (thin solid line). Lognormal distributions of hydraulic conductivity for fractures and conduits were obtained using aperture and diameter data shown in Figure 2.3. Fracture permeability (medium solid line) was calculated using equation (2.1). Laminar and turbulent conduit hydraulic conductivity (heavy solid lines) were calculated using equations (2.2) and (2.4), respectively.

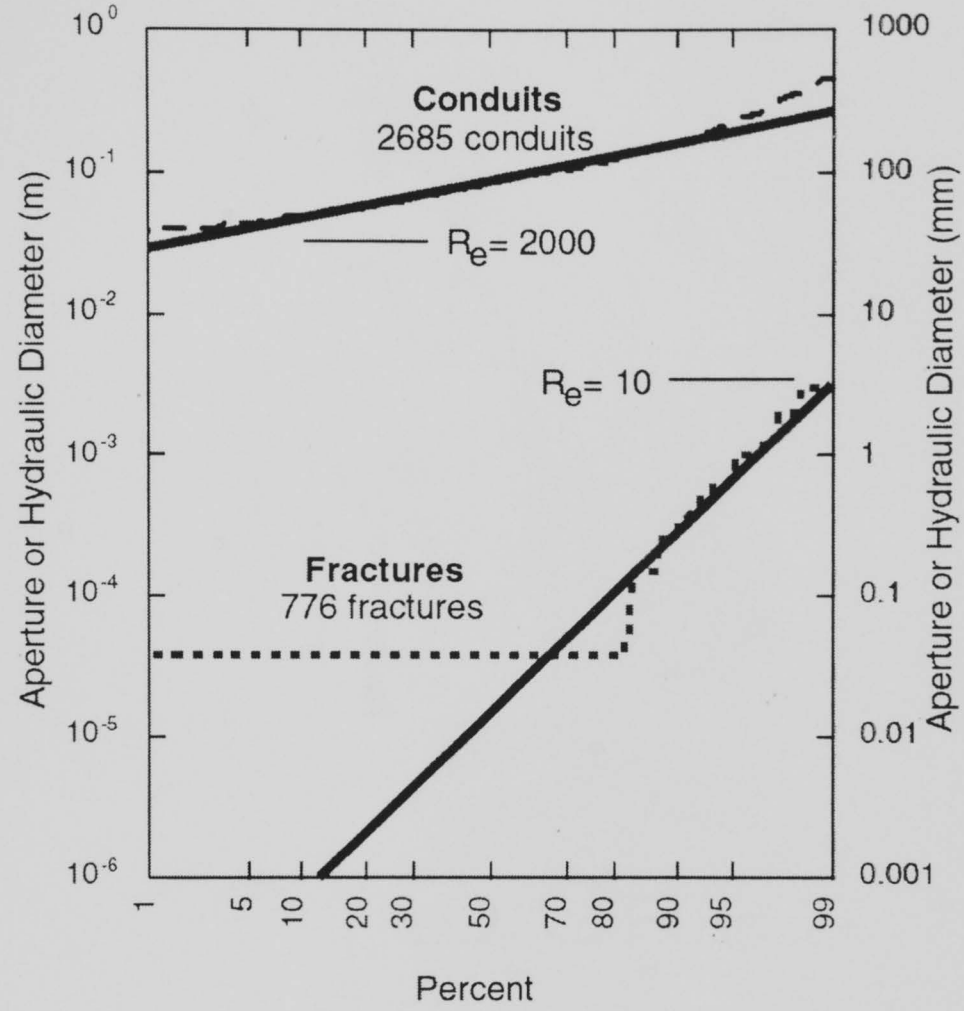

Figure 2.3: Conduit and fracture size distribution.

Fracture data shown for 776 fracture aperture measurements illustrated along with lognormal model of distribution. Uniform distribution of fractures below the 80th percentile is due to the measurement limit. Hydraulic diameter data shown for 2685 conduits. Reynolds numbers are shown for non-linear laminar ($10<R_e<2000$) transition for fractures and turbulent ($R_e>2000$) transition for conduits calculated using estimates of hydraulic gradient (0.11-0.42 m km^{-1}) for the Edwards aquifer (McKinney and Watkins, 1993).

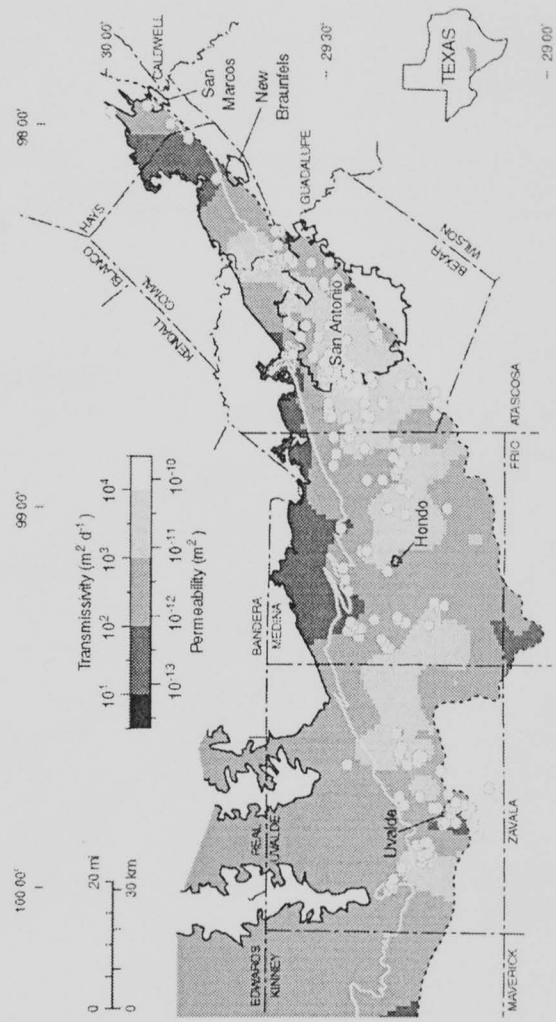

Figure 2.4: Map of the San Antonio segment of the Edwards aquifer.

Location of zero drawdown wells (wells with no measurable drawdown during pumping) is shown with white circles. Smoothed kriging of the transmissivity field included for comparison with locations of zero drawdown wells (Mace, in press; Hovorka et al., 1988). Legend for transmissivity includes estimate of permeability using average aquifer thickness of 170 meters to convert values. Solid dark line indicates northern physical boundary for the San Antonio segment of the Edwards. Dashed line indicates the bad water line which forms the southern chemical boundary for the aquifer. The white line indicates the recharge boundary which approximates the confined/unconfined boundary for the aquifer.

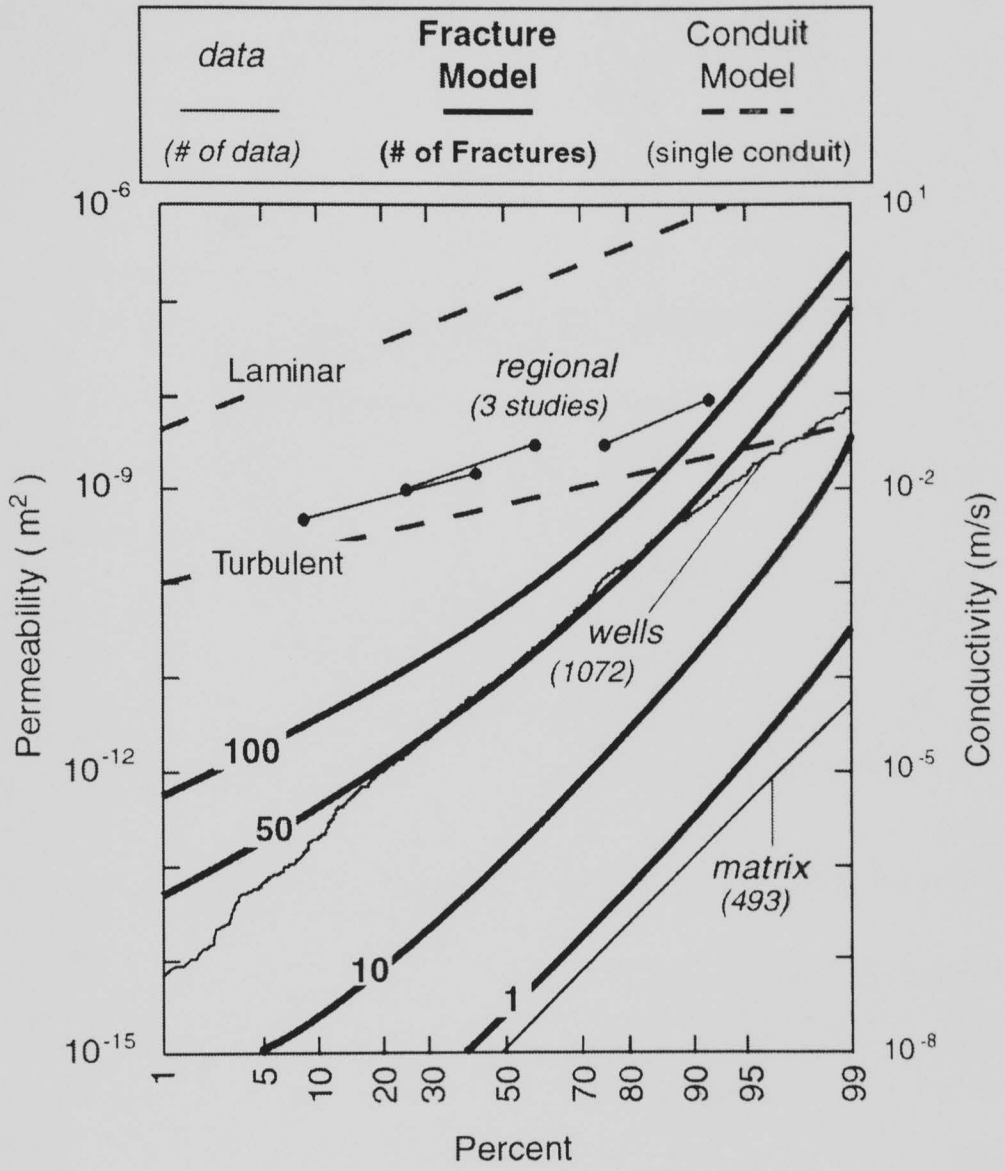

Figure 2.5: Monte Carlo models for matrix + multiple horizontal fractures and matrix + single horizontal conduit combination models.

Matrix, well, and regional distributions shown for comparison.

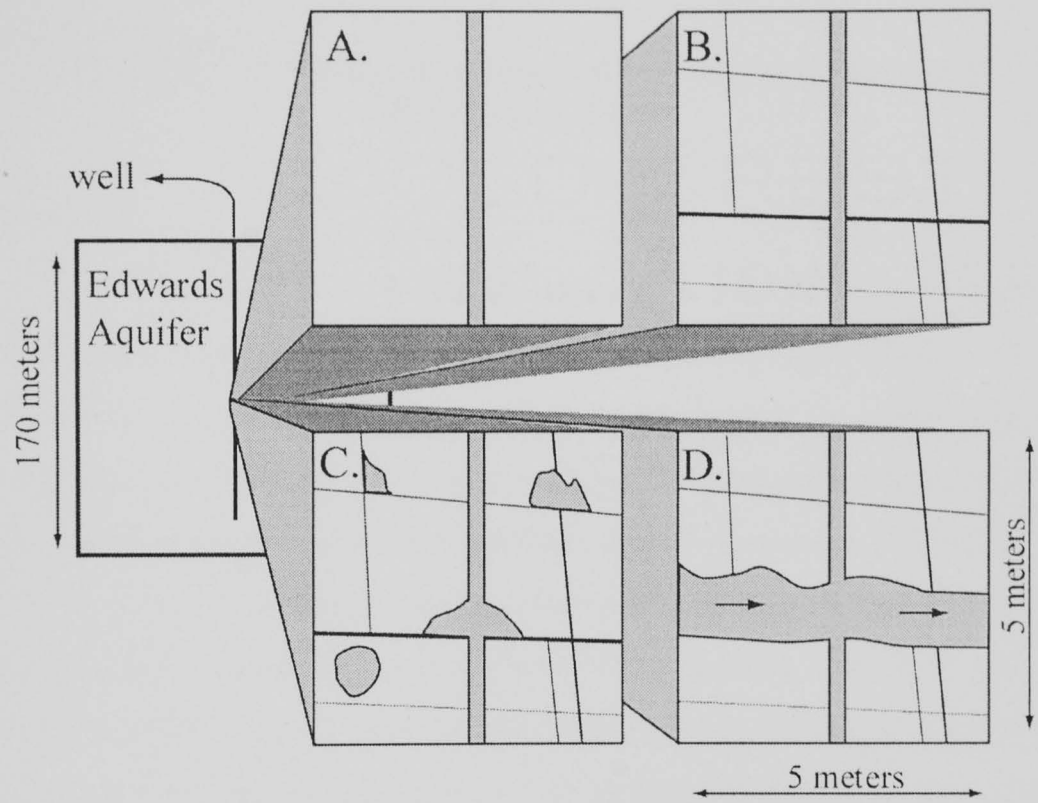

Figure 2.6: Four possible models of heterogeneities controlling the response of Edwards aquifer wells.

Model A represents a well located in a carbonate matrix that does not intercept any fractures or conduits. Model B represents a well that intercepts fractures. Model C represents a well that intercepts fractures and dissolution features of limited lateral extent resulting in a well with an irregular wall and bit drops during drilling. Model D represents a well that intercepts a laterally continuous, hydraulically active conduit. The majority of wells in the Edwards are probably best represented by model C, but a single well may have elements of all four models. Models B,C, or D are all plausible models for causing zero drawdown wells (wells with no measurable drawdown).

CHAPTER 3: Asymmetric Dipole-Flow Test in a Fractured Carbonate Aquifer

ABSTRACT

In fractured aquifers, continuum assumptions may not be appropriate because heterogeneities and discrete flow zones dominate the groundwater flow. To overcome this problem, a large number of measurements for characterizing these zones must be collected. Therefore, hydraulic testing methods need to be inexpensive, fast, and sensitive to heterogeneities. The hydraulic dipole flow test is a relatively new technique that was developed from the use of recirculation wells. This technique may overcome many of the problems inherent in other testing methods. In this study analytical solutions were developed and then applied to modified dipole-flow test with a single packer at the Bissen Quarry test site (Wisconsin, USA). This packer separated a well at various intervals, and fluids were pumped from the upper segment (chamber) of the well to the lower segment (chamber). The head was monitored at 11 observation points and in both segments of the well. Conductivities of the well segments were then determined. The tests at 7 different packer elevations in the well were rapid (<1 hour to reach steady-state). Asymmetric dipole-flow tests demonstrated the ability to quantify heterogeneities of the fractured aquifer.

INTRODUCTION

Groundwater equations are most sensitive to permeability. In nature, permeability has a range covering at least 17 orders of magnitude, with up to 9

orders of magnitude variation in a single aquifer (Halihan et al., 2000). Given the large range of possible values and the sensitivity to this parameter, accurate permeability data are critical for evaluating groundwater. This variability is a key factor to understanding the transport of solutes in the subsurface (Rehfeldt et al., 1989). Obtaining permeability data in fractured rock aquifers is difficult because of the permeability scale effect (Kiraly, 1975), problems with fracture connectivity, and the difficulty in obtaining sufficient data at an appropriate scale. Commonly used hydraulic testing techniques fail to provide enough information for characterizing these aquifers.

With these impediments, the selection of appropriate permeability data for use in models or for aquifer interpretation is difficult (Botha and Verwey, 1992). Well tests may have multiple interpretations, and each can generate an independent model of how the aquifer functions (Botha and Verwey, 1992). This ambiguity makes aquifer interpretation difficult at the well-scale. Therefore, it is necessary to develop techniques for testing fractured aquifers that can overcome some of these impediments without being overly complex, expensive, or time consuming. Dipole flow testing was originally developed as an aquifer remediation technique but has evolved into a technique to evaluate the vertical conductivity of porous media (Herrling and Stamm, 1992; Kabala, 1993). In this paper, asymmetric dipole flow equations are presented to interpret a series of tests conducted in fractured dolomite wells.

PREVIOUS WORK

The standard pumping test and specific capacity test are probably the most widely used hydraulic experiments. However, when investigating heterogeneous aquifers, they have a number of problems: 1) only a single averaged values of transmissivity is obtained for a test (Rehfeldt et al., 1989); 2) in a fractured aquifer, these tests may take days to weeks to obtain reliable results, and the flow may not be radial (Geier et al., 1995); 3) the results of these tests are questionable because of the complex nature of some heterogeneous aquifers. In the latter case, the results cannot be properly used to infer aquifer structure (Botha and Verwey, 1992).

Botha and Verwey (1992) suggest that packer tests "seem to be the only worthwhile approach to use...in a multi-layer aquifer." These tests are useful in determining small-scale hydraulic properties. However, they can be complicated by a single test intersecting multiple fractures, nonconductive fractures, or variations in the fracture plane (Geier, et al., 1995). Another difficulty is that by limiting the measurement to one location, the tested fractures may interconnect away from the borehole, and the response would measure some network instead of a single fracture or zone (Geier, et al., 1995). Finally, packer tests may suffer from the skin effect, caused by flow in the well bore around a packer (Kabala and Xiang, 1992; Taylor et al., 1990).

A new class of hydraulic tests is evolving that shows promise in overcoming some of the difficulties of standard techniques. These are referred to as recirculation or dipole tests (Clement et al., 1997). It is a packer test where

water is pumped from one segment of an aquifer to another. The test can be conducted in a vertical configuration in a single well (Kabala, 1993) or in multiple wells to conduct horizontal or azimuthal tests (Clement et al., 1997). This configuration is also used as an *in situ* remediation technique for contaminated aquifers (Herrling and Stamm, 1992). Kabala (1993) proposed dipole flow tests to improve characterization of anisotropic behavior in porous medium aquifers. Theoretical development of the dipole flow test was continued by Zlotnik and Ledder (1994) who examined the effects of boundary conditions on the test. The theoretical basis for the test was improved and a technique for understanding of the area of influence was developed (Zlotnik and Ledder, 1996). However, the dipole flow test has not been extensively field tested as a means of aquifer characterization (Zlotnik and Zurbuchen, 1998). There are few, if any, theoretical developments or experimental data on how such tests perform in fractured or karstic aquifers.

The dipole flow test offers a number of benefits when compared to other aquifer testing techniques. This test differs from other pumping tests in that the flow field can be vertical instead of only horizontal, and the test requires no fluids be injected or removed from the aquifer. At our field site in Bissen quarry, Wisconsin (USA), a standard pumping test required over 275,000 liters of water to be taken out of the aquifer during a 24 hour period, while the largest dipole test required only 900 liters to be moved inside the aquifer. The fluid used for the test remains localized in the aquifer minimizing or eliminating the difficulty of treating contaminated fluid. The dipole test is able to obtain more data in less

time than standard hydraulic testing methods by reaching steady-state quickly (5 minutes to 1 hour). By reaching steady-state quickly, these tests give the ability to test conceptual models in a reasonable amount of time. Permeability tensors can be tested, and no curve fitting is required since the solutions are steady-state analytical solutions.

The dipole test has drawbacks as well. The equipment required for testing has a higher initial cost when compared to standard pumping test equipment, but this may be offset eventually by decreased labor costs. In addition, the dipole test cannot be performed easily in a cased well (Kabala, 1993). Due to the vertical flow in the configuration, the test would be controlled by the skin effect, with the majority of flow occurring in the gravel pack outside of the well screen (Taylor et al., 1990; Kabala and Xiang, 1992). For fractured aquifers, many wells are completed open hole, making dipole aquifer testing reasonable when the appropriate drilling techniques are utilized. The dipole flow test as described by Kabala (1993) has the difficulty of requiring 3 packers to execute each test. Additionally, the analytical solutions provided by Zlotnik and Ledder (1996) require that the dipole chambers be the same length.

In this study, solutions were developed for a steady-state asymmetric dipole test in an anisotropic aquifer. The three packer/equal chamber solutions developed by Kabala (1993) and Zlotnik and Ledder (1996) require approximately equivalent permeabilities in the dipole chambers. Since fractured aquifer wells would rarely meet this criterion, an asymmetric single packer

approach was taken. The solutions were then applied to a series of asymmetric dipole flow tests conducted in a fractured high permeability dolomite aquifer.

SITE DESCRIPTION

The Bissen Quarry hydrogeologic test site, which was closed in the fall of 1998, is located approximately 7 kilometers (4.5 miles) southwest of Sturgeon Bay, Wisconsin (USA) (Figure 3.1). It quarries the Silurian Byron Dolomite. The Byron Dolomite is part of a regional aquifer along the western flank of the Michigan Basin. Recharge occurs through vertical fractures, and rapid lateral flow occurs through regional horizontal high permeability zones (Bradbury and Muldoon, 1992; Muldoon and Bradbury, 1996; Tsoflias and Sharp, 1998).

The Wisconsin Geological and Natural History Survey (WGNHS) conducted intensive studies on an approximately 40 m x 25 m surface of exposed dolomite with visible vertical fractures. Nineteen wells were installed at an approximate 3 m spacing grid, most to 11 m in depth (Figure 3.1). Site hydrogeology was characterized with a series of hydraulic tests, borehole logs, stratigraphic analysis of cores, outcrop studies, surface mapping of vertical fractures, and GPR surveys. These studies identified four major horizontal fractures (1.35, 4.25, 6.4 and 12 m below surface), two dissolution zones (2.72 and 7.45 m below surface), and an orthogonal set of sub-vertical fractures (strikes of ~ N75°E and N25°W). For this study, these zones are listed as fractures 1-6 with fracture 1 being the closest to the surface. Hydraulic conductivity data show a bimodal distribution ranging seven orders of magnitude, indicating high conductivity fractures vs. lower conductivity rock matrix (Muldoon and

Bradbury, 1996). WGNHS studies show that lithologies and horizontal stratigraphic discontinuities control both aquifer storage capacity and distribution of preferred flow paths. Preferred flow zones form along bedding planes, diagenetic surfaces, and cycle sequence boundaries. These features are further enhanced by dissolution.

Asymmetric dipole testing was conducted in well 13 (Figure 3.1), which had a diameter of 3 inches (76 mm). Observations of the head field were made at 11 additional observation locations in 4 additional wells (Figures 3.1 and 3.2). Previous work has determined a bulk transmissivity of 2.5 x 10^{-3} m^2 s^{-1} for well 13. Caliper logs and double packer testing of well 13 determined that the upper portion of the well was dominated by the horizontal fractures with the lowest fracture (fracture 6) controlling the majority of flow in the well (Figure 3.3) (Muldoon and Bradbury, 1998). Additionally, double packer testing indicated a region of high permeability in the bottom of the well that was not observed at most of the other nearby wells.

FIELD METHODS

The equipment used to conduct the dipole profiling included: (1) inflatable packer; (2) nitrogen tank, pressure gauge, and tubing to inflate the packer; (3) in-line flow meter; (4) variable rate pump, controller, and generator (MP-1, Grunfos Pumps Corp.); (5) tubing to connect packer and pump to flowmeter; (6) transducers, cables, and datalogger (Hermit 2000, In-Situ Corp.); (7) cable to raise and lower assembly in wells (Figure 3.4). For the small diameter (3 inch) well available, the system could not use rigid pipe. With shallow wells, the system

could be raised and lowered by hand. For larger diameter wells, the system can be adapted to include pipe and in-line pumps.

To conduct the tests, the following procedures were used:

1. The packer with attached nitrogen line, lower transducer, and tubing was lowered to the desired position in the well. The position will be referred to by the center point elevation.
2. The pump with attached control cable and tubing and the upper transducer with cable were lowered down the well to just above the packer location.
3. The system was bled of all air by running the pump with the packer uninflated.
4. Transducers were prepared for logging.
5. The packer was inflated.
6. Pump and data logger were started at a flow rate, Q, designed to obtain a reading in both chambers without exceeding the limits of the lower transducer.
7. Transducers were monitored to observe when the test reached steady-state (5-30 minutes), and values of head for the two chambers were recorded.
8. Drawdown or negative buildup normalized to the pumping rate was plotted relative to curves for hydraulic conductivities assuming homogeneous, isotropic conditions.

To obtain an asymmetric dipole profile for the well, the steps were repeated until tests were conducted at 7 locations. Conducting tests at multiple flowrates as suggested by Zlotnik and Zurbuchen (1998) is not as crucial in this

configuration since previous and subsequent tests provide a check on the test value. If the transmissivity of the upper chamber does not increase as the packer is lowered on sequential tests, with the transmissivity decreasing in the lower interval, the tests should be repeated or examined for skin effect problems.

The flowrate for an asymmetric dipole test must be set to avoid two problems. The pumping rate must be low enough to avoid dewatering the upper chamber (Zlotnik and Zurbuchen, 1998). Additionally in a fractured aquifer, the lower permeability often present at the bottom of a well will cause high pressures to build up in the lower interval once the packer is set below the more permeable zones in the well. Therefore, if the pumping rate is too high, hydraulic fracturing may occur or equipment may be damaged. The former problem is generally of concern higher in the well, while the later is a problem lower in the well. Setting the flowrate to avoid these problems is difficult to predict *a priori*, but conservative estimates are advised.

THEORY - HOMOGENEOUS ANISOTROPIC AQUIFER

Consider the drawdown induced by a dipole consisting of a linear source and sink distributed along a line r = 0 in an anisotropic aquifer of thickness, b (Figure 3.5). This is a special case of the solution of Hantush (1961, p. 90) where the well has two screened sections. One section is used for injection and another for extraction.

The drawdown induced by the upper extraction chamber, $s_1(r,z,t)$, is given by (see notation list for variable definition):

$$s_1(r,z,t) = \left(\frac{Q}{4\pi K_r b}\right)\left[W(u) + \frac{4b}{\pi A}\sum_{n=1}^{\infty}\frac{1}{n}K_0\left(\frac{n\pi r}{ab}\right)\sin\left(\frac{n\pi A}{b}\right)\cos\left(\frac{n\pi z}{b}\right)\right] \qquad (3.1)$$

where Q is the discharge rate [$L^3\ t^{-1}$], K_r is the horizontal hydraulic conductivity [$L\ t^{-1}$], A is the length of the extraction chamber [L], a is the anisotropy ratio [dimensionless], W(u) is the well function [dim], and K_0 is a zero-order modified Bessel function of the second kind. Similarly for the lower chamber, the drawdown is given by:

$$s_-(r,z,t)=\left(\frac{-Q}{4\pi K_r b}\right)\left[W(u)+\frac{4b}{\pi B}\sum_{n=1}^{\infty}\frac{1}{n}K_0\left(\frac{n\pi r}{ab}\right)\sin\left(\frac{-n\pi(A+D)}{b}\right)\cos\left(\frac{n\pi z}{b}\right)\right] \quad (3.2)$$

where D is the packer length [L] and B is the length of the injection chamber [L]. The total drawdown after time:

$$t > \frac{S_s b^2}{2K_r} \quad (3.3)$$

is merely a superposition of s_- and s_+ which yields the steady-state solution:

$$s(r,z)=s_-(r,z,t)+s_+(r,z,t)=$$
$$\left(\frac{Q}{\pi K_r A}\right)\sum_{n=1}^{\infty}\frac{1}{n}K_0\left(\frac{n\pi r}{ab}\right)\sin\left(\frac{n\pi A}{b}\right)\cos\left(\frac{n\pi z}{b}\right) +$$
$$\left(\frac{Q}{\pi K_r B}\right)\sum_{n=1}^{\infty}\frac{1}{n}K_0\left(\frac{n\pi r}{ab}\right)\sin\left(\frac{n\pi(A+D)}{b}\right)\cos\left(\frac{n\pi z}{b}\right) \quad (3.4)$$

Simple hydraulic head measurements can be obtained in the upper and lower chambers of an asymmetric dipole test, so the drawdown obtained in each chamber is useful for field testing. Integrating the local drawdown over the chamber (Hantush, 1961), solutions for the total upper and lower chamber drawdown are obtained:

$$s_u=\left(\frac{Q}{\pi^2 K_r \bar{A}}\right)\sum_{n=1}^{\infty}\frac{1}{n^2}K_0\left(n\pi\bar{r}_w\right)\sin\left(n\pi\bar{A}\right)\left[\frac{1}{\bar{A}}\sin\left(n\pi\bar{A}\right)+\frac{1}{\bar{B}}\sin\left(n\pi\left(\bar{A}+\bar{D}\right)\right)\right] \quad (3.5)$$

similarly, the head in the lower chamber would be:

$$s_l=\left(\frac{Q}{\pi^2 K_r \bar{B}}\right)\sum_{n=1}^{\infty}\frac{1}{n^2}K_0\left(n\pi\bar{r}_w\right)\sin\left(n\pi\left(\bar{A}+\bar{D}\right)\right)\left[\frac{1}{\bar{A}}\sin\left(n\pi\bar{A}\right)+\frac{1}{\bar{B}}\sin\left(n\pi\left(A+D\right)\right)\right] \quad (3.6)$$

where:

$$\bar{A} = \frac{A}{b}, \quad \bar{B} = \frac{B}{b}, \quad \bar{D} = \frac{D}{b}, \quad \text{and } \bar{r_w} = \frac{r_w}{ab}. \tag{3.7}$$

Radial hydraulic conductivity can be calculated for the upper chamber using:

$$K_r = \left(\frac{Q}{\pi^2 s_u \bar{A}} \right) \sum_{n=1}^{\infty} \frac{1}{n^2} K_0(n\pi\bar{r_w}) \sin(n\pi\bar{A}) \left[\frac{1}{\bar{A}} \sin(n\pi\bar{A}) + \frac{1}{\bar{B}} \sin(n\pi(\bar{A}+\bar{D})) \right] \tag{3.8}$$

similarly, the conductivity for the lower chamber would be:

$$K_r = \left(\frac{Q}{\pi^2 s_l \bar{B}} \right) \sum_{n=1}^{\infty} \frac{1}{n^2} K_0(n\pi\bar{r_w}) \sin(n\pi(\bar{A}+\bar{D})) \left[\frac{1}{\bar{A}} \sin(n\pi\bar{A}) + \frac{1}{\bar{B}} \sin(n\pi(\bar{A}+\bar{D})) \right] \tag{3.9}$$

For the tests conducted, conductivity was calculated for both an isotropic aquifer and an anisotropic aquifer with an anisotropy ratio ($K_r K_z^{-1}$) of 10 and 0.1. The thickness of a fractured aquifer is a difficult parameter to quantify, and the bottom of the well was taken to represent the bottom of the aquifer (Muldoon and Bradbury, 1998). (The response of the asymmetric dipole equations to variations in the dimensionless parameters is given in Appendix A.)

CONDUCTIVITY OF SINGLE INTERVAL

The conductivity of a single interval can be calculated using the results from two individual tests. If the change in conductivity between tests results from the addition or removal of a permeable feature from a chamber, the conductivity of that zone can be calculated using the change in chamber transmissivity. If chamber transmissivity is defined as:

$$T_c = K_c b_c \tag{3.10}$$

where T_c is the chamber transmissivity [$L^2 t^{-1}$], K_c is the chamber conductivity [$L t^{-1}$], and b_c is the chamber length [L], then the conductivity of an interval can be calculated as:

$$K_i = \frac{T_L - T_S}{b_i} \qquad (3.11)$$

where K_i is the conductivity of a single interval between tests, T_L is the transmissivity of the longer chamber, and T_S is the transmissivity of the shorter chamber, and b_i is the interval thickness.

RESULTS

The results of the testing are examined for a single asymmetric dipole test (test 5). After the behavior of a single test is understood, the profile for the upper chamber is examined to determine what the testing indicates about the structure of permeability for the well. Next, the lower chamber is examined to determine if the interpretation of the well properties are consistent between chambers. Finally, the highest permeability feature, fracture 6, is examined to determine how the asymmetric dipole test compares with double packer tests for the fracture.

Asymmetric Dipole Test 5

The results for a single asymmetric dipole test (test 5) are illustrated in Figures 3.2, 3.6, and 3.7 (The results of the remaining 6 tests are located in Appendix B). For the single packer location, the drawdown in the upper chamber is greater than the buildup in the lower chamber (Figure 3.6). If both values were equal, the transmissivities of the two chambers would be equal, however at this location, the lower chamber of the well is more transmissive than the upper chamber. This is the result of the high permeability fracture 6 being located in the lower chamber during the test. For the upper pole, the test reached steady-state after 5 minutes, while the lower chamber reached a steady buildup after only 1

minute. The dipole field generated from test 5 developed a pressure field demonstrating the expected r^{-2} dependence for the test. The test had a region of influence greater than 20 meters. The lowest piezometers in the observation network (D and E) did not have a significant response to the test.

Upper Chamber Profile

The asymmetric dipole profile of the upper chamber illustrates qualitatively that the upper portion of the well responded similarly to a continuum (Figure 3.8 and Appendix C). The changes in conductivity that occurred as the packer was lowered for subsequent tests resulted in a profile that closely follows the path for a continuous change in conductivity. The lowest test (test 7) illustrates the difficulty of obtaining values when the conductivity contrast between the two poles is extreme. For the lowest test, the permeable regions of the well were all above the packer, so as to avoid damaging the lower transducer or generating fractures, the flowrate could not be set high enough to generate measurable drawdown. In fact, the response measured was buildup for both chambers. A simple one layer continuum model cannot simulate this response. The final test only gave an indication that between test 6 and 7, a permeable feature was included in the chamber that was not there in the previous test. The quantitative values of conductivity for the upper portion of the well are similar to the bulk value obtained with a standard pumping test (Tsoflias et al, in review). Without performing a numerical model to test the results versus other techniques, it is difficult to determine if the test yields values that are higher than other

methods or if an anisotropy or heterogeneity in the aquifer is the cause of the measured drawdown.

Lower Chamber Profile

The profile of the lower chamber contrasts with the upper chamber but provides a similar interpretation of the well (Figure 3.9). The upper tests (1-5) indicated that the buildup in the lower chamber did not change as the packer was lowered in the well during sequential tests. This indicates that lowering the packer did not appreciably reduce the bulk transmissivity of the chamber. This indicates that a feature lower in the well controlled the conductivity of the well. Test 6 generated a much higher buildup, indicating that the high permeability feature was no longer contained within the lower chamber. The values in test 6 and 7 are similar to low conductivity values found using double packer tests at the Bissen site. This contrasts with double packer tests from the lower portion of well 13. The repeated results of the dipole test using an identical portion on the well for test 6 and 7 and the lack of high values at similar elevations indicates that the lower portion of the well is not highly conductive.

Conductivity of Fracture 6

The conductivity of the region that was available in test 5, but was subsequently covered in test 6 was calculated using equation 3.11 as 9.2×10^{-3} m s^{-1}, which is similar to double packer testing of fracture 6 which obtained a value of 4.11×10^{-3} m s^{-1}. A lower value for the dipole profile can be obtained if a higher vertical conductivity is assumed, but the interval used between the two tests was different, so a strict comparison is not appropriate.

CONCLUSIONS

Hydraulic testing is one of the most accurate ways to obtain permeability values for site characterization. However, the difficulties with standard testing methods make them unattractive in fractured media. Asymmetric dipole profiling may provide a useful alternative for characterizing wells in fractured media.

Asymmetric dipole profiling provided a rapid technique to assess the bulk properties of well 13. With the seven tests conducted, the well could be divided into an upper fractured portion that behaves as a continuum, a large fracture that is the highest conductivity portion of the well, and a lower non-conductive (or likely non-fractured) region. The quantitative values for the asymmetric dipole test appear to yield values that are generally high compared to double packer tests. Numerical modeling of these tests in layered media may illustrate the discrepancy between the asymmetric dipole tests and double packer testing. Three packer dipole tests may be useful in the upper portion of the well to delineate further the permeability field.

Asymmetric dipole profiling provides an alternative technique to develop quantitative conceptual models of fractured aquifers. The ability to conduct the tests rapidly without extracting fluids from the aquifer make the technique attractive for accessing contaminated sites. The difficulty of obtaining results for the entire well profile due to draining the upper chamber with no resulting buildup in the lower chamber high in the well, and no drawdown or excessive buildup in the lower chamber limit the technique in some cases. Additional work is needed

to determine how localized anisotropy and heterogeneity affects the results of the tests.

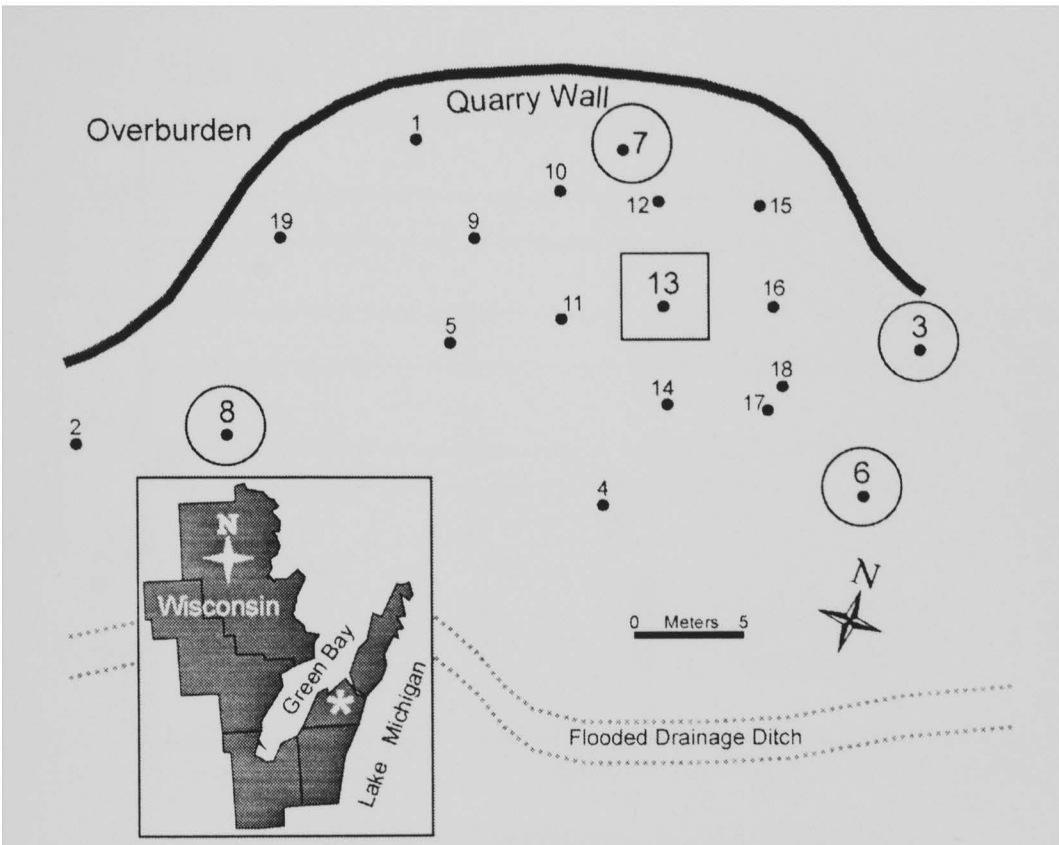

Figure 3.1: Map of location of Bissen quarry (inset) and location of wells in quarry.

Well 13 (in square) was utilized for dipole-flow testing. Wells 3, 6, 7, and 8 (in circles) were used as observation points for the test.

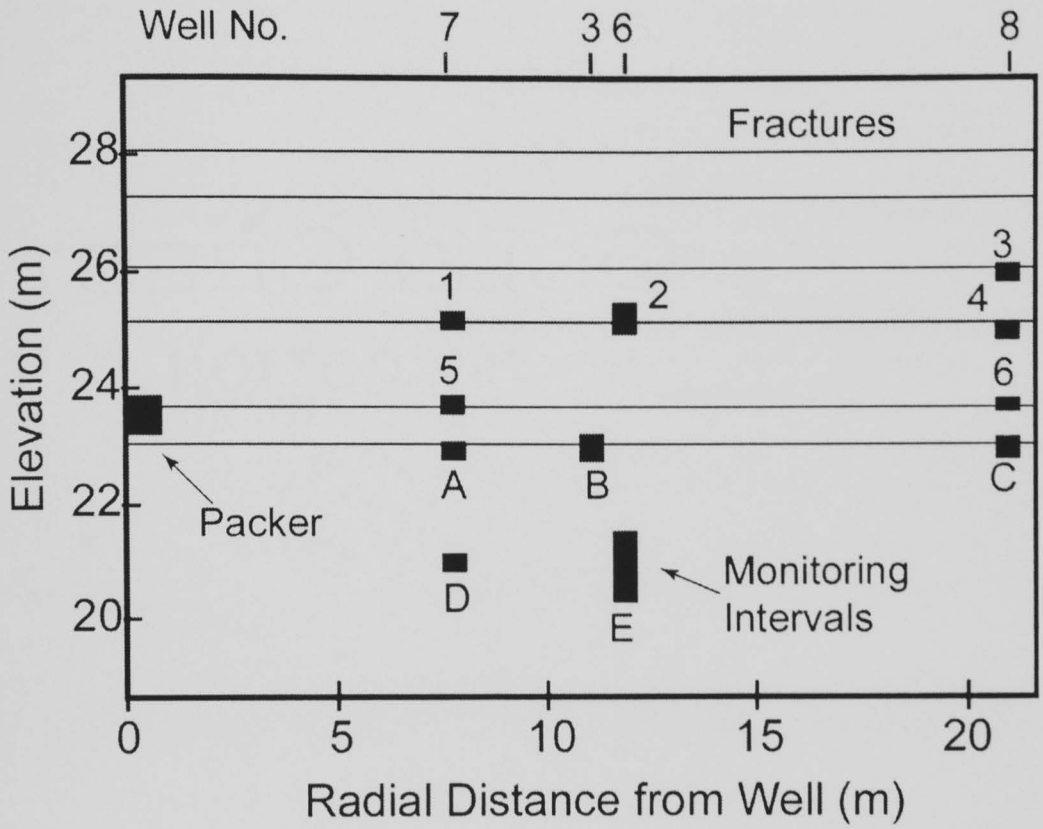

Figure 3.2: Observation network cross-sectional view for tests conducted at well 13.

Packer location illustrated for test results illustrated in figures 3.6 and 3.7. Previous work at the site has delineated 6 prominent fracture zones with fracture 6 (lowest fracture) having the highest permeability (Muldoon and Bradbury, 1998). Observation point numbers (1-6) and letters (A-E) correlate with results illustrated in figure 3.7.

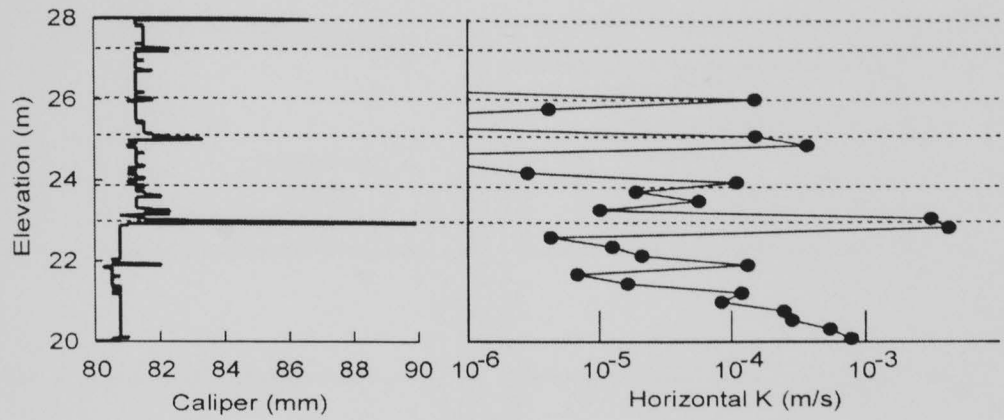

Figure 3.3: Caliper log and double packer profile for well 13 (Muldoon and Bradbury, 1998).

Location of six fracture zones illustrated with dashed lines. Double packer tests were conducted over 27 cm (0.9 foot) interval at 22.5 cm (0.75 foot) increments.

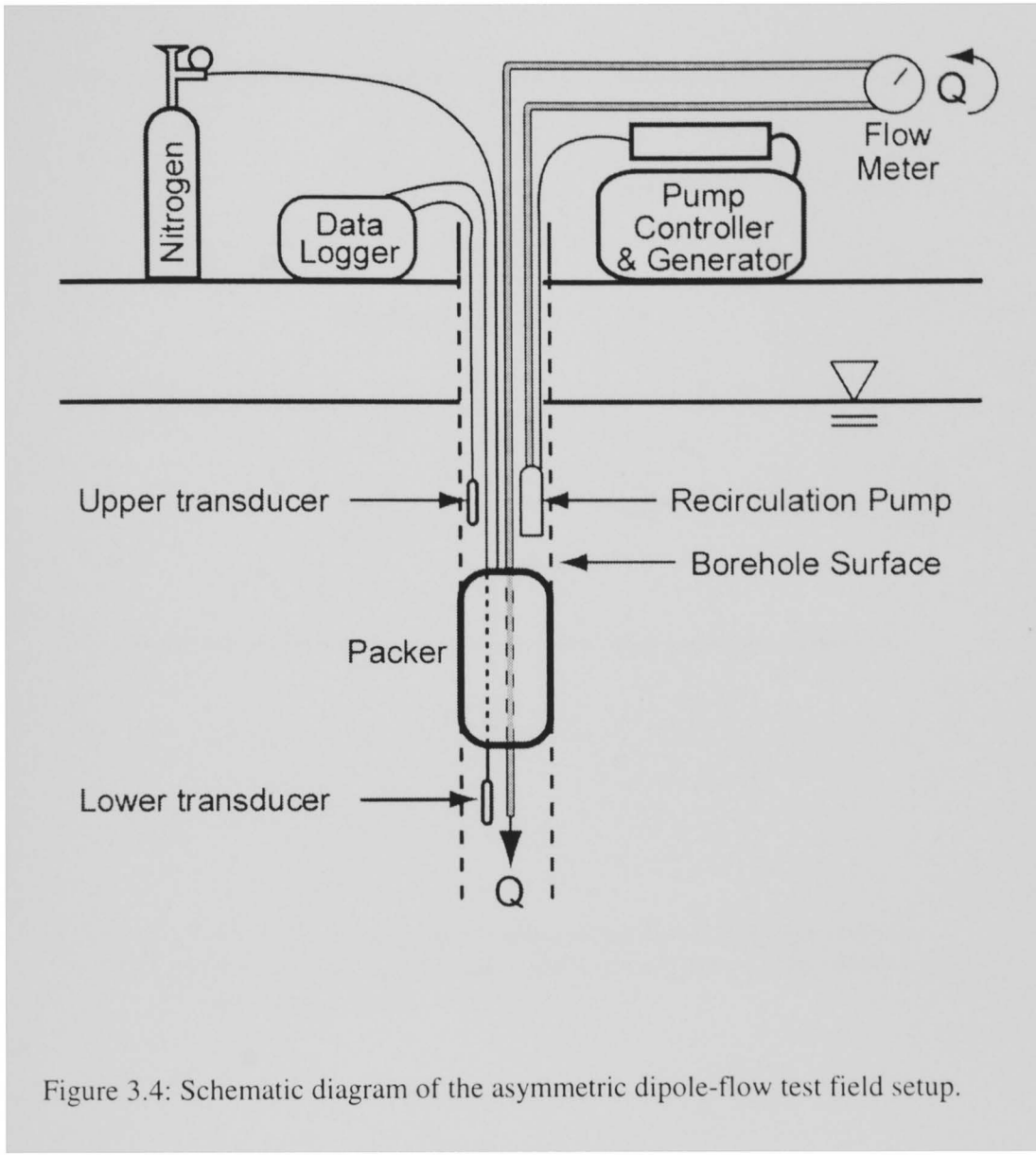

Figure 3.4: Schematic diagram of the asymmetric dipole-flow test field setup.

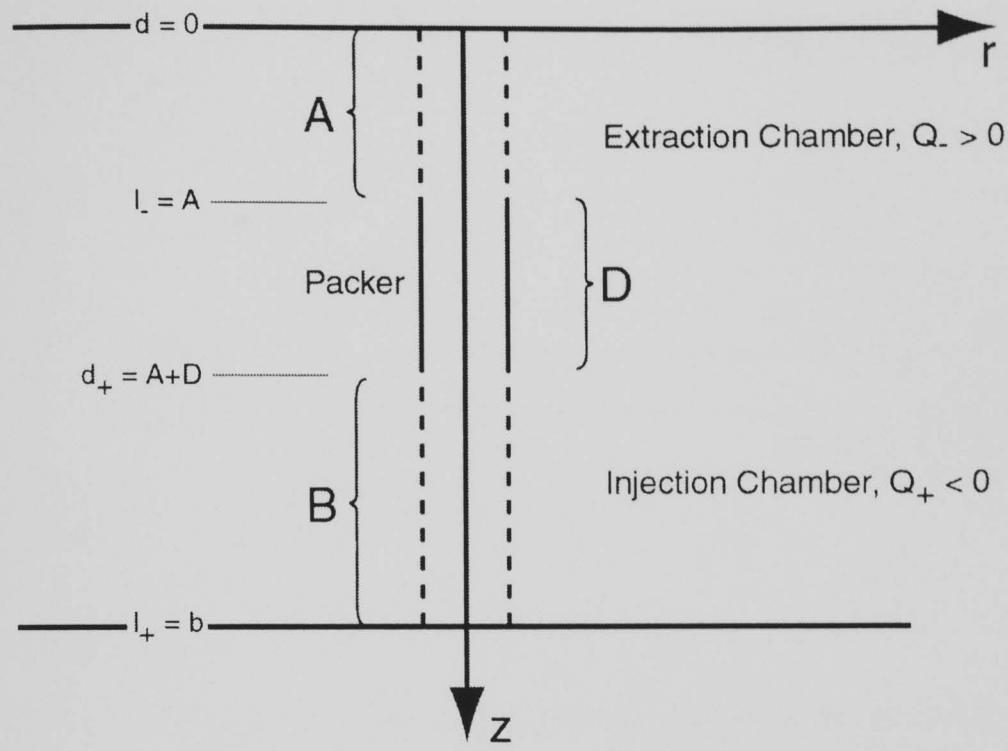

Figure 3.5: Schematic diagram of an asymmetric dipole configuration for homogeneous, anisotropic aquifer shows the variable definitions and coordinate scheme.

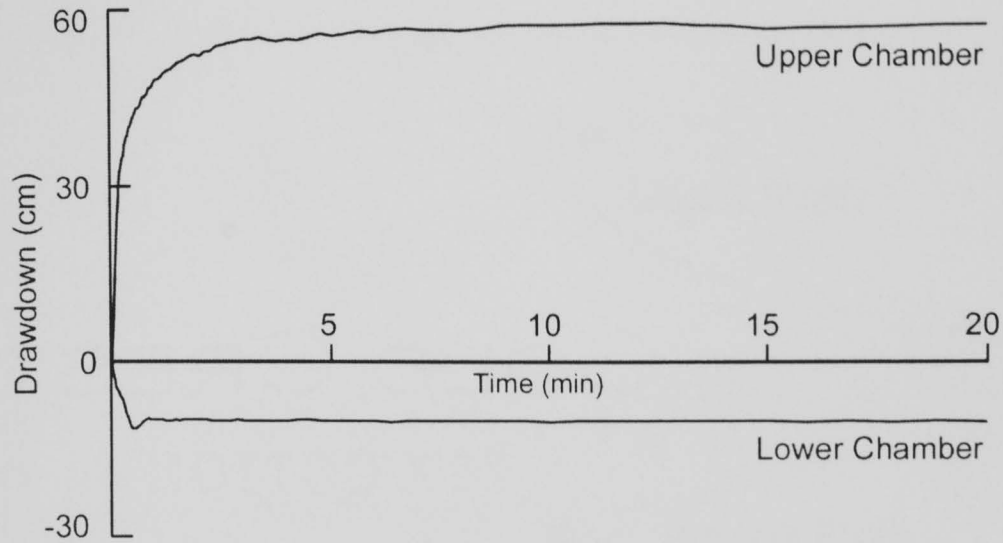

Figure 3.6: Transducer response in upper and lower chamber of the asymmetric dipole-flow test.

Figure 3.2 illustrates packer location for test.

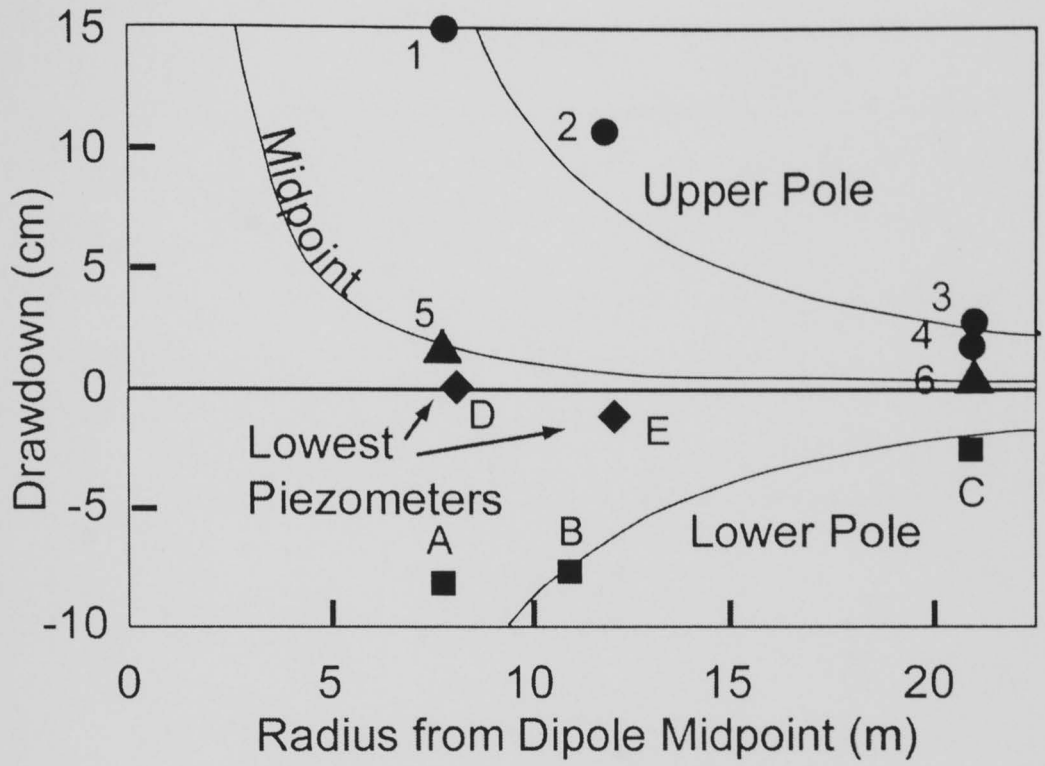

Figure 3.7: Pressure field generated by asymmetric dipole test with packer at location illustrated in figure 3.2.

Circles indicate monitoring locations for the upper pole of the test. Squares indicate locations for the lower pole. Diamonds indicate monitoring points on the lower pole that were not in the primary fracture network (See Figure 3.2). Triangles indicate points at the test midpoint. Solid lines indicate that the decrease of head in radial direction invoked by the dipole-flow test follows generally the R^{-2} law.

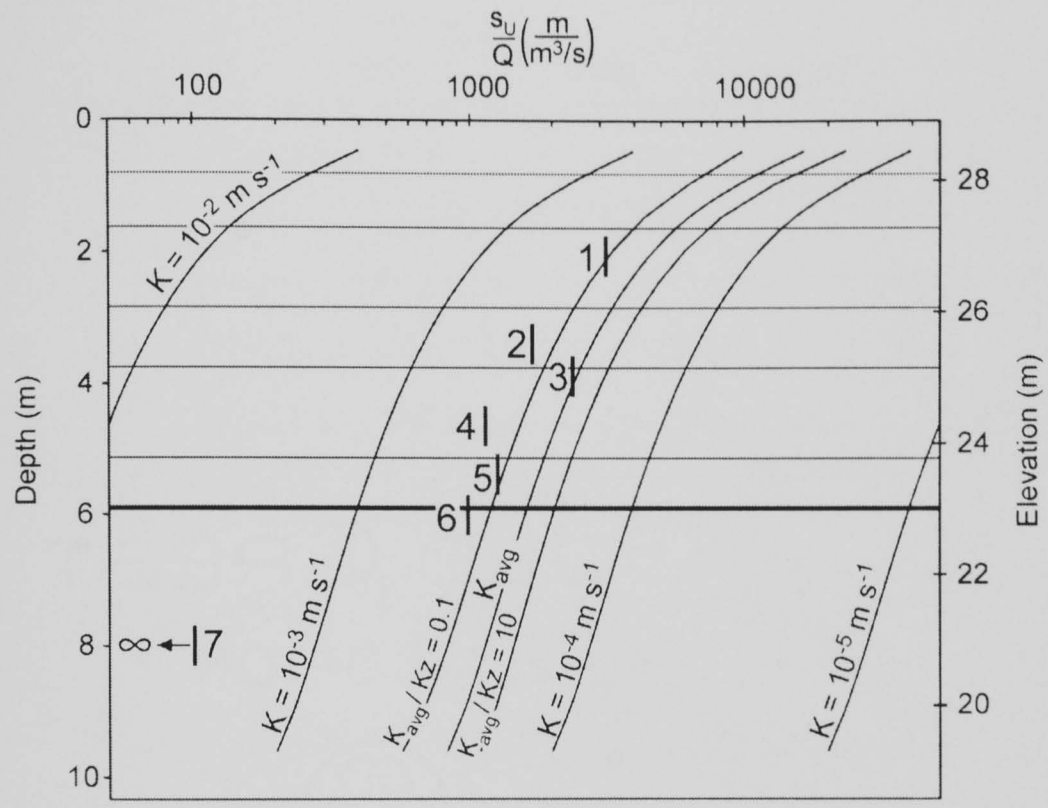

Figure 3.8: Asymmetric dipole profile s_U/Q as a function of the packer depth for the upper chamber of well 13.

Solid curves indicate type curves corresponding to the various values of K_r calculated from equation 3.5. Vertical lines indicate test measured s_U/Q plotted against the elevation of the packer. The lowest test (test 7) is plotted with an arrow indicating that no measurable drawdown was obtained for the test.

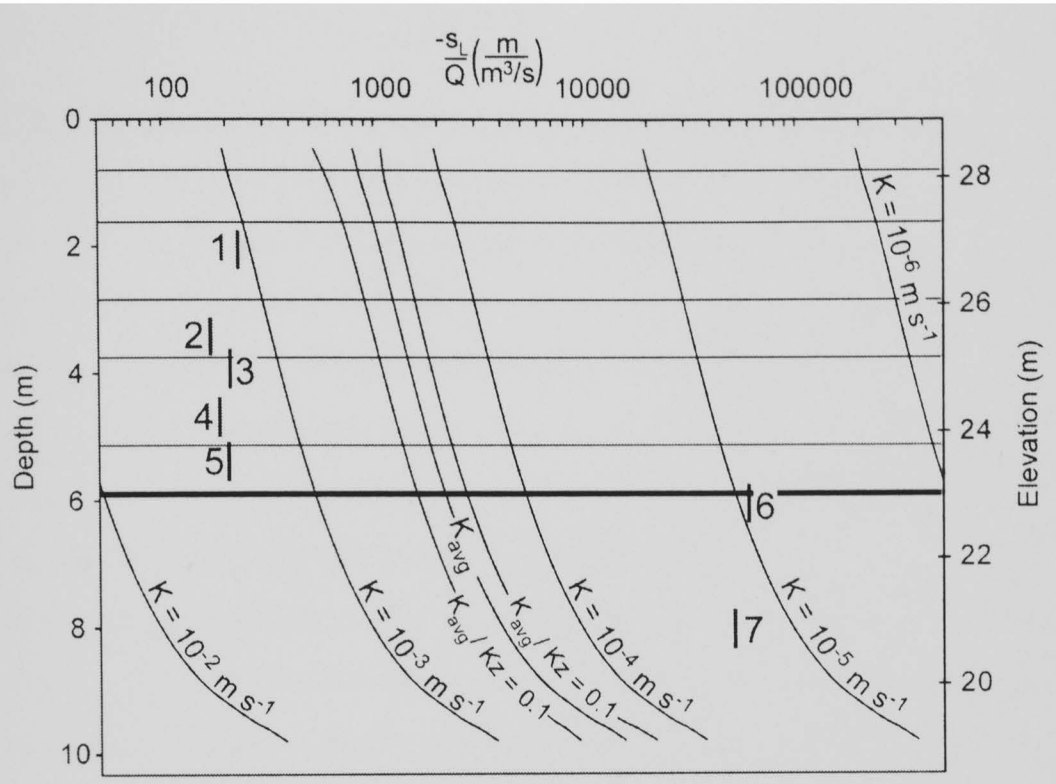

Figure 3.9: Asymmetric dipole profile $-s_L/Q$ as a function of the packer depth for the lower chamber of well 13.

Solid curves indicate type curves corresponding to the various values of K_r calculated from equation 6. Vertical lines indicate test buildup (negative drawdown) $-s_L/Q$ plotted against the elevation of the packer.

Notation	Definition
a	anisotropy ratio, where $a^2 = K_r / K_z$ [dim]
A	length of extraction (upper dipole) chamber [L]
b	aquifer thickness [L]
B	length of injection (lower dipole) chamber [L]
d	top of chamber [L]
D	packer length [L]
K	horizontal hydraulic conductivity [$L\ t^{-1}$]
K	vertical hydraulic conductivity [$L\ t^{-1}$]
l	bottom of chamber [L]
n	index of summation [dim]
Q	discharge rate [$L^3\ t^{-1}$]
r	radial coordinate [L]
r_w	well radius [L]
s	local drawdown in the aquifer [L], (- = drawdown, + = buildup)
t	time [t]
W(u)	well function [dim]
z	vertical coordinate measured downward from the top of the aquifer [L]

Table 3.1: Variables used for asymmetric dipole-flow equations.

CHAPTER 4: Evaluating Fracture Connections Using Asymmetric Dipole Tests

ABSTRACT

Fractured rock aquifers are difficult to characterize because of their heterogeneous nature. Developing an understanding of the permeability and connections of fractures is difficult and time consuming in these aquifers. Field testing techniques for determining the location and connections of fractures in these aquifers are lacking when compared to modeling capabilities. In the Clare Valley, South Australia, well interference is an important issue for a major viticultural area located on a fractured aquifer. Five fracture sets exist in the aquifer, with four sets dipping 60 degrees or greater. In this setting, we evaluate the ability of asymmetric dipole-flow tests to determine the permeability and connections between wells and piezometers. The test series involves packing a well at multiple intervals and pumping fluid from the upper segment of the well to the lower segment. By monitoring the response of the hydraulic dipole field, the connectivity of the fractures between boreholes can be evaluated by examining whether drawdown or buildup occurred in observation bores and piezometers. The results indicate that the boreholes were connected in complex geometries with drawdown occurring above and below areas of pressure buildup.

INTRODUCTION

Evaluating connections between wells is required to predict well interference and recharge mechanisms. Connectivity of wells is also important for determining potential flowpaths of contaminants or the efficiency of remediation techniques. In porous media aquifers, connections are assumed to follow lithology with wells connecting horizontally in most cases. Analysis of hydraulic testing in wells generally assumes horizontal flow *a priori* (e.g., Theis, 1935). In a fractured aquifer, the horizontal assumption may apply in areas where horizontal fractures control the aquifer. However, in geological settings where complex or poorly connected fractures control the aquifer, determining connections between wells can be difficult.

Outcrop analysis in fractured aquifers has provided some insight into how wells may connect (LaPointe and Hudson, 1985; Wiltschko et al., 1991). Simple analysis of primary fracture orientation can provide insight regarding the assumption of horizontal flow. Theoretical work has provided models to interpret hydraulics in these aquifers (Snow, 1969; Streltsova, 1976). Theoretical work on the connectivity of fractures has been used to determine when fractures are connected sufficiently to provide flow (Berkowitz, 1995; Renshaw, 1999). Additionally, complex numerical models allow fractures to be connected as planes or pipes (Dershowitz and Fidelibus, 1999).

While previous work has allowed a better understanding of how fracture networks may respond and how to model them, field techniques to determine connections between wells at a specific site are still limited. Marine (1980)

discussed the use of tracers to track the connections of fractures, however the technique is limited in cases with multiple connections. Hydraulic testing using double packers is useful, but is limited by both multiple connections and the time required to determine locations using a small segment of the well during a single test (Botha and Verwey, 1992).

Dipole flow tests are a relatively recent technique applied to both porous media aquifers (Kabala, 1993; Zlotnik and Zurbuchen, 1998) and fractured media (Halihan, 1999; Halihan and Zlotnik, in preparation). The dipole field can be useful for determining connections in a fractured aquifer because of the presence of two hydraulic signals (drawdown and buildup). Our hypothesis is that using this advantage, asymmetric dipole tests can provide an improved method of determining the location of fracture connections between observation points in a fractured aquifer.

SITE DESCRIPTION

The Clare Valley, South Australia is a major viticultural region located approximately 100 km north of Adelaide. The geology of the region is dominated by the Hill River Syncline that is composed of low-grade metamorphic Proterozoic rocks. The lithology at the well site consist of vertically dipping beds of silty dolomite which contain five major fracture sets, 4 steeply dipping and 1 gently dipping (Figure 4.1).

Hydrogeologic investigations of the Clare Valley were conducted to aid in evaluating groundwater resources for the expanding viticultural industry in the area. One area of major interest was how wells may interact with each other in

the complex set of fractures present at the site. Wells for this study were located at the Wendouree Vineyard approximately 5 km south of the town of Clare. Work at the site demonstrated that the wells respond only at fracture locations and that the lithology has low hydraulic conductivity (Morton et al., 1998; Cook et al., 1999). Three wells on the site were utilized for this study. Well Clare 105 is a 100-meter deep, 8-inch (203-mm) diameter open borehole used for asymmetric dipole testing (Figure 4.2). Four deep piezometers were available for observations in well 36385, and six shallow piezometers were available in well 41497 (Figure 4.3).

FIELD METHODS

Asymmetric dipole-flow testing in well Clare 105 followed the procedure of Halihan and Zlotnik (in preparation). A single packer was inflated in the open borehole and fluids were pumped from the upper chamber to the lower chamber of the well. To scale the testing up to larger bores (203-mm diameter, 100-meter deep), solid pipe was used instead of flexible tubing from the intake screen to the surface (Figure 4.4). The flow was then routed through a flowmeter and returned below the packer using flexible tubing connected to a return valve above the packer. Nine asymmetric dipole tests were conducted in the well, and observations of drawdown were taken in both testing poles and in the 10 piezometers. Tests reached steady state after 20-30 minutes, which is longer than the testing required by Halihan and Zlotnik, but was expected due to the chamber length dependence for the transient portion of the test.

CONNECTION THEORY

Asymmetric dipole-flow testing is beneficial for testing hydraulic connections because it provides an additional piece of information over standard double packer or open borehole pumping or injection tests. By having drawdown occurring in one portion of the well, while buildup is occurring in the other portion, three possible observations can be made at observation points (piezometers or wells) in the aquifer. Drawdown, buildup, or no measurable response may occur at observation locations. To predict the connections present in an aquifer between a well and observation locations, the dipole field generated by an asymmetric dipole test must be understood.

Two different viewpoints of aquifer connectivity can be utilized. The first is a continuum model using representative elementary volumes to describe the connections. The other model would assume that all connections in the aquifer are discrete, nearly independent connections. The actual situation should be somewhere between these two extremes. The theoretical asymmetric dipole field generated for the Wendouree vineyard under homogeneous, isotropic conditions is calculated and discussed to evaluate the expected response in piezometers if the continuum assumption was valid in this aquifer. For the discrete case, with single connections present, a single connection analysis is evaluated. Finally, the analysis for multiple discrete connections is presented.

Homogeneous, Isotropic Aquifer

The equations are presented in Chapter 3 for an asymmetric dipole field in a homogenous, anisotropic aquifer. To solve for the drawdown at a given radius and depth from the well, the following equation is used:

$$s(r,z) = s_{-}(r,z,t) + s_{+}(r,z,t) =$$
$$\left(\frac{Q}{\pi K_r A}\right)\sum_{n=1}^{\infty}\frac{1}{n}K_0\left(\frac{n\pi r}{ab}\right)\sin\left(\frac{n\pi A}{b}\right)\cos\left(\frac{n\pi z}{b}\right) +$$
$$\left(\frac{Q}{\pi K_r B}\right)\sum_{n=1}^{\infty}\frac{1}{n}K_0\left(\frac{n\pi r}{ab}\right)\sin\left(\frac{n\pi(A+D)}{b}\right)\cos\left(\frac{n\pi z}{b}\right) \qquad (4.1)$$

This equation was solved for three different packer locations to illustrate the pressure field that would be generated by an asymmetric dipole test (Figure 4.5). This will provide some intuition about how the field should respond in a hydraulic continuum.

Single Hydraulic Connections

If an aquifer consisted of discrete hydraulic connections that had only single links between a well and an observation location, asymmetric dipole testing of the well could demonstrate where the well is connected to observation locations. The simplest way to illustrate how to determine these discrete connections is to use an example. In Figure 4.6 a single open borehole is connected to two observation locations, each with a single connection. Asymmetric dipole-flow testing is performed by conducting 5 individual tests, inflating a packer at 5 different locations in the well (Tests A-E). For asymmetric dipole test A, drawdown will occur above the packer, and buildup will occur below the packer. Since both piezometers (P1 and P2) are connected to the lower

pole, both observation locations will observe buildup. For a second test, B, the observation in piezometer 1 would still indicate buildup during the test. However, piezometer 2 would now indicate drawdown as the piezometer is connected with the upper chamber of the dipole. A third test, C, would give the same qualitative result as test B. A fourth test, D, would again show drawdown piezometer 2, but now the connection with piezometer 1 is no longer available, so no drawdown or buildup would be detected. Finally, test E would generate drawdown at both piezometers.

The observation from this example is that individual discrete connections can be observed by examining for a single test whether an observation point has drawdown, buildup, or no response. By profiling a well with multiple tests, the location of a connection can be determined by evaluating when the observations at a piezometer change sign. Thus in our example (Figure 4.6), piezometer 2 is connected between the tests conducted at location A and B. Piezometer 1 is connected somewhere between test C and E, with a possible connection beneath the packer during test D. However the magnitude of the response at test C and E will dictate whether a null response can be detected in the field. This example also illustrates that to determine n discrete connections, a minimum of $n+1$ tests must be performed.

To evaluate single connections, the connection locations in the wellbore were evaluated through asymmetric dipole testing. The locations of step changes in hydraulic conductivity were used to estimate fracture locations. The location of the fractures can also be done using salinity contrasts (Love et al., 1999),

borehole video, or geophysical surveys (Morton et al., 1998). Once the fracture connection locations were established, the connections to these locations were determined by evaluating the observations made in the 10 piezometers. If a single sign change in the piezometer was available, the location of the connection to the wellbore was determined. If multiple sign changes occurred in the data, no single connection could be evaluated; multiple connections were required to explain the response.

Multiple Hydraulic Connections

In a three-dimensional fracture network, multiple paths may connect discrete locations in wellbores or piezometers. Connections can be established using asymmetric dipole-flow tests using the signal generated between the locations where connections are evaluated. In order to determine multiple connections, the fracture locations in the wellbore being tested must be established the same as in the single connection method. The quantitative response for the asymmetric dipole-flow tests at an individual fracture location is recorded by determining the pressure response in the wellbore generated through the profile at the depth of the fracture. For the example in Figure 4.6, the fracture from P2 intercepting the wellbore would observe buildup for the first test followed by 4 tests with drawdown. These data provide the input signal that can be used to monitor piezometers to observe connections between the individual fracture and piezometers. This quantitative data record is generated for each fracture location.

At an observation location, the response of every asymmetric dipole test is recorded. For multiple connections between the testing wellbore and the observation location, the response at the observation point is a function of the hydraulic conductivity and the length of the connection from the well to the observation location. First, we assume a piezometer only monitors an individual fracture. Second, we assume the response due to an individual connection from a piezometer to the wellbore is a linear function of the response in the wellbore being tested. If these assumptions are valid, the response at a piezometer is a linear sum of all connections that occur between the wellbore being tested and the observation location.

In order to evaluate the multiple connections, the linear connections can be evaluated in matrix form by first writing a matrix, **M** for all the connection locations in the wellbore as:

$$M = \begin{bmatrix} s_{11} & s_{12} & \cdots & s_{1j} \\ s_{21} & s_{22} & \cdots & s_{2j} \\ & \cdots & & \\ s_{i1} & s_{i2} & \cdots & s_{ij} \end{bmatrix} \tag{4.2}$$

where s_{ij} is the drawdown (negative drawdown is buildup) at fracture i during test j. The response at a piezometer can be written as the vector, **A** as:

$$A = \begin{bmatrix} s_1 \\ s_2 \\ \cdots \\ s_j \end{bmatrix} \tag{4.3}$$

where A_j is the drawdown at the piezometer during test j. The connections between the wellbore and the piezometer can then be evaluated using:

$$MU = A \tag{4.4}$$

where **U** is the vector of the connection coefficients with U_i representing the relative connection strength between fracture i and the observation location. To solve for **U**, a matrix inversion is required. Since M is unlikely to be symmetric, the vector **U** is solved for by using transpose matrices and solving:

$$U = \left(M^T M\right)^{-1}\left(M^T A\right). \tag{4.5}$$

The matrix, **M**, was augmented to account for fractures that may have been covered during the testing sequence. The matrix was augmented by adding fracture signals that include a null response where the fracture may have been covered. In the tests conducted at Clare, adding a second signal for fracture 2 and 4 converted the 9x5 matrix to a 9x7 matrix. In solving for the matrix coefficients, only one of the fracture signals can be used in the final connection solution.

In solving the connections, the physical system provides a strong constraint on the inversion. The connection coefficients cannot be negative. A negative connection coefficient would imply that generating a drawdown at a fracture would cause a pressure buildup at some other location in the aquifer. With this constraint, inversions that produced negative coefficients could be discounted as physically unrealizable models. If no models fit the physical system with all of the fracture signals included in **M**, individual signals were removed until the physical model with the smallest mean error was obtained.

For qualitative connections, the strong signal generated by the asymmetric dipole test enables a single connection to be determined by observation of the sign change present in the signals for individual fractures. However, to determine

quantitatively the vector **U** for each piezometer, a separate inverse problem must be solved. For the 10 piezometers monitored, 10 inverse problems must be evaluated.

RESULTS

The results from the Clare Valley indicate that insights available from porous media approaches are not useful in this aquifer. The asymmetric dipole tests conducted indicate that continuum assumptions are not appropriate for this aquifer at the well scale. Discrete hydraulic connections can be established between many locations in the aquifer, with fracture connections occurring in three dimensions. These connections are analyzed based on examining the simplest connections first.

Homogeneous, Isotropic Aquifer

Symmetric dipole testing (Kabala, 1993) in a continuum generates a symmetric field with the location of the central packer providing a plane of symmetry between drawdown and buildup. Asymmetric dipole-flow testing causes the plane of symmetry to be displaced in the direction of the larger testing pole (Figure 4.5). Evaluating the results of testing in the Clare Valley in a nearly symmetric test (Figures 4.3 and 4.7), the dipole field generated in the testing well is inverted in the 15 meter radial distance to the observation piezometers. Drawdown is observed approximately 15 meters below the packer midpoint in well 36385 – piezometer B. Buildup is observed 45 meters above the packer in well 41497 – piezometer 1. This inversion of the dipole field is not unusual

considering the orientation of the fracture planes, but cannot be explained using continuum models of the aquifer.

Fracture Connection Locations in Well Clare 105

Evaluating the response of the lower pole of the asymmetric profile, 4 discrete jumps in bulk hydraulic conductivity occur (Figure 4.8). These indicate that discrete conductive features have been removed from the lower chamber instead of a gradual decrease in average hydraulic conductivity (Halihan and Zlotnik, in preparation). With the available data, five permeable locations are available for connections, the four features that were eliminated during the profile, and the conductive zone above test 1. Double packer testing in the well indicates the same five zones can be interpreted except fracture 2 which is likely two or more different fractures that the dipole testing did not resolve (Figure 4.8). The signal for each fracture intercepting well Clare 105 is the response of the testing chamber that the fracture was located in during each test (Figure 4.9). The results of the testing and the interpreted response of each fracture at the well are compiled in Table 4.1.

The matrix approached yielded models for every piezometer. The signal for fracture 2 assuming that the packer covered the fracture during test 2 yielded stronger connection coefficients than the signal assuming the fracture was always open. The signal from fracture 4 was stronger without being altered. In both cases, the results would not be changed for which fractures were connected, only the magnitude of the connection coefficients.

Piezometers 5, 6, C and D

Piezometers 5 and 6 (well 41497) and piezometers C and D (well 36385) have a similar response during the test series (Figures 4.10 and 4.11). All of the tests in the piezometers do not have a significant drawdown signal observed (> 5 mm) during any of the tests except for test 9 at piezometer C which has only 1 centimeter of drawdon (Figure 4.11; Table 4.1). This indicates that either the connection between Clare 105 and the piezometers is very weak or can be considered unconnected. This may be expected at the depth that these piezometers are placed (Figure 4.3). The signals observed in all four piezometers do have a single sign change. So if a connection was interpreted, piezometers 5, C, and D would be connected to fracture 1, and piezometer 6 would be connected to fracture 2.

The matrix solution for these piezometers indicates roughly the same response as interpreted from examining the sign change (Figures 4.10 and 4.11; Table 4.2). The connection coefficients are generally small. The interpretation would be that these locations are poorly connected if at all.

Piezometers A and B

Piezometers A and B (well 36385) have a quantitatively similar response during the test series (Figure 4.12; Table 4.1). Both piezometers have results that look similar to the signal from fracture 5, however almost all of the tests observe drawdown during the testing instead of buildup as would be expected from fracture 4 or 5. Fracture 2 is a likely connection to provide drawdown during the majority of tests, except test 1. Fracture 1 does not make a good candidate for a

strong connection because it would cause test 1 to have more drawdown than is observed. The matrix inversion suggests that the piezometers are strongly connected to fractures 2 and 4 with a weaker connection to fracture 1 (Table 4.2).

Piezometers 1 and 2

Piezometers 1 and 2 (well 41497) have nearly identical signals (Figure 4.13; Table 4.1). Both signals look very similar to the response from fracture 2 and indicate a strong connection with that fracture. However, test 1 requires positive drawdown to be generated at the both piezometers, which cannot occur with fracture 2. This indicates that fracture 1 must also be connected. The increase observed at both piezometers between test 1 and 2 and the positive drawdown observed for both tests indicate that it must be connected to both fractures 1 and 2. The piezometers must also have a weak connection to fracture 5. This is indicated by buildup occurring during test 7 for both piezometers. Additionally, the trend in both piezometers is steeper than expected for a connection with only fracture 1 and 2. So using both the magnitude and sign of the signal at the piezometers, 3 connections can be interpreted for these piezometers.

The matrix inversion results in the same conclusion for the piezometers (Table 4.2). The weak connection with fracture 5 can be detected because of the strong signal generated at that location. To improve the quantitative values of the connection coefficients from fractures 1 and 2, a higher pumping rate for tests higher in the well would need to be imposed to generate a stronger signal for the upper fractures.

Piezometer 3

The signal observed at piezometer 3 is relatively complicated (Figure 4.14a; Table 4.1). A simple connection to fracture 4 or 5 can be observed due to the persistent buildup observed during most of the tests. However the connections that generate the large positive drawdown on test 3, and the null response on test 5 are difficult to interpret. It is unlikely that fracture 1 would generate the observed signal with the response observed on test 1. The nearest piezometers 2 and 4 have connections to fractures 2 and 3. These seem like the most likely candidates to explain the response observed. The response at this piezometer illustrates that a signal can get complex enough that matrix inversion would be required for analysis. The matrix inversion for piezometer 3 indicates a complex connection pattern with relatively strong connections to four fractures (Table 4.2).

Piezometer 4

The observations in piezometer 4 (well 41497) indicate a sign change between tests 8 and 9 (Figure 4.14b; Table 4.1). This indicates a connection to fracture 5. However, the signal from fracture 5 does not explain why the magnitude of the signal in the piezometer is greater higher in the well. If only fracture 5 was connected, the magnitude of the signal should increase with depth in parallel with fracture 5. If fracture 3 is included as a second connection, the tests from the upper portion of the well would have fracture 3 and 5 acting together to generate drawdown at piezometer 4, while after test 3, the two

fractures would have signals with opposite signs. The matrix inversion indicates three connections with the strongest connection at fracture 3 (Table 4.2).

DISCUSSION

The results of the asymmetric dipole-flow testing of well Clare 105 illustrate the connections present between the well and the piezometers (Figure 4.15). The results indicate that a continuum approach to understanding flow at this scale at this site is not appropriate. The connection structure demonstrated by testing is not unusual for a fractured aquifer with high angle fracture sets.

The difficulty in interpreting geophysical logs or correlating double packer data between wells in this aquifer is easily demonstrated with this technique. While double packer testing can demonstrate the conductive intervals in Clare 105, these conductive intervals do not horizontally correlate with the observation network. Fracture 5 provides a high conductivity pathway between the upper conductive portion of the aquifer and deepest portions of the well. Fracture 3 provides a conductive pathway for fluids and contaminants, but the majority of the available monitoring network is not useful for monitoring this location. These difficulties in monitoring a discrete fracture network are not new, but asymmetric dipole-flow tests can improve the characterization of the connections and the permeability structure of an aquifer at the site scale.

The primary weakness of asymmetric dipole-flow tests is the area of influence of the test. Standard hydraulic testing, extraction or injection, results in a radial inverse dependence (R^{-1}) on the testing signal generated at the wellbore. This allows for observations to be made some distance from the wellbore. Dipole

testing instead has an R^{-2} dependence. This rapid loss of signal with radial distances limits the ability of the test to examine large areas of an aquifer from a single well. The loss of signal at the piezometers makes some of the connection interpretation ambiguous. Increasing the drawdown or buildup signal is only useful for a small range in the profile as either the upper pole will drain completely, or the lower pole will buildup too much hydraulic head. The corollary to this signal strength problem is that this method will preferentially evaluate the strongest connections at a site with locations of decreasing hydraulic connection strength preferentially excluded from analysis.

Another difficulty with fracture connection analysis at the site-scale that affects this and any other testing method is the location of the monitoring network. Piezometers 5, 6, C and D may not respond to any hydraulic testing since they may be located within unfractured matrix and only respond to long term changes in hydraulic head at the site. While asymmetric dipole tests can evaluate the locations of connections, if no connections are available, the analysis may be ambiguous for distinguishing between a poor connection and no connection.

CONCLUSIONS

Asymmetric dipole-flow testing is useful for determining hydraulic connections between locations closer than 20 meters apart in a fractured aquifer. By utilizing the contrast in signal between drawdown generated in the upper pole of a test with the buildup generated in the lower portion of a test, the response at piezometers can be interpreted to determine the location of discrete connections in

a fractured aquifer. The hydraulic response of these sites can not be interpreted using continuum hydrology at this scale. The technique is limited by the R^2 influence of the technique, but allows for testing connections without *a priori* horizontal assumptions.

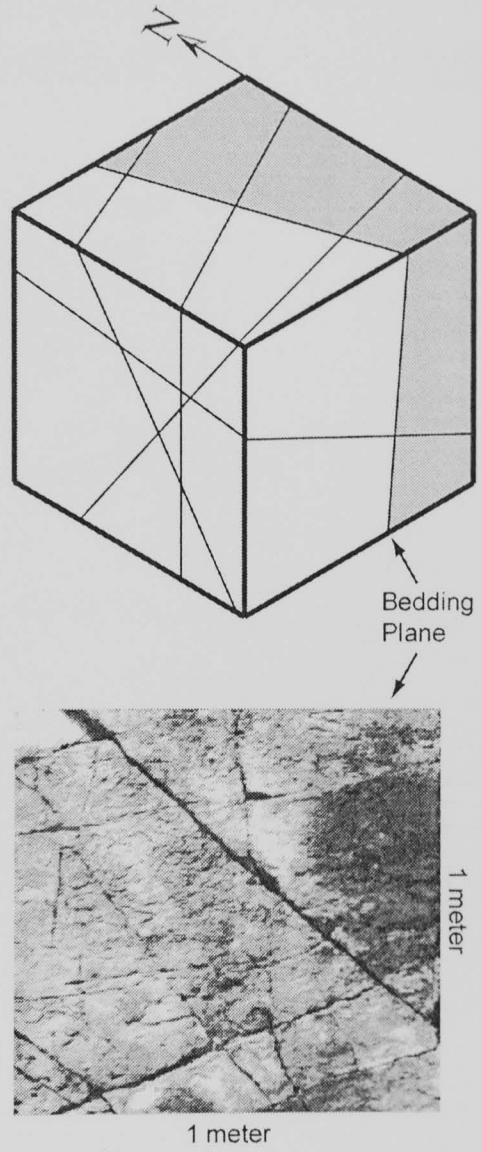

Figure 4.1: Block diagram and outcrop picture of the lithology of the Wendouree Vineyard field site.

The block diagram illustrates major fracture sets present at the Wendouree vineyard. Photograph illustrates a view of the bottom of vertical bedding at a location in the town of Clare, South Australia.

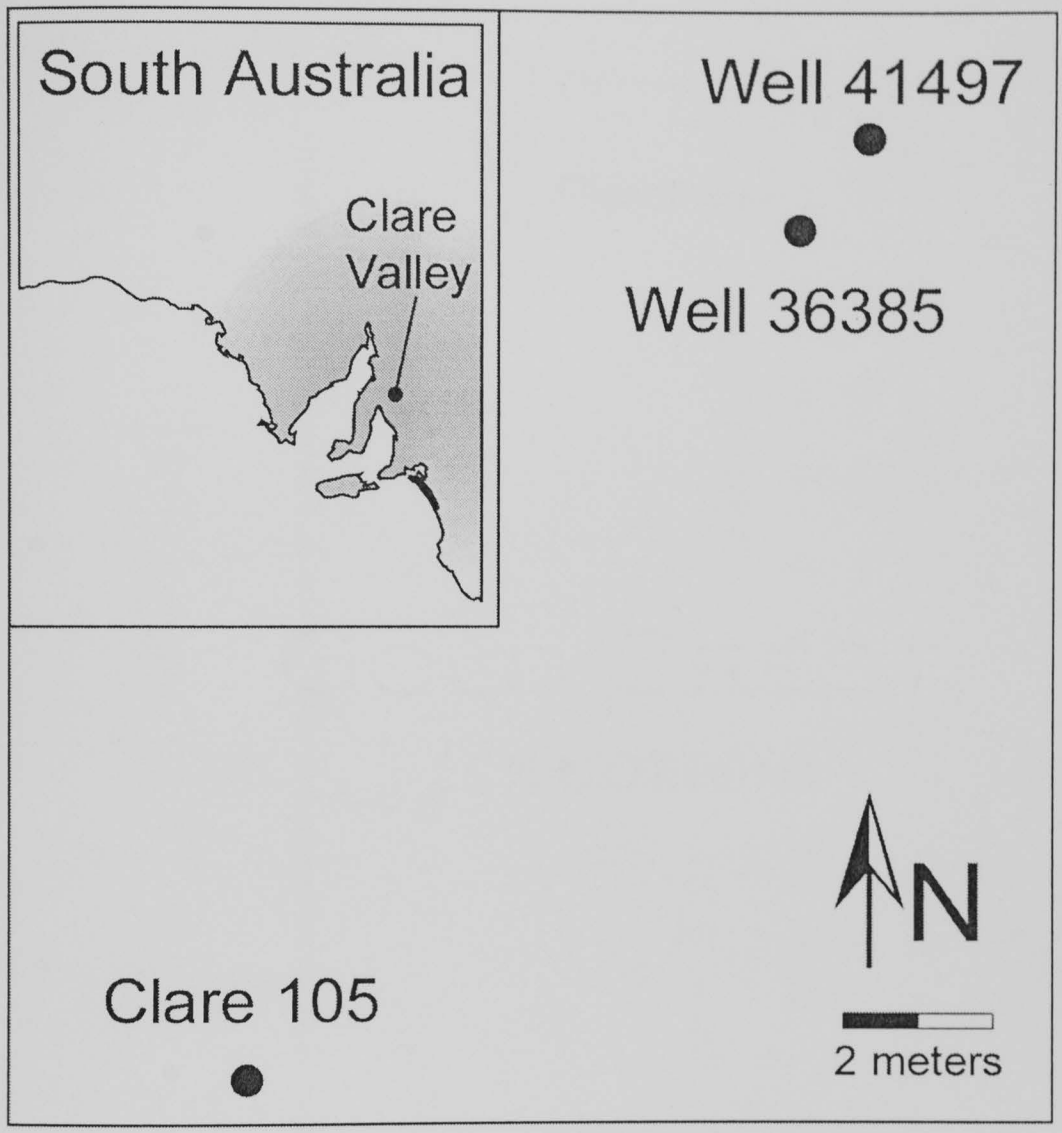

Figure 4.2: Well locations for the Wendouree vineyard.

The location of the three wells used in this study. Inset illustrates the location of the Clare Valley, South Australia.

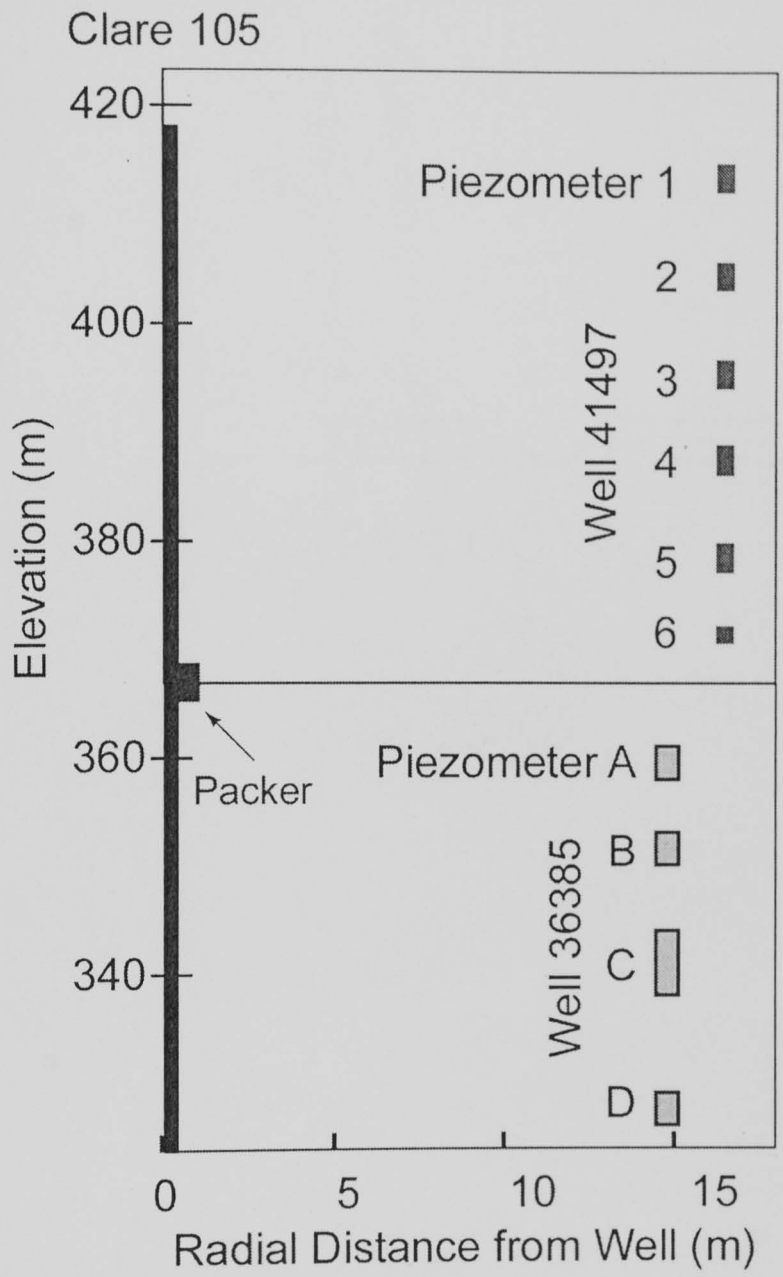

Figure 4.3: Cross-sectional view of Wendouree field site.

Dipole-flow testing was performed in well Clare 105, six observation locations were available in well 41497, with 4 additional observation locations available in well 36385. Packer illustrates location for results given in Figure 4.7.

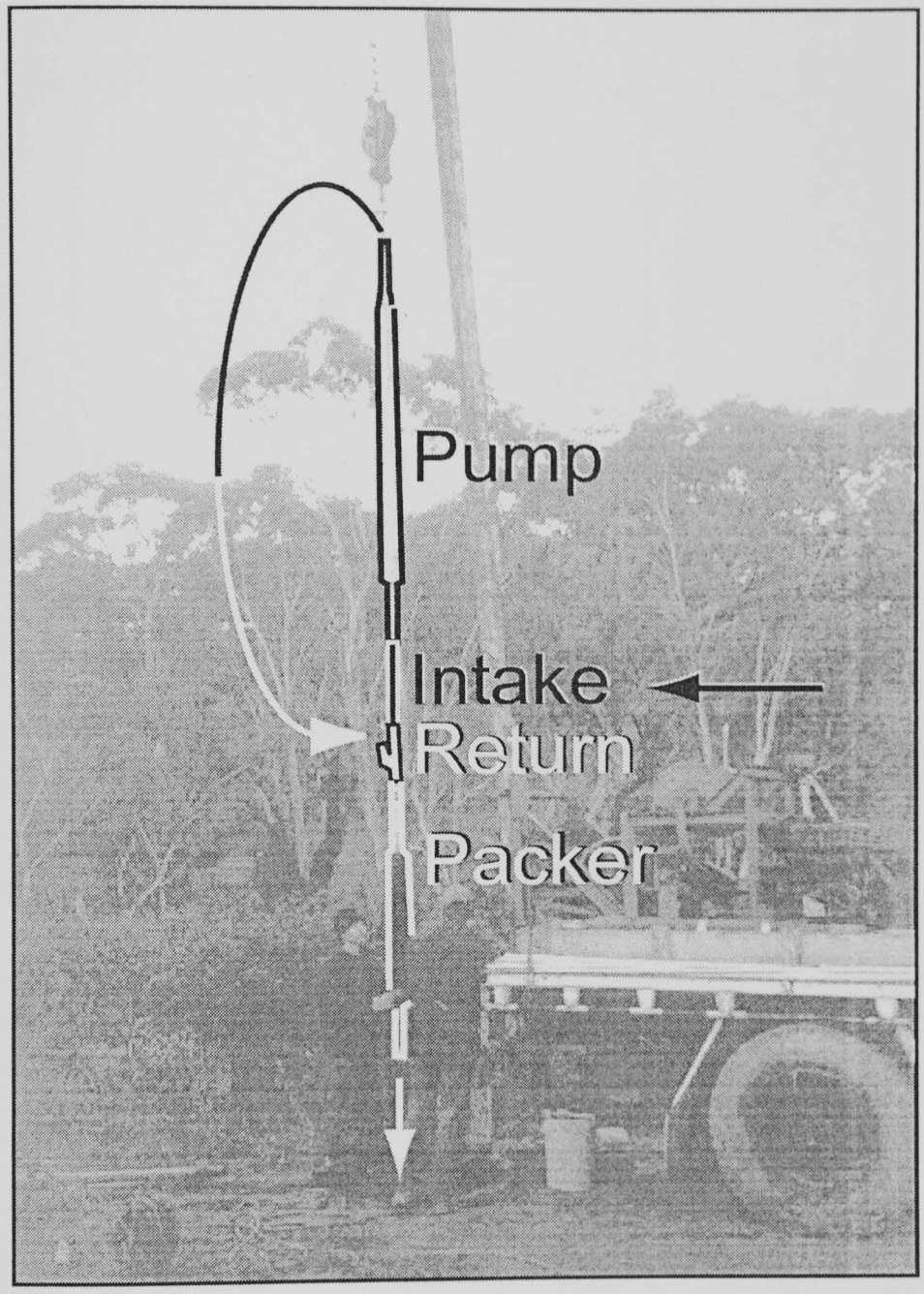

Figure 4.4: Asymmetric dipole-flow tool used to test well Clare 105.

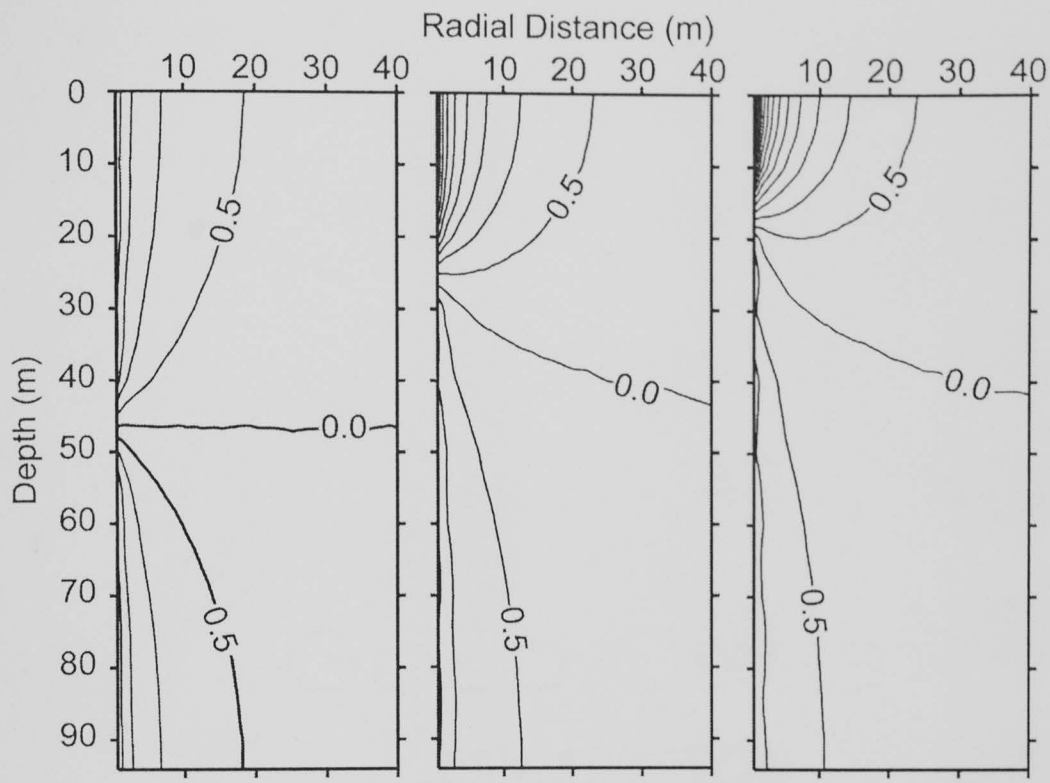

Figure 4.5: Theoretical asymmetric dipole-flow field generated for packers in three different locations.

Packer midpoint is located at the interception of the 0.0 contour with the y-axis.

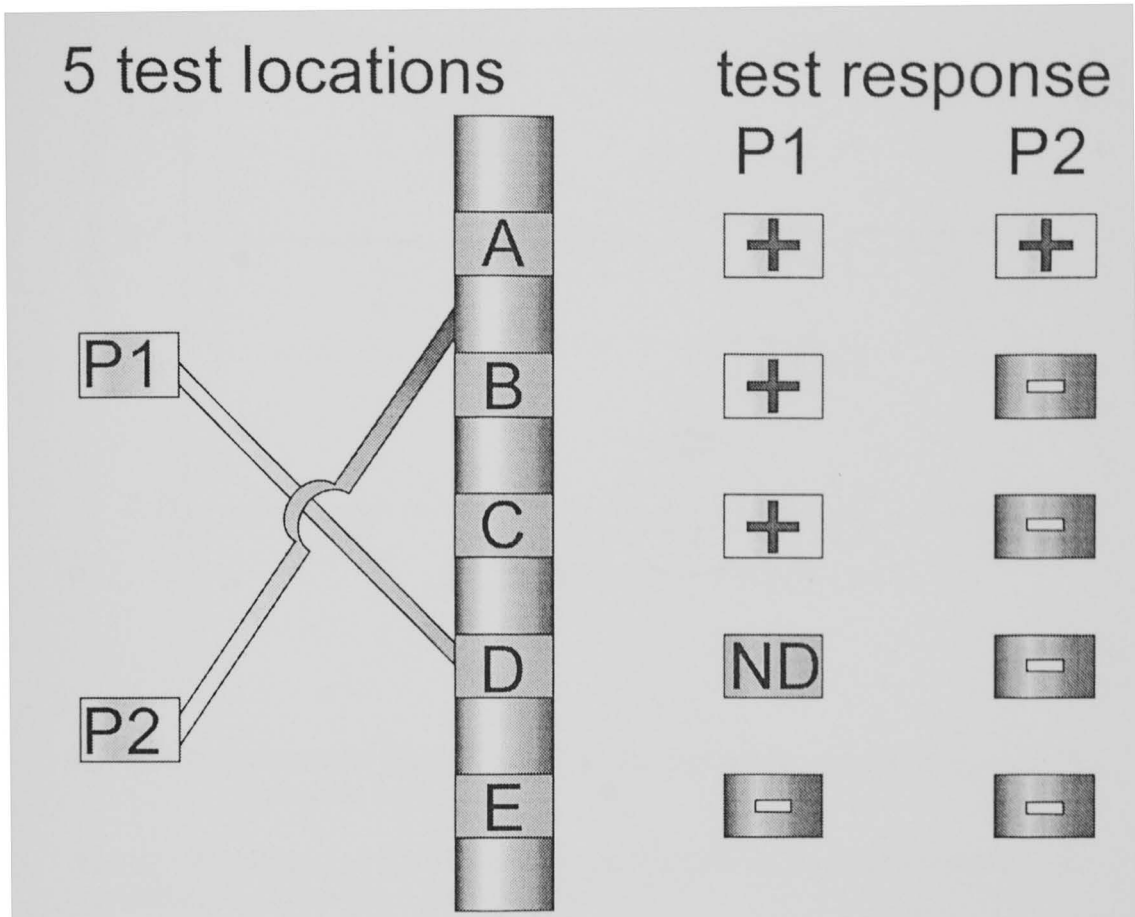

Figure 4.6: Conceptual model for single connection analysis.

2 single fractures connect piezometers P1 and P2 to the wellbore. 5 asymmetric dipole tests (A-E) generate the given test responses.

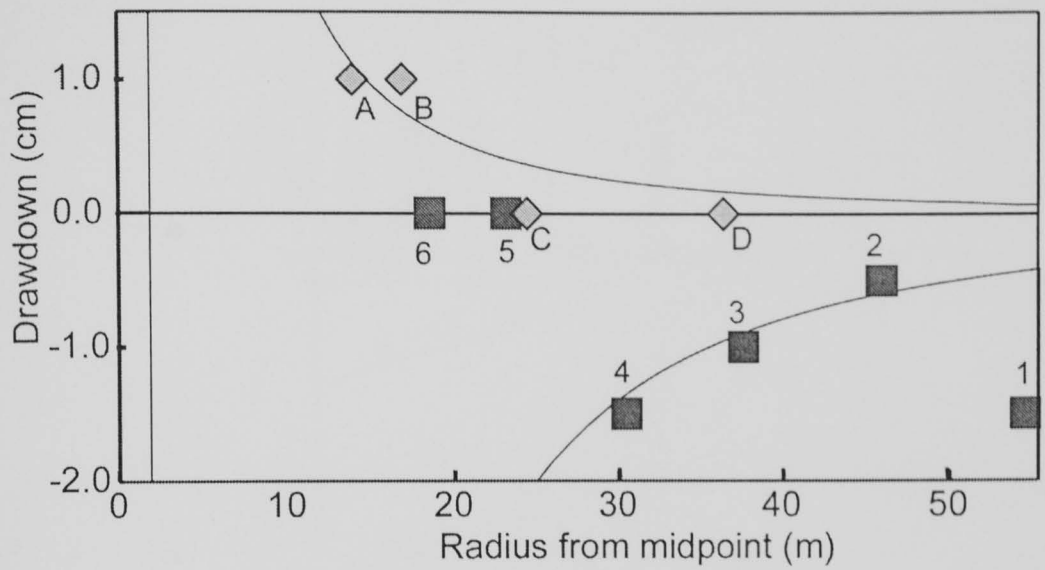

Figure 4.7: Asymmetric dipole field generated with packer located at position illustrated in Figure 4.3.

Note R^{-2} dependence of the dipole field even though the piezometers aren't along continuous rays from the dipole midpoint.

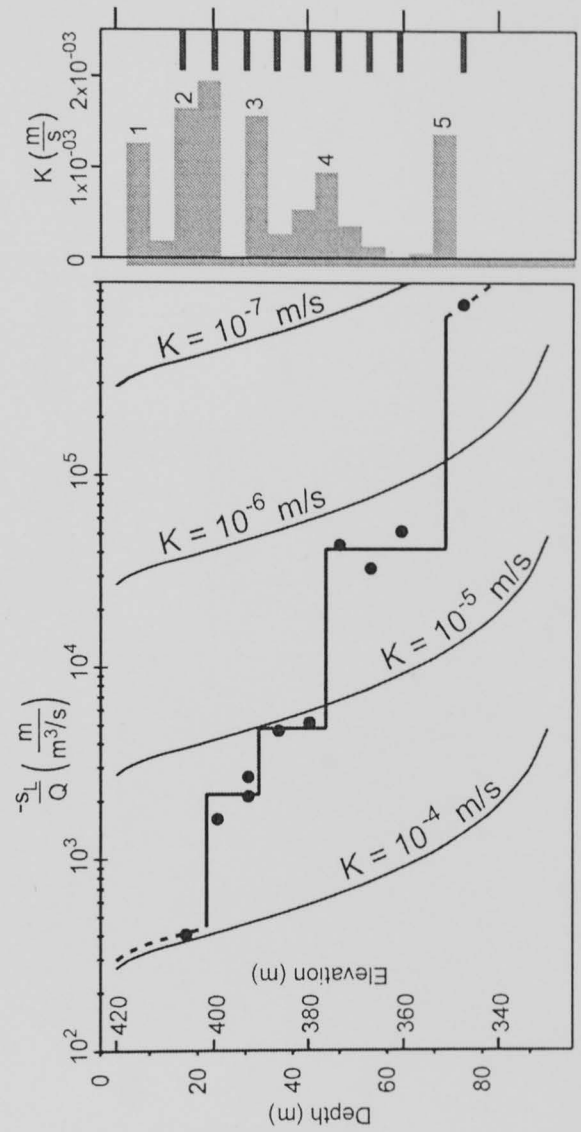

Figure 4.8: Response of hydraulic testing of Clare 105.

Graph on left illustrates 4 discrete jumps in hydraulic conductivity that are observed during a series of asymmetric dipole-flow tests. These jumps are interpreted as fracture locations. The graph on the right illustrates conductivities obtained from double packer testing conducted over 5-meter intervals and the fracture number assigned to each high conductivity interval. The bars on the far right indicate packer locations for the asymmetric dipole-flow tests.

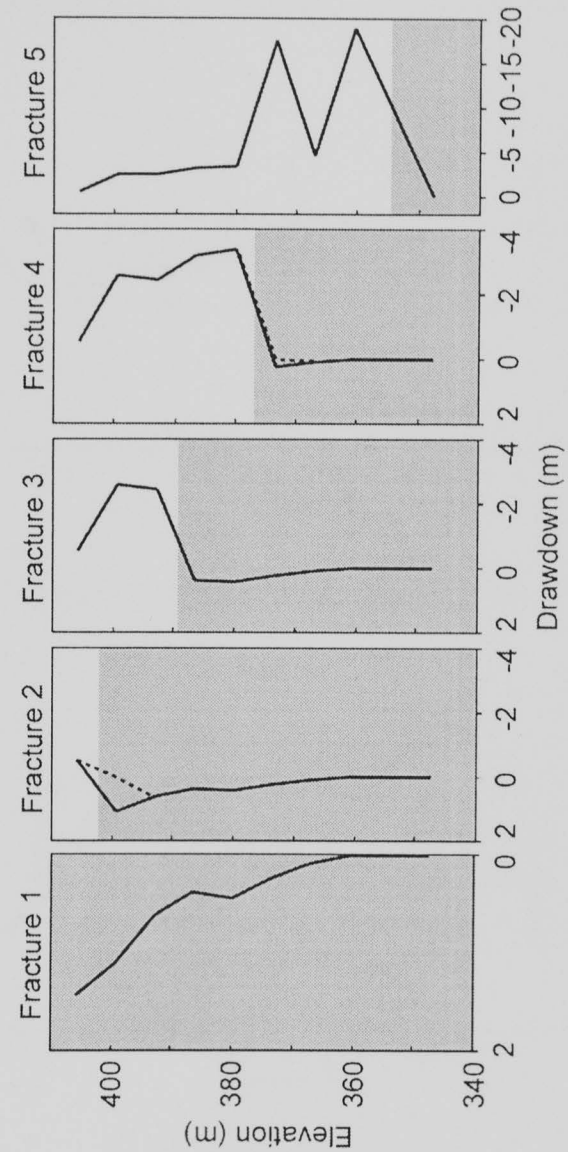

Figure 4.9: Hydraulic signals generated at fractures 1 to 5 in well Clare 105.

The shaded portions of the graphs indicate the portion of the signal where drawdown occurs. The unshaded areas indicate a buildup signal. The dashed lines in fractures 2 and 4 indicate the alternative signal generated if the packer covered the fracture during testing.

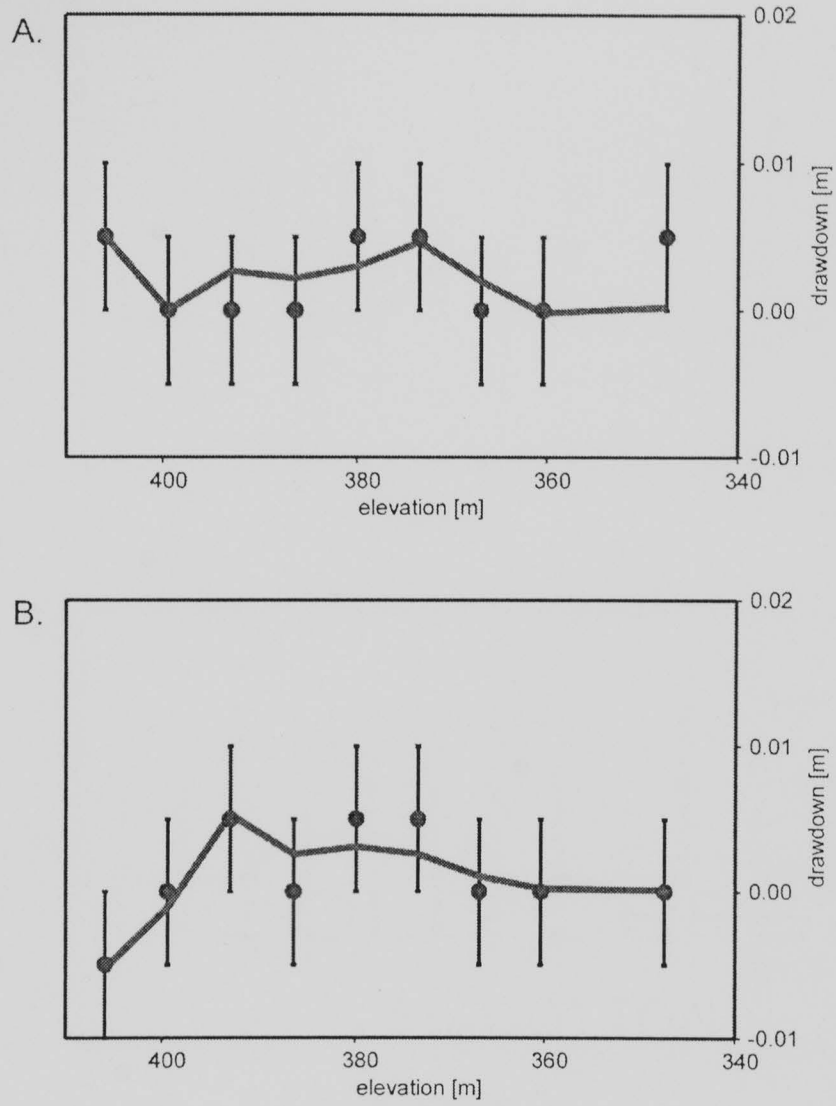

Figure 4.10: Observations and model drawdown for piezometers 5 and 6.

A) Asymmetric dipole-flow test elevations versus drawdown data observed at piezometer 5 (Well 41497) with 5 mm error bars. Continuous lines indicate matrix inversion model results for connections to Clare 105. B) Field data and model results for piezometer 6 (Well 41497)

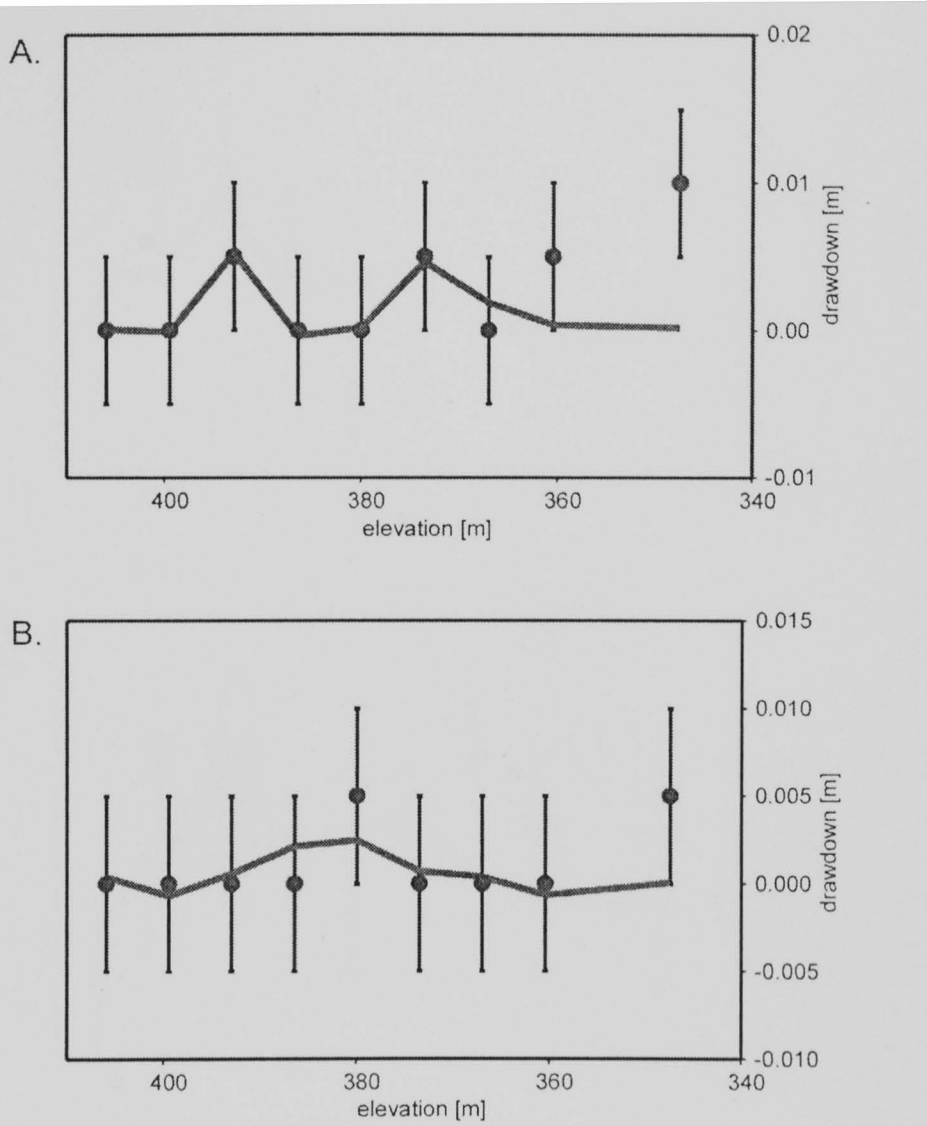

Figure 4.11: Observations and model drawdown for piezometers C and D.

A) Asymmetric dipole-flow test elevations versus drawdown data observed at piezometer C (Well 36385) with 5 mm error bars. Continuous lines indicate matrix inversion model results for connections to Clare 105. B) Field data and model results for piezometer D (Well 36385)

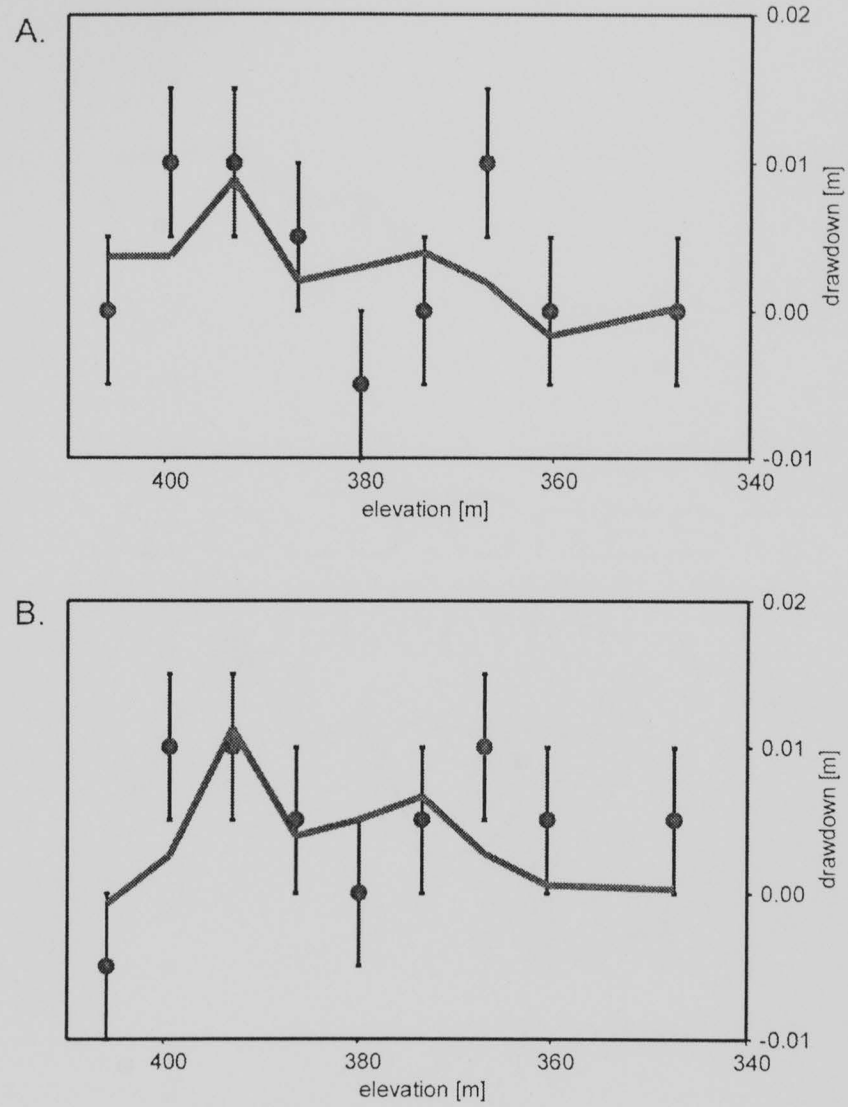

Figure 4.12: Observations and model drawdown for piezometers A and B.

A) Asymmetric dipole-flow test elevations versus drawdown data observed at piezometer A (Well 36385) with 5 mm error bars. Continuous lines indicate matrix inversion model results for connections to Clare 105. B) Field data and model results for piezometer B (Well 36385)

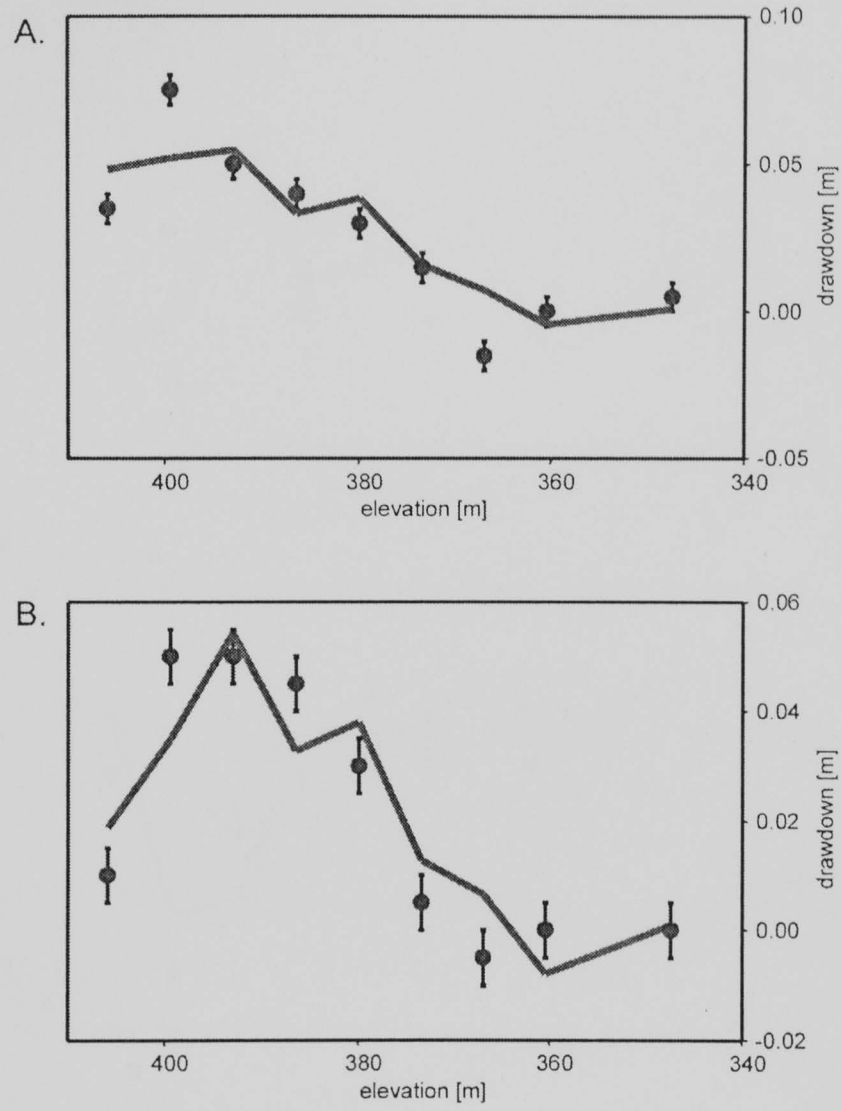

Figure 4.13: Observations and model drawdown for piezometers 1 and 2.

A) Asymmetric dipole-flow test elevations versus drawdown data observed at piezometer 1 (Well 41497) with 5 mm error bars. Continuous lines indicate matrix inversion model results for connections to Clare 105. B) Field data and model results for piezometer 2 (Well 41497)

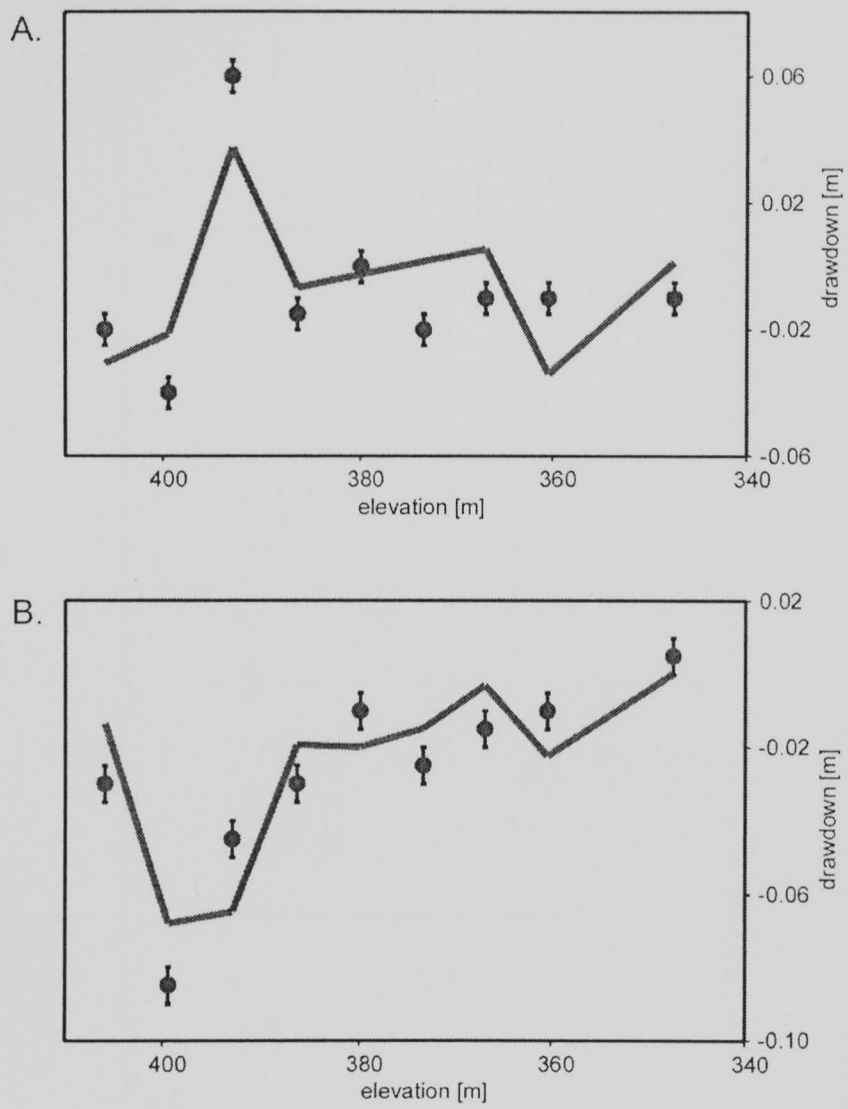

Figure 4.14: Observations and model drawdown for piezometers 3 and 4.

A) Asymmetric dipole-flow test elevations versus drawdown data observed at piezometer 3 (Well 41497) with 5 mm error bars. Continuous lines indicate matrix inversion model results for connections to Clare 105. B) Field data and model results for piezometer 4 (Well 41497)

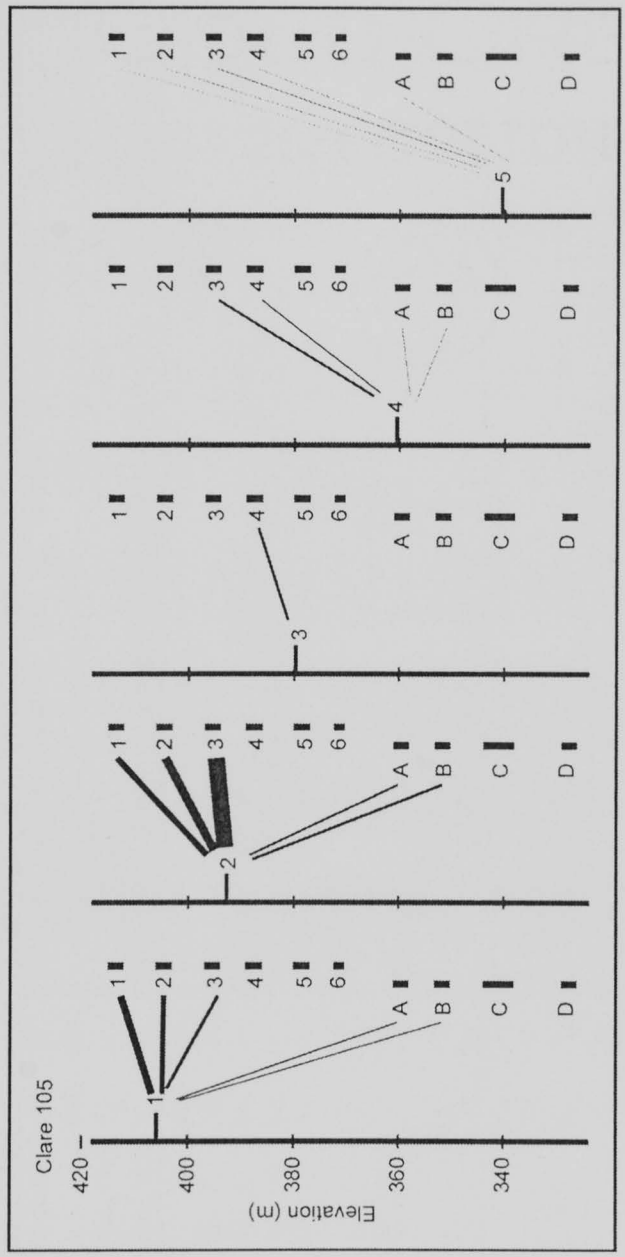

Figure 4.15: Fracture connections interpreted for well Clare 105.

Line weights indicate connection strength. Piezometers 5, 6, C, and D are interpreted as unconnected to Clare 105.

Table 4.1: Testing results of 9 asymmetric dipole-flow tests conducted in well Clare 105.

Test				1	2	3	4	5	6	7	8	9
Midpoint Elevation			m	405.92	399.42	392.92	386.42	379.92	373.42	366.92	360.42	347.42
		Q	l/s	1.23	1.2	0.91	0.68	0.66	0.4	0.11	0.37	0.03
Clare 105		s_U	m	1.44	1.11	0.42	0.39	0.27	0.07	0.07	0.02	0.01
Clare 105		s_L	m	-0.50	-2.55	-2.43	-3.17	-3.37	-17.43	-4.57	-18.95	-22.71
Well 41497	1	Δs	m	0.035	0.075	0.050	0.040	0.030	0.015	-0.015	0.000	0.005
	2	Δs	m	0.010	0.050	0.050	0.045	0.030	0.005	-0.005	0.000	0.000
	3	Δs	m	-0.020	-0.040	0.060	-0.015	0.000	-0.020	-0.010	-0.010	-0.010
	4	Δs	m	-0.030	-0.085	-0.045	-0.030	-0.010	-0.025	-0.015	-0.010	0.005
	5	Δs	m	0.005	0.000	-	0.000	0.005	0.005	0.000	0.000	0.005
Well 36385	6	Δs	m	-0.005	0.000	0.005	0.000	0.005	0.005	0.000	0.000	0.000
	A	Δs	m	0.000	0.010	0.010	0.005	-0.005	0.000	0.010	0.000	0.000
	B	Δs	m	-0.005	0.010	0.010	0.005	0.000	0.005	0.010	0.005	0.005
	C	Δs	m	0.000	0.000	0.005	0.000	0.000	0.005	0.000	0.005	0.010
	D	Δs	m	0.000	0.000	0.000	0.000	0.005	0.000	0.000	0.000	0.005
Fracture Signal	1	Δs	m	1.440	1.110	0.630	0.390	0.450	0.245	0.100	0.020	0.010
	2	Δs	m	-0.500	1.11 / 0.0	0.630	0.390	0.450	0.245	0.100	0.020	0.010
	3	Δs	m	-0.500	-2.550	-2.430	0.390	0.450	0.245	0.100	0.020	0.010
	4	Δs	m	-0.500	-2.550	-2.430	-3.170	-3.370	0.245 / 0.0	0.100	0.020	0.010
	5	Δs	m	-0.500	-2.550	-2.430	-3.170	-3.370	-17.430	-4.570	-18.950	0.010

	Well 41497*						Well 36385*			
	1	2	3	4	5	6	A	B	C	D
1	48	32	22	0	8.1	0	8.1	6.6	4.9	1.7
2a	41	56	107	0	9.7	10	14	18	12	3.1
3	0	0	0	18	1.8	0	0	0	0	1.0
4	0	0	16	7.2	1.7	0.4	2.0	1.9	2.2	0
5	0.3	0.5	1.9	1.2	0.03	0	0.11	0	0	0.04

* all values multiplied by 1000

Table 4.2: Connection coefficients between fractures in Clare 105 and piezometers. Each column represents values for the vector, **U**.

Chapter 5: Conclusions

Continuum approximations of aquifer permeability have provided many useful techniques to examine groundwater. However, in heterogeneous fractured and karstic aquifers, the assumption of a hydrologic continuum may not hold. In these settings, the permeability of the aquifer may depend on the scale of measurement. The value of permeability obtained by a given technique may yield a value which is useful for determining the quantity of flow, but in these aquifers, the value may only be appropriate at a given scale and location. Additionally, if the direction and rate of flow is required, heterogeneities may dominate the aquifer causing poor or incorrect estimates when using continuum techniques.

A quantitative analysis of outcrop data in the Edwards aquifer of central Texas illustrates that the permeability scale effect first described by Kiraly (1975) can be explain as a change in sampling volume between tests. The analysis indicates that outcrop-scale data can be useful for prediction on larger-scale. The analysis illustrates the fundamental importance of the distribution of fracture apertures in predicting the quantity of flow in fractured aquifers. Based on aperture alone, excluding other fracture properties, a small number of fractures will control a flow system even though thousands of fractures may be present. Additionally, invoking conduit flow though an aquifer as a mechanism to explain large spring flows or small drawdowns during well testing is difficult to do on a quantitative basis. The probability of intercepting a continuous conduit with a

well is very small, and fractures can provide sufficient flow to reproduce the observed effects in high permeability aquifers.

Asymmetric dipole-flow tests provide a technique that is particularly suited to investigating fractured aquifers at the site scale. This new technique is sensitive to heterogeneities, allowing aquifer investigations to examine high conductivity features that control flow. This testing prevents focusing on small open fractures or kinematic fractures that don't provide a significant amount of fluid to a well, but may appear important when using other geophysical techniques. Asymmetric dipole-flow tests evaluate changes in average conductivity and provide the ability to determine how the bulk properties of a set of fractures respond. Additionally, this technique allows fracture networks to be evaluated to determine the three-dimensional response of a fractured aquifer instead of being restricted to a one- or two-dimensional analysis.

Future work in outcrop analysis needs to test outcrop data in a purely fractured aquifer where no karst conduits are present. This will allow further testing of how accurately outcrop aperture distributions can reproduce conductivity values from hydraulic tests in wells. Additional work is needed to determine if the fracture density of conductive fractures can be determined *a priori*. Finally, better steady state permeability combination models are needed to increase or decrease estimated well- and regional-scale conductivities based on the distribution of not only fracture aperture, but fracture spacing, length, and roughness.

Future work in dipole-flow testing in fractured aquifers needs to critically examine the data generated by the technique in these aquifers. How do the values of dipole-flow tests compare with other forms of testing in these settings? Can connections between fractures in three-dimensions be determined with dipole testing, or does the ill-posedness of the inverse problem combined with the lack of dipole resolution limit the usefulness of this technique? To answer these questions, additional modeling work will be required to test the dipole technique under well constrained model conditions comparing the results of dipole tests with other hydraulic techniques. Additionally, a well-characterized field site with the potential for conducting a three-dimensional series of tests over a block approximately 10 meters on a side would provide better insight into these questions.

Appendix A: Analytical Model of Asymmetric Dipole-Flow Test

For the equations presented in Chapter 3 for the asymmetric dipole-flow test, the response of the dimensionless quantities to variations needs to be understood to properly utilize the analytical models. The analytical model also needs to be tested to determine the field testing limits (Equations are in Chapter 3 and variable definitions are in Table 3.1). Variations in the analytical model are tested for a 0.1-meter radius well located in a 100-meter thick aquifer with a horizontal hydraulic conductivity of 10^{-5} m s^{-1}. For the majority of simulation, a 1.0-meter packer, a 1.0-l s^{-1} pumping rate, and isotropic conditions are utilized for parameter values.

The variations of $\overline{A}$ and $\overline{B}$ in equations 3.5 and 3.6 are illustrated in Figure A.1. As the chambers reach zero length, the absolute value of the chamber drawdown approaches infinity. As the chambers increase in length, the drawdown approaches zero as the pumping rate becomes too little to generate measurable drawdown.

$\overline{D}$ in many case would have very little effect on asymmetric dipole-flow test equations 3.5 and 3.6 (Figure A.2). For typical values of $\overline{D}$ in the range of 0.01-0.1 (1% to 10% of aquifer thickness), very little variability is observed in the response of the test. Only when $\overline{D}$ reaches values of 30% of aquifer thickness or greater is a noticeable effect observed. This indicates that substituting packers of different lengths will not provide much variability in test results.

The dimensionless well radius, $\overline{r_w}$, combines the well radius and the anisotropy (Figure A.3; Equation 3.7). For large values of $\overline{r_w}$, the model predicts no drawdown will occur in a chamber (Equations 3.5 and 3.6). This large value case would likely be due to strong vertical conductivity as opposed to large diameter boreholes. Diameters large enough to demonstrate this effect cannot have a packer placed to conduct a test.

The case of small values of $\overline{r_w}$ will be the normal case for the majority of field conditions. For infinitely small values of $\overline{r_w}$ the analytical solution is not valid. The solution has a singularity at $\overline{r_w} = 0$ which would coincide with an well of infinitesimally small diameter, or an infinitely low vertical conductivity. In a fractured rock aquifer, the case of infinitely low vertical conductivity may be encountered when fracture networks are unconnected except by a borehole. In this case, it is expected that each testing chamber should respond as individual pumping and injection chambers whose response would be governed by the equations for partially penetrating wells (Hantush, 1961).

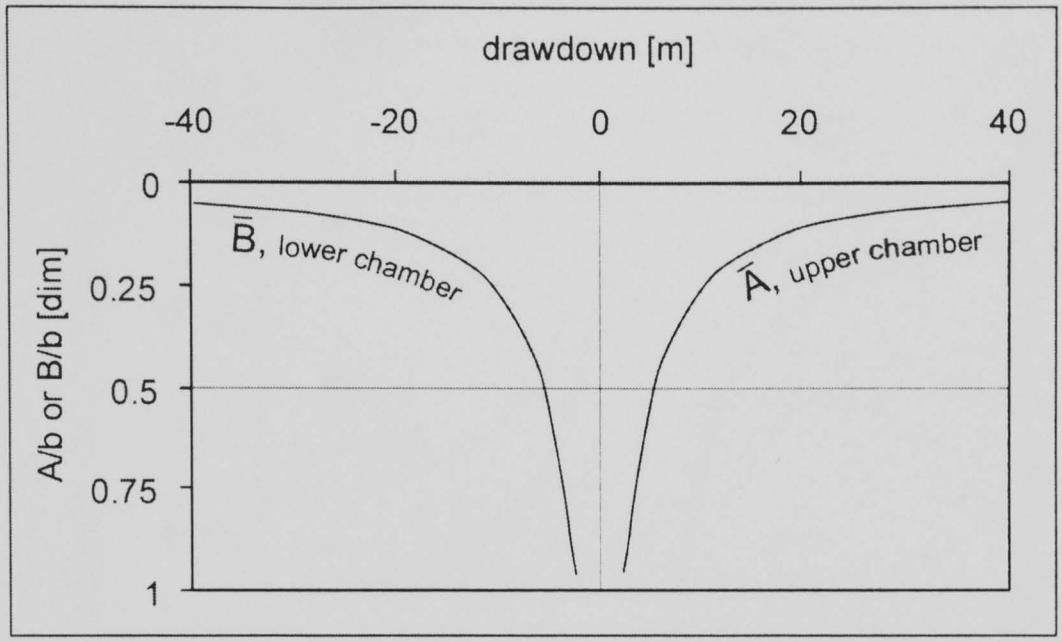

Figure A.1: Drawdown variation in response to variations in $\overline{A}$ and $\overline{B}$.

As the chamber size approaches zero the absolute value of chamber drawdown approaches infinity, and as the chamber size approaches infinity, the chamber drawdown approaches zero.

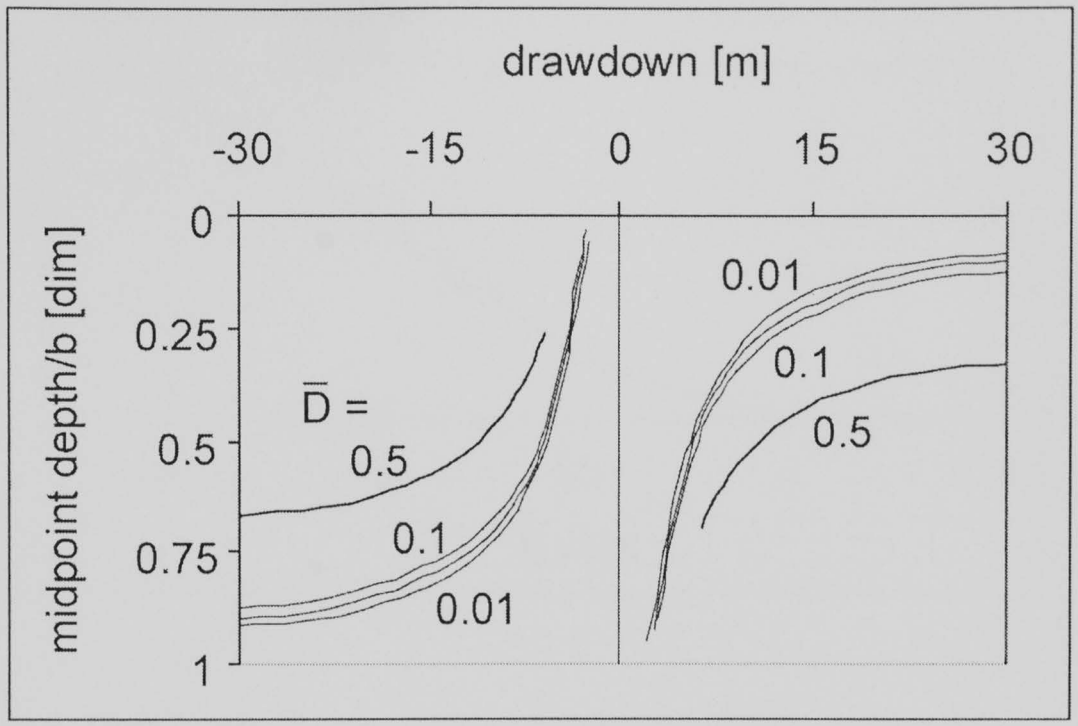

Figure A.2: Drawdown variations in response to variation of $\bar{D}$.

Values of $\bar{D}$ are presented for all lines except where $\bar{D} = 0.05$. For realistic values of $\bar{D}$, the variation in packer size will not strongly affect the test.

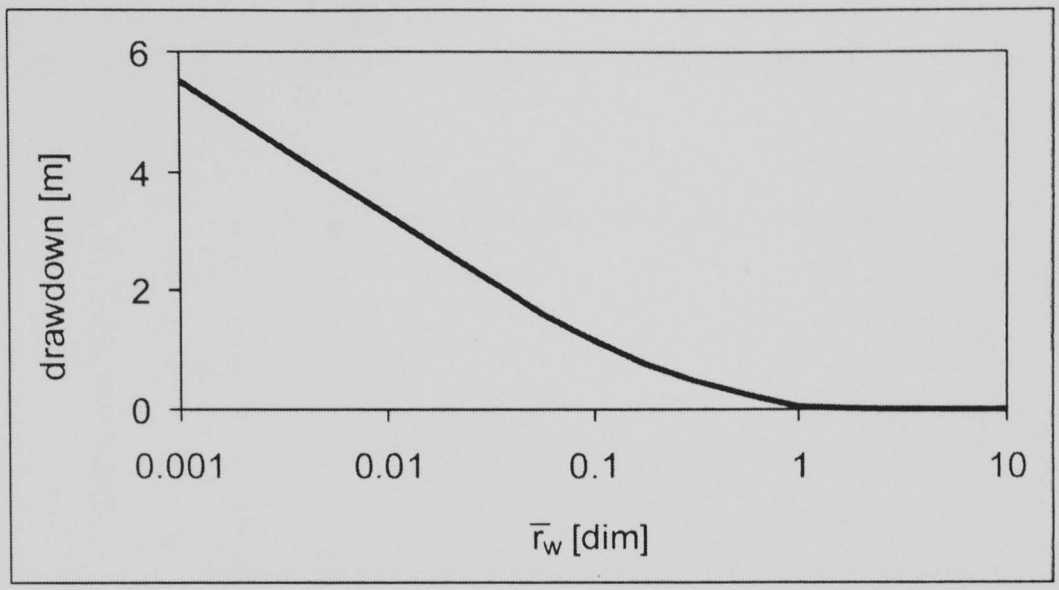

Figure A.3: Variation in drawdown with changes in $\overline{r_w}$.

As r_w or $\overline{r_w}$ gets large (or anisotropy, a, gets small), the chamber drawdown approaches zero. As r_w or $\overline{r_w}$ gets small (or anisotropy, a, gets large), the chamber drawdown continually increases.

Appendix B: Asymmetric Dipole-flow Test Results from Bissen Well 13

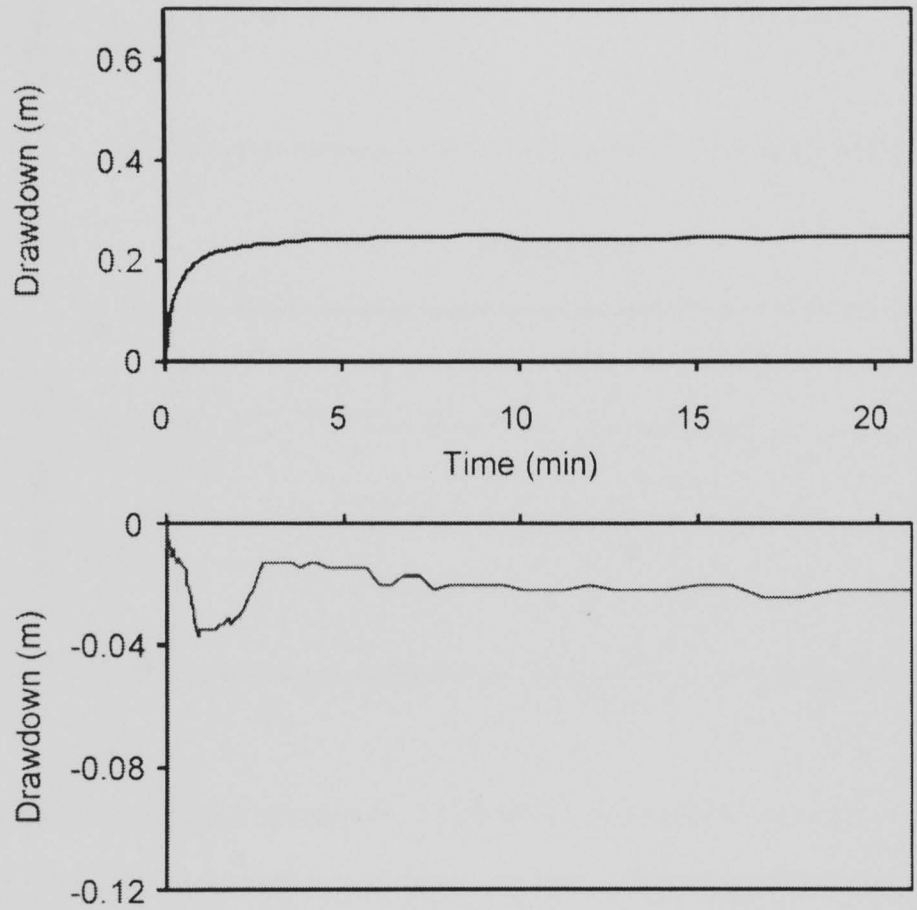

Figure B.1: Transducer response for upper and lower chambers for test 1.

Upper graph illustrates response of upper chamber with positive drawdown. Lower graph illustrates response of lower chamber with negative drawdown (buildup). Note the scale for drawdown in the chambers is different for the upper and lower chamber, but the scales are the same for tests 1-5. Numerical data can be obtained from the author for all tests.

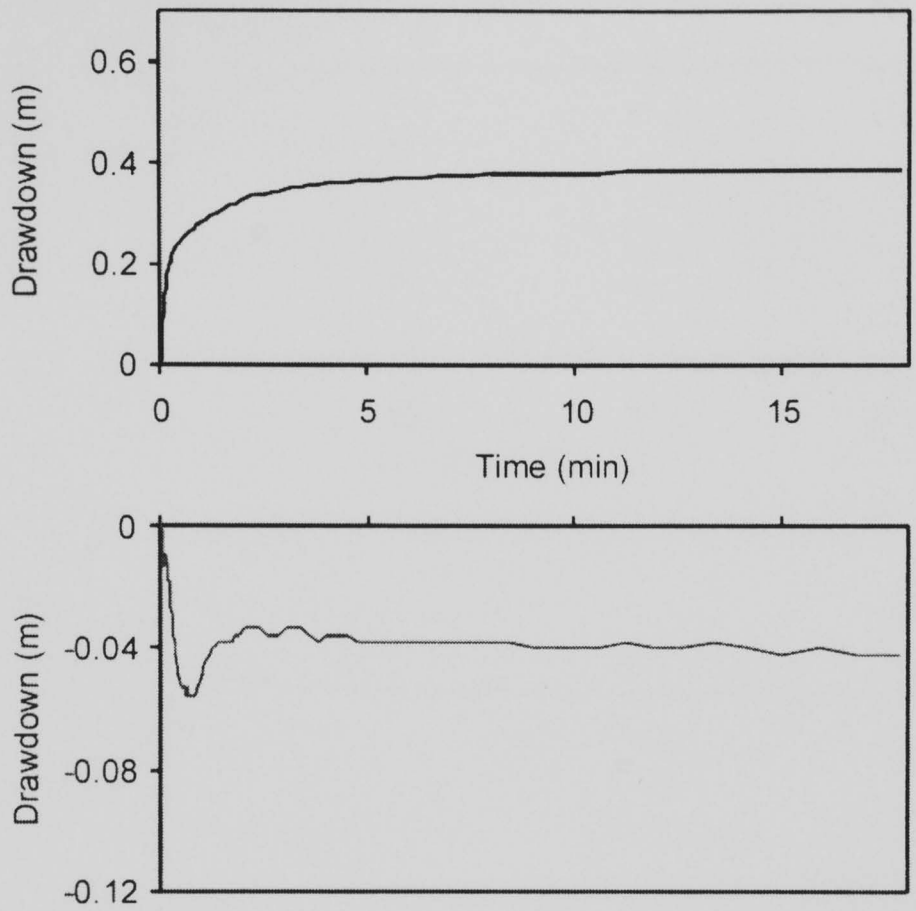

Figure B.2: Transducer response for upper and lower chambers for test 2.

Upper graph illustrates response of upper chamber with positive drawdown. Lower graph illustrates response of lower chamber with negative drawdown (buildup). Note the scale for drawdown in the chambers is different for the upper and lower chamber, but the scales are the same for tests 1-5.

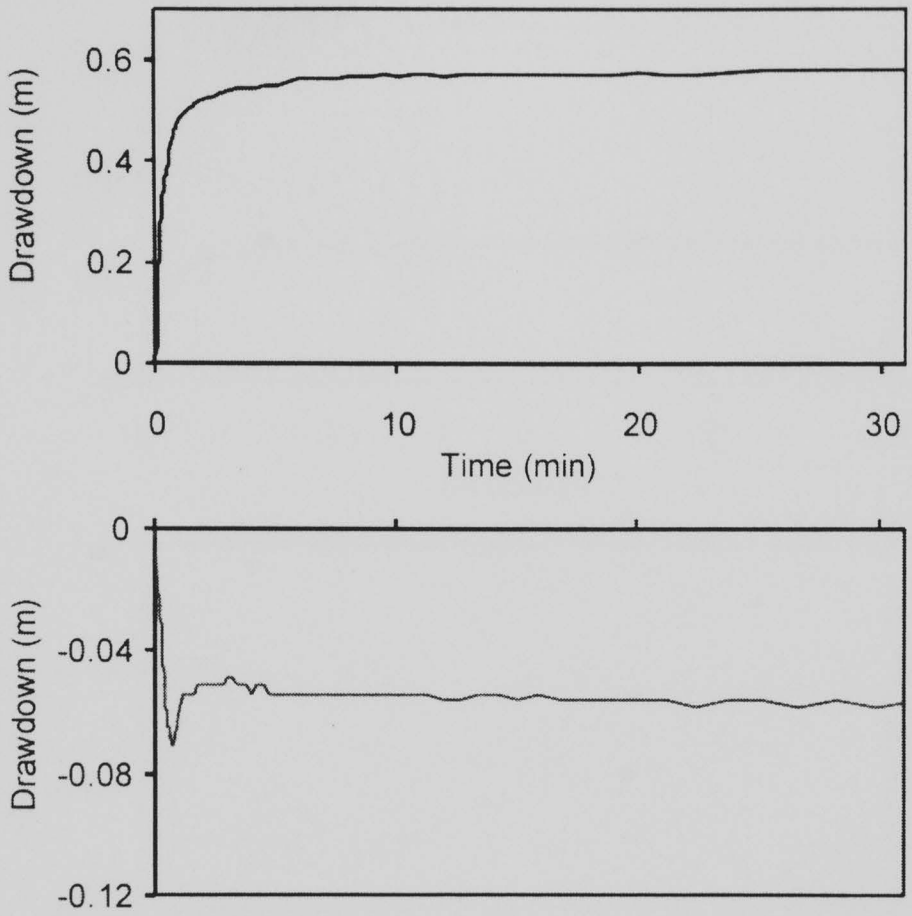

Figure B.3: Transducer response for upper and lower chambers for test 3.

Upper graph illustrates response of upper chamber with positive drawdown. Lower graph illustrates response of lower chamber with negative drawdown (buildup). Note the scale for drawdown in the chambers is different for the upper and lower chamber, but the scales are the same for tests 1-5.

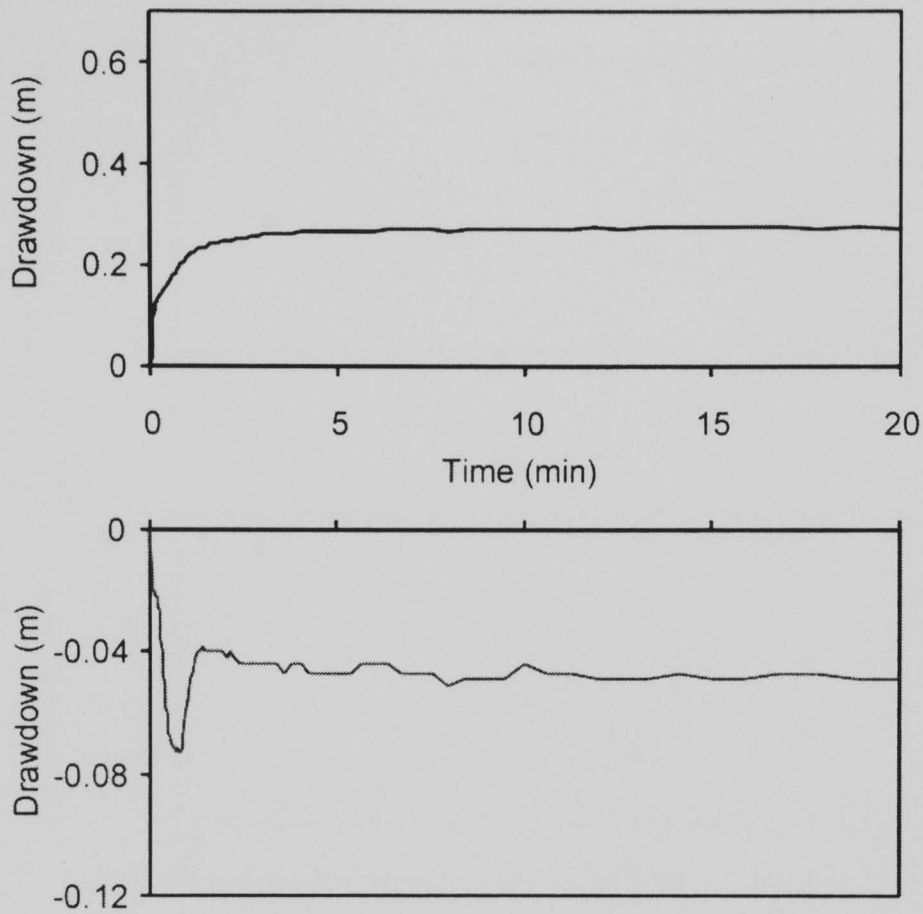

Figure B.4: Transducer response for upper and lower chambers for test 4.

Upper graph illustrates response of upper chamber with positive drawdown. Lower graph illustrates response of lower chamber with negative drawdown (buildup). Note the scale for drawdown in the chambers is different for the upper and lower chamber, but the scales are the same for tests 1-5.

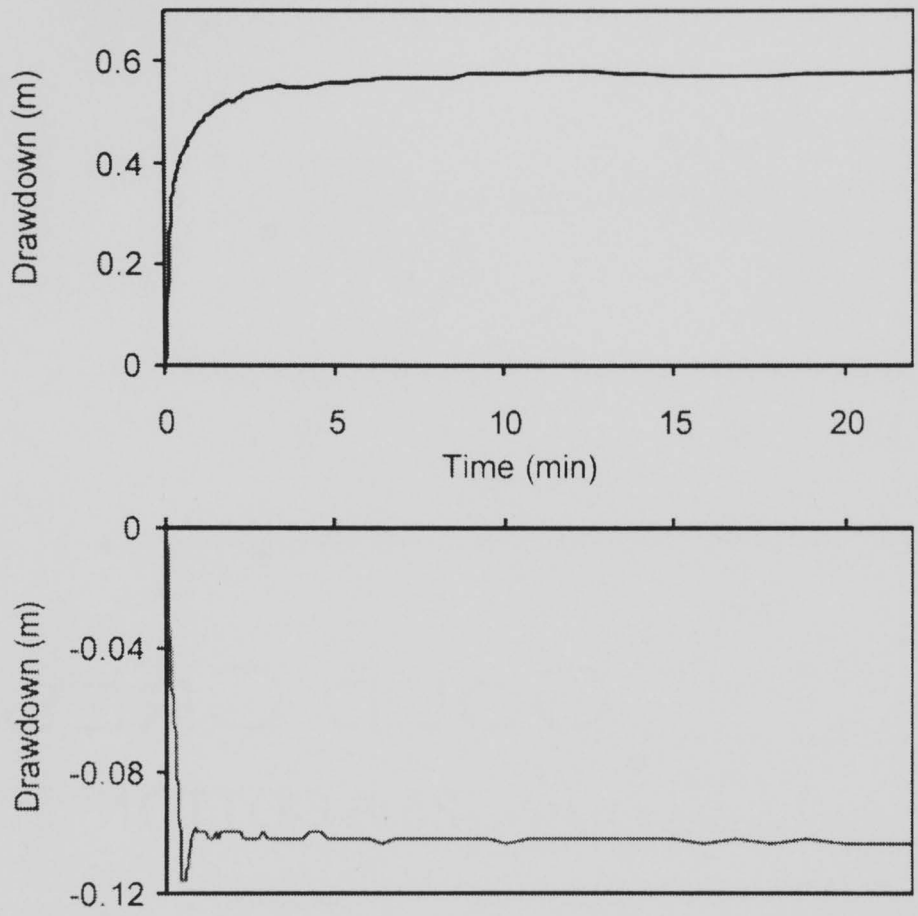

Figure B.5: Transducer response for upper and lower chambers for test 5.

Upper graph illustrates response of upper chamber with positive drawdown. Lower graph illustrates response of lower chamber with negative drawdown (buildup). Note the scale for drawdown in the chambers is different for the upper and lower chamber, but the scales are the same for tests 1-5.

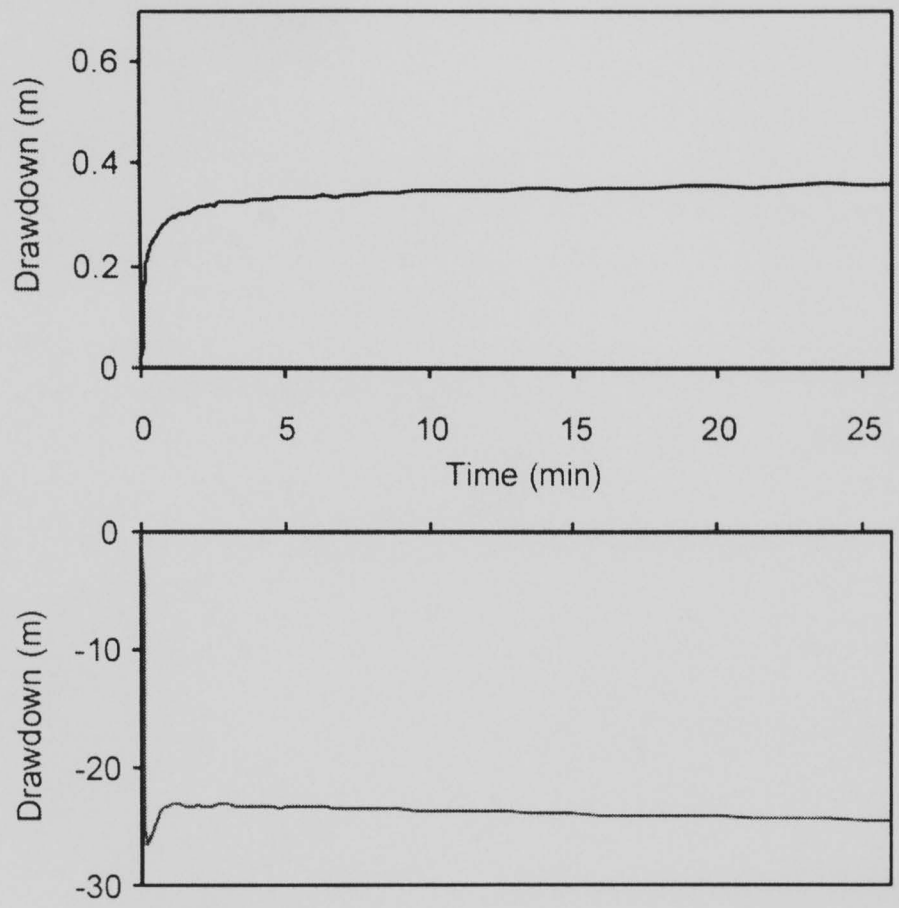

Figure B.6: Transducer response for upper and lower chambers for test 6.

Upper graph illustrates response of upper chamber with positive drawdown. Lower graph illustrates response of lower chamber with negative drawdown (buildup). Note the scale for drawdown in the chambers is different for the upper and lower chamber.

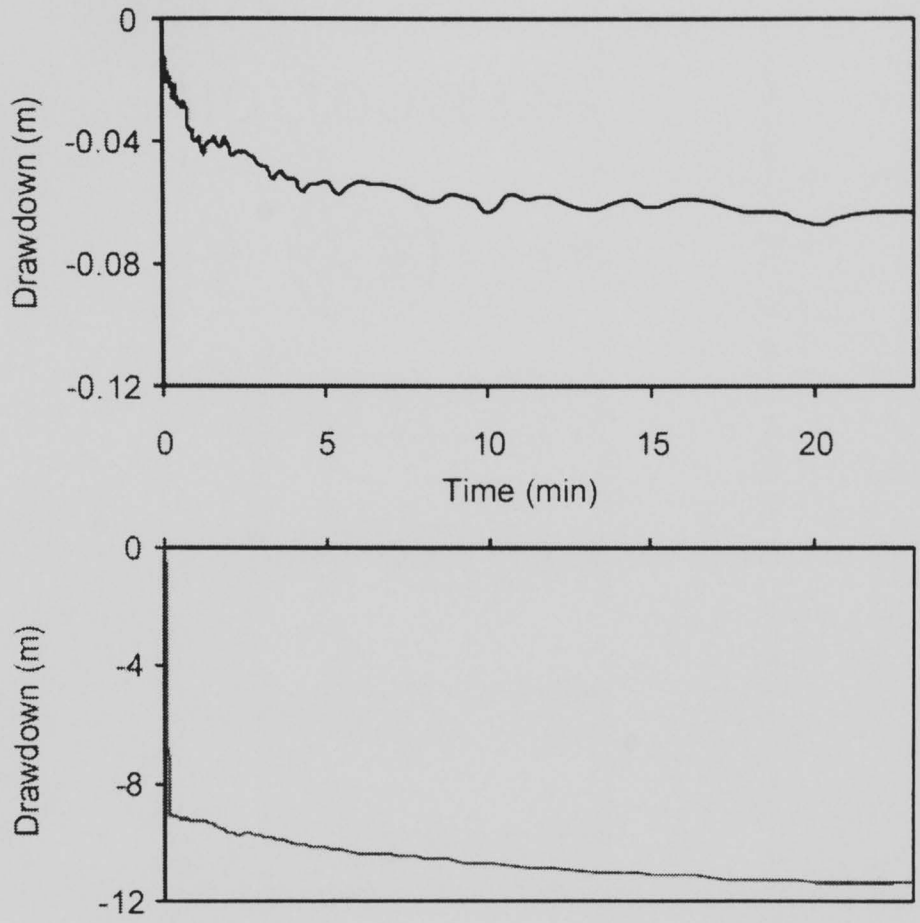

Figure B.7: Transducer response for upper and lower chambers for test 7.

Upper graph illustrates response of upper chamber with negative drawdown (buildup). Lower graph illustrates response of lower chamber with negative drawdown (buildup). Note the scale for drawdown in the chambers is different for the upper and lower chamber. This response cannot be explained with a single layer model, but can occur with a two layer simulation (Halihan, 1999a).

Table B.1: Steady state response of dipole tests in Well 13.

Test Number	Packer Midpoint Elevation [m]	Steady State Upper Drawdown [m]	Steady State Lower Buildup [m]	Q Discharge Rate [l/s]	A Upper Chamber [m]	B Lower Chamber [m]	s/Q Upper [$m/m^3/s$]	-s/Q Lower [$m/m^3/s$]
1	26.849	0.251	0.020	0.088	1.722	7.976	2860	228
2	25.477	0.387	0.042	0.252	3.124	6.604	1540	167
3	25.020	0.581	0.056	0.270	3.576	6.147	2150	207
4	24.258	0.273	0.049	0.263	4.343	5.385	1040	186
5	23.496	0.580	0.104	0.506	5.105	4.623	1150	206
6	22.886	0.364	24.540	0.408	5.715	4.013	892	60100
7	20.905	-0.063	11.382	0.221	7.678	2.032	-286	51600

D = 2 ft = 0.61 m
b = 33.89 ft = 10.33 m
r_w = 0.125 ft = 0.038 m

Appendix C: Model Dipole Response in Layered Aquifers

Numerical modeling was conducted to determine the hypothetical of the asymmetric dipole-flow test response to various heterogeneities. The results from the numerical modeling can then be used to help interpret the field data from a well characterized site to determine the usefulness of asymmetric dipole-flow tests in fractured aquifers.

Numerical modeling was performed with FRAC3DVS 3.1 on three different aquifer configurations: a homogeneous aquifer, an aquifer with a single horizontal fracture, and a two layer aquifer with an order of magnitude permeability contrast (Therrien and Sudicky, 1996). Hydraulic conductivity for the matrix was selected as an average permeability for wells ($K = 10^{-5}$ m/s). The high permeability matrix was an order of magnitude higher. The fracture aperture used was 1.1 mm ($K = 10^{0}$ m/s). The model aquifer was 100 m in thickness, with a well diameter of 0.25 m. The profiling simulations were conducted from 20 to 80 meters depth to avoid boundary effects and excessively high heads.

The numerical modeling was conducted as steady state experiments. (The input files for FRAC3DVS for the single fracture simulation are located at the end of this appendix). The boundaries were selected as constant head nodes. Negligible effects were observed for changing the boundaries to no-flow. This is due to the small region of influence of the dipole test relative to the distance from the boundaries.

UPPER CHAMBER RESPONSE

The response of the upper chamber to the numerical simulations indicate that for the homogeneous case a smooth curve is developed as is expected from the analytical modeling (Figure C.1). For the simulation of a single fracture, the upper chamber response is the same response of the matrix alone until the chamber encounters the fracture. At that point the profile leaves the matrix curve and attains a value that is an average of the matrix and the fracture conductivity. As the chamber begins to include additional matrix the average value for the conductivity changes very little and a nearly straight line profile is developed lower in the well.

For the two-layer model, a different result is obtained (Figure C.1). The chamber follows the curve for the high conductivity upper layer for the upper portion of the well. For the lower portion, the conductivity is an average that includes small additions of lower conductivity matrix. The profile leaves the homogenous curve and traces a nearly straight line through the lower portion of the well.

LOWER CHAMBER RESPONSE

The lower chamber response for the homogeneous case is again a smooth curve as expected from analytical modeling (Figure C.2). For the simulation of a single fracture, the profile follows an average value between the fracture and the matrix for the upper half of the well. Once the fracture is excluded from the lower chamber, the response follows the homogenous curve for the matrix permeability (Figure C.2).

For the layered simulation, the lower chamber traces out a curve that is an average of the high and low conductivities (Figure C.2). As the high conductivity matrix is removed from the chamber, the drawdown moves towards the lower matrix homogeneous profile. Once the chamber only has the lower conductivity matrix, the test response follows the low conductivity homogenous curve.

CONCLUSIONS

The asymmetric dipole-flow models illustrated that fracture zones could be distinguished from layered media in the dipole profile (Figures C.1 and C.2). The homogenous case for $K=10^{-4}$ m/s and K^{-5} m/s forms curves that illustrate that as the smaller segment of the dipole reaches zero length, the head developed in that segment approaches infinity or in reality the packer ruptures or hydraulic fracturing occurs. In the other chamber, as the larger dipole segment reaches infinity, the head difference developed from the initial state is zero. If a single fracture is present, steps in the head profile are observed where the fracture is intersected (Figures C.1 and C.2). The simulations indicate that the test is sensitive to the transmissivity of each individual segment, and is not strongly influenced by the other pole of the test. In the layered simulations, the profile changes head gradually, finally reaching the homogenous curve when the test segment only includes the homogenous media (Figures C.1 and C.2).

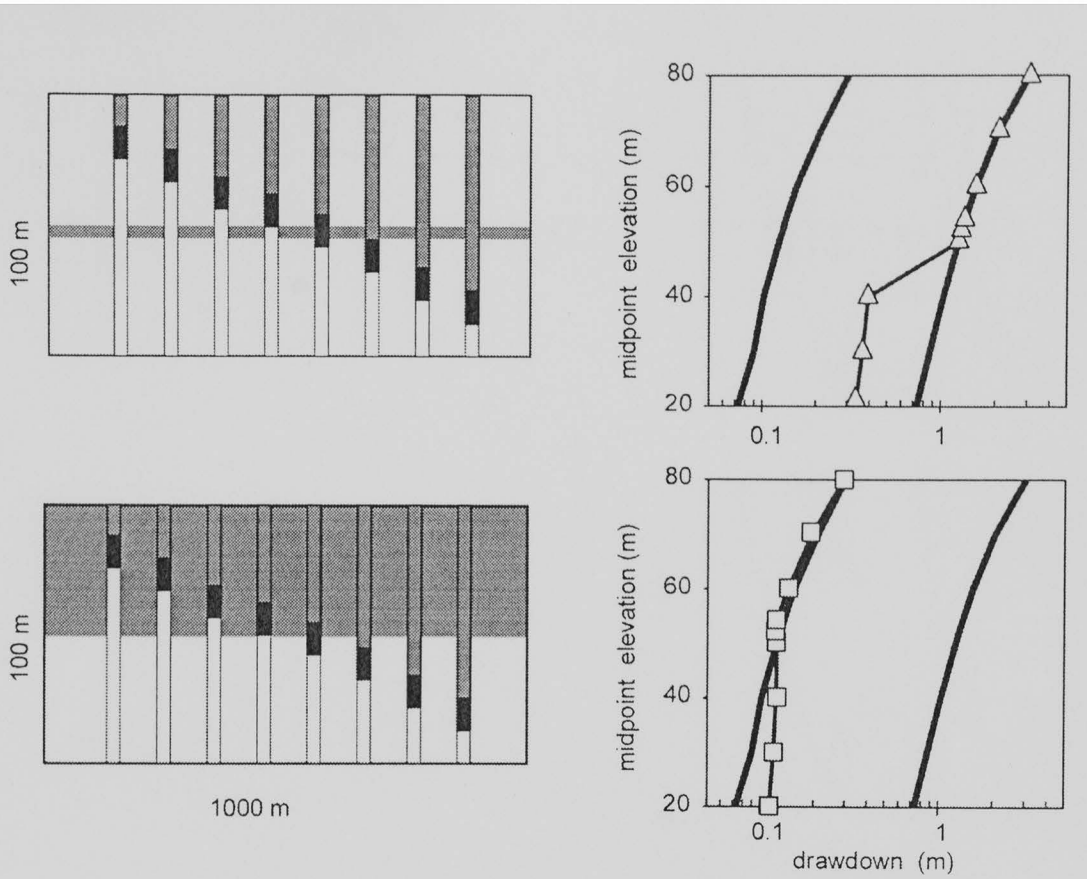

Figure C.1 Numerical model of response of upper chamber.

The left side of the figure illustrates the numerical models tested. The upper model is a single 1.1 mm fracture located in a 100 m thick aquifer. The lower model is a layered model with the upper layer having a conductivity an order of magnitude above the lower layer. The numerical results for the upper chamber are presented on the right. The smooth curves indicate the results for homogenous aquifers with a single value for conductivity. The data points indicate the profile obtained moving down though the model aquifers.

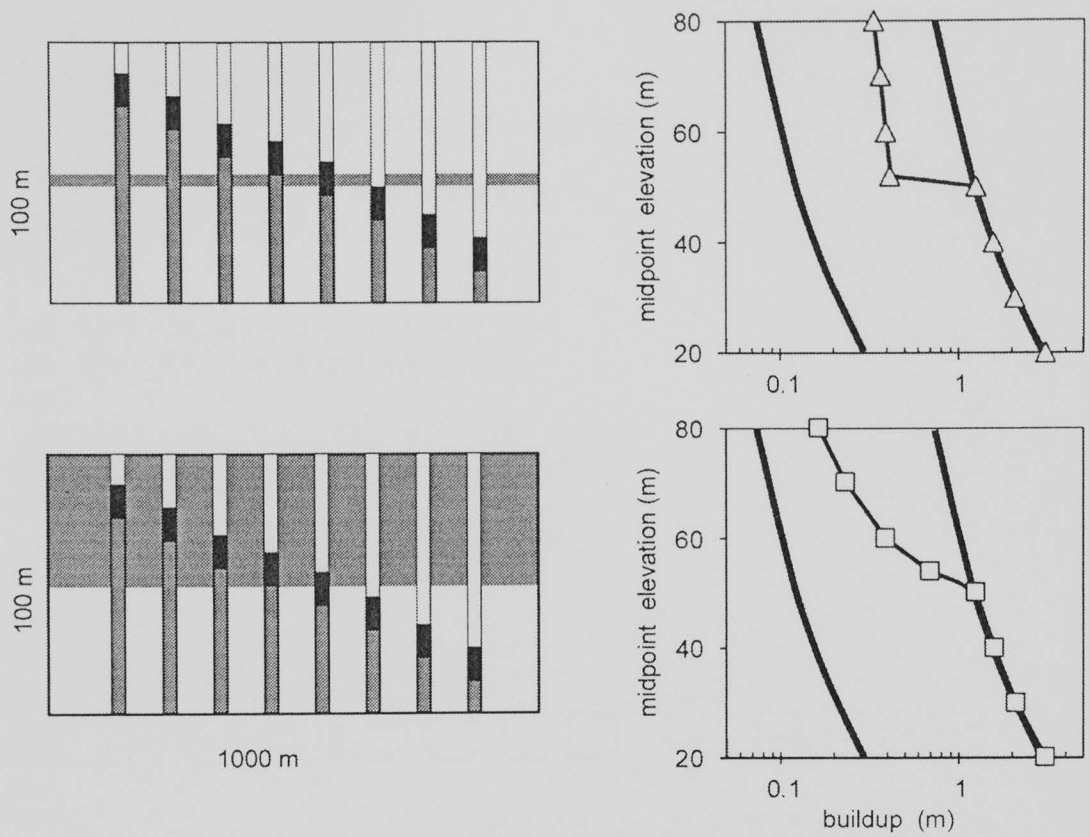

Figure C.2 Numerical model of response of lower chamber.

The left side of the figure illustrates the numerical models tested. The upper model is a single 1.1 mm fracture located in a 100 m thick aquifer. The lower model is a layered model with the upper layer having a conductivity an order of magnitude above the lower layer. The numerical results for the lower chamber are presented on the right. The smooth curves indicate the results for homogenous aquifers with a single value for conductivity. The data points indicate the profile obtained moving down though the model aquifers.

FRAC3DVS FILE DIPOLE7.NP

Asymmetric dipole flow test model for single fracture

```
! Preparing 1000 (m2) grid with rectangles (31 x 31)
Generate variable rectangles
31
31
0.00, 150., 300., 450., 460., 470., 480., 490.
495., 496., 497., 498., 498.5, 499., 499.5
500.
500.5, 501., 501.5, 502., 503., 504., 505.
510., 520., 530., 540., 550., 700., 850., 1000.

0.00, 150., 300., 450., 460., 470., 480., 490.
495., 496., 497., 498., 498.5, 499., 499.5
500.
500.5, 501., 501.5, 502., 503., 504., 505.
510., 520., 530., 540., 550., 700., 850., 1000.

Generate layers from slice
.true.
.true.
.true.
0.
1
Edwards
50
.true.
100.

Done grid definition
! Echo coordinates
! Echo incidences

!Transient flow
!Adaptive timesteps
!Output times
!11
!1.
!10.
!60.
```

```
!100.
!600.
!1000.
!6000.
!10000.
!60000.
!100000.
!360000.

clear chosen nodes
Choose nodes x plane
0.0
1.e-5
specified head
1
0.0, 100.0

clear chosen nodes
choose nodes x plane
1000.0
1.e-5
specified head
1
0.0, 100.0

clear chosen nodes
choose nodes y plane
0.0
1.e-5
specified head
1
0.0, 100.0

clear chosen nodes
choose nodes y plane
1000.0
1.e-5
specified head
1
0.0, 100.0

! make horizontal fracture
```

```
Clear chosen faces
Choose faces z plane
50.
1.e-5
Make fractures
fracture
Echo fracture incidences

! initial conditions
Choose nodes all
Initial head
100.0

! make 2 wells with one over the other segments
Make well
500. 500. 0.
500. 500. 28.
6.3e-4       ! 10 gpm
0.25
0.25
7.664e04
0.0
Make well
500. 500. 32.
500. 500. 100.
-6.3e-4
0.25
0.25
7.664e04
0.0

Make observation point
500. 500. 24.
Make observation point
500. 500. 76.
```

FRAC3DVS FILE MPROPS

```
Generic Matrix
1.0e-5     ! kx
1.0d-5     ! ky
1.0d-5     ! kz
0.0        ! specific storage
0.02       ! porosity
.true.    ! tabular data follows if true
2,              ! # of pressure - relative k values
-4.50, 0.3502       ! pressure,  relative k
0.000, 1.00
2,              ! # of saturation - relative k values
0.3502,  3.4d-12       ! saturation,  relative k
1.00,    1.00
0.0             ! longitudinal dispersivity
0.0             ! transverse dispersivity
0.0             ! transverse vertical dispersivity
0.1             ! tortuosity
2.65            ! bulk density
0.0
0.0
```

FRAC3DVS FILE FPROPS

```
fracture
1.0          fracture storage coefficient
.true.       true if fracture
1.0          frack if not fracture
0.011        aperture
.true.       tabular data
2
0.0 1.0
-1.0 1.0     ! dummy line
2
0.0 1.0
1.0 1.0      ! dummy line
1
1.0 1.0      ! dummy line
1.0          alfrac
1.0          atfrac
```

References

Alexander, K.B., 1990, Correlation of structural lineaments and fracture traces to water-well yields in the Edwards aquifer, central Texas [Masters Thesis]: Austin, The University of Texas at Austin, 113 p.

Atkinson, T.C., 1985, Present and future directions in karst hydrogeology: Annales. Societe Geologique de Belgique, v. 108, p. 293-296.

Berkowitz, B., 1995, Analysis of fracture network connectivity using percolation theory: Mathematical Geology, v. 27, n. 4, p. 467-483.

Bhattacharya, R., and Gupta, V.K., 1990, Application of central limit theorems to solute dispersion in saturated porous media: from kinetic to field scales, in Cushman, J.H., ed., Dynamics of Fluids in Hierarchical Porous Media: London, Academic Press, p. 91-96.

Botha, J.F., and Verwey, J.P., 1992, Aquifer test data and numerical models, in Russell, T.F., Ewing, R.E., Brebbia, C.A., Gray, W.G., and Pinder, G.F., eds., Computational Methods in Water Resources IX, Volume 1, Numerical Methods in Water Resources: New York, Elsevier Scientific, p. 459-466.

Brace, W.F., 1984, Permeability of crystalline rocks: New in situ measurements: Journal of Geophysical Research, v. 89, no. B6, p. 4327.

Bradbury, K.R., and Muldoon, M.A., 1990, Hydraulic conductivity determinations in unlithified glacial and fluvial materials, in Nielsen, D.M., and Johnson, A.I., eds., Ground Water and Vadose Zone Monitoring, ASTM STP 1053: Philadelphia, American Society for Testing and Materials, p. 138-151.

Bradbury, K. R., and Muldoon, M.A., 1992, Hydrogeology and groundwater monitoring of fractured dolomite in the Upper Door Priority Watershed, Door County, Wisconsin: Wisconsin Geological and Natural History Survey Open File Report, WOFR 92-2.

Cacas, M.C., Ledoux, E., De Marsily, G., and Tillie, B., 1990, Modeling fracture flow with a stochastic discrete fracture network: calibration and validation, 1. The flow model: Water Resources Research, v. 26, no. 3, p. 479-489.

Clauser, C., 1992, Permeability of Crystalline Rocks: EOS, Transactions AGU, v. 73, no. 21, p. 233-238.

Clement, T.P., Truex, M.J., and Hooker, B.S., 1997, Two-well test method for determining hydraulic properties of aquifers: Ground Water, v. 35, no. 4, p. 698-703.

Cook, P.G., Love, A.J., Halihan, T., and Cresswell, R., 1999, Measuring groundwater flow in fractured rocks with environmental isotopes, Clare Valley, South Australia: Water 99 Joint Congress, Brisbane, Australia, 6-8 July, 1999, p. 417-422.

Dagan, G., 1986, Statistical theory of groundwater flow and transport: Pore to laboratory, laboratory to formation, and formation to regional scale: Water Resources Research, v. 22, no. 9, p. 120S-134S.

Dershowitz, W. S. and Fidelibus, C., 1999, Derivation of equivalent pipe network analogues for three-dimensional discrete fracture networks by boundary element method: Water Resources Research, v. 35, no. 9, p. 2685-2691.

Dershowitz, W., Lee, G., Hitchcock, S., and LaPointe, P., 1993, FracMan Version 2.306 Interactive Discrete Feature Data Analysis, Geometric Modeling, and Exploration Simulation: User Documentation: Seattle, WA, Golder Associates, Inc.

Dyke, C., 1995, The detection and characterization of natural fracture permeability whilst drilling, in Myer, Cook, Goodman, and Tsang, eds., Fractured and Jointed Rock Masses: Rotterdam, Balkema, p. 591-601.

Fetter, C.W., 1994, Applied Hydrogeology: New York, Macmillan, 691 p.

Ford, D.C. and Williams, P.W., 1989, Karst Geomorphology and Hydrology: London, Unwin Hyman, 601 p.

Freeze, R.A., and Cherry, J.A., 1979, Groundwater: Englewood Cliffs, New Jersey, Prentice Hall, 604 p.

Geier, J., Dershowitz, W.S., Wallmann, P.C., and Doe, T.W., 1995, Discrete fracture modelling of in-situ hydrolic and tracer experiments, in Myer,

L.R., Tsang, C.F., Cook, N.G.W., and Goodman, R.E., eds., Fractured and Jointed Rock Masses: Rotterdam, Balkema, p. 511-518.

Gelhar, L.W., Mantoglou, A., Welty, C., and Rehfeldt, K.R., 1985, A review of field-scale physical solute transport processes in saturated and unsaturated porous media: Research Report EPRI EA-4190, Project 2485-5, Palo Alto, CA, Electric Power Research Institute, 116 p.

Gernand, J.D., and Heidtman, J.P., 1997, Detailed pumping test to characterize a fractured bedrock aquifer: Ground Water, v. 35, no. 4, p. 632-637.

Gupta, R.S., 1989, Hydrology and Hydraulic Systems: Englewood Cliffs, New Jersey, Prentice Hall, 739 p.

Halihan, T., 1998, Multiscale estimation of permeability in fractured aquifers: EOS, 1998 Spring AGU, Boston, poster.

Halihan, T., 1999a, Asymmetric dipole flow profiling in a fractured carbonate aquifer: Water 99 Joint Congress, Brisbane, Australia, 6-8 July, 1999, p. 807-812.

Halihan, T., 1999b, Preliminary anisotropy characterization of fractured Ordovician metasediments in Wagga Wagga, New South Wales: unpublished report to CSIRO Land and Water and Wagga Wagga council.

Halihan, T., Hansen, C.N., and Sharp, J.M., Jr., 1999a, LUST characterization in urban fractured karst aquifers: Karst Waters Institute, Symposium on Karst Modeling, Feb 24-27, 1999, Charlottesville, VA, poster.

Halihan, T., Love, A.J., and P.G. Cook, 1999b, Use of outcrop, well, and creek data to develop a regional conceptual model of the fractured rock aquifer of the Clare Valley, South Australia: Abstracts with Program, Geological Society of America Annual Meeting, Denver, CO.

Halihan, T., Mace, R.E., and Sharp, J.M., Jr. 2000., Flow in the San Antonio segment of the Edwards aquifer: matrix, fractures, or conduits?, in Sasowsky, I.D. and Wicks, C.M., eds., Groundwater flow and contaminant transport in carbonate aquifers: Rotterdam, Balkema, p. 129-146.

Halihan, T., Sharp, J.M., Jr., and Mace, R.E., 1999c, Interpreting flow using permeability at multiple scales, in Palmer, Palmer, and Sasowsky, eds., Karst Modeling: Proceedings of the symposium held Feb 24-27, 1999,

Charlottesville, VA: Special Publication 5, Karst Waters Institute, p. 82-96.

Halihan, T., Wicks, C.M., and Engeln, J.F., 1998, Physical response of a karst drainage basin to flood pulses: Example of the Devil's Icebox cave system (Missouri, USA): Journal of Hydrology, v. 204, p. 24-36.

Halihan, T. and Wicks, C.M., 1998, Modeling of storm responses in conduit flow aquifers with reservoirs: Journal of Hydrology, v. 208, p. 82-91.

Halihan, T., and Zlotnik, V.A., in preparation, Asymmetric dipole-flow test in a fractured carbonate aquifer.

Hantush, M.S., 1961, Drawdown around a partially penetrating well: Journal of the Hydraulic Division, American Society of Civil Engineers, v.87, no. HY4, p. 83-98.

Herrling, B., and Stamm, J., 1992, Numerical results of calculated 3D vertical circulation flows around wells with two screen sections for in situ or on-site aquifer remediation, in Computational Methods in Water Resources IX, Volume 1, Numerical Methods in Water Resources: New York, Elsevier Scientific, p. 483-492.

Hovorka, S.D., 1997, personal communication.

Hovorka, S.D., Mace, R.E., and Collins, E.W., 1995, Regional distribution of permeability in the Edwards aquifer: Report 95-02, San Antonio, TX, Edwards Underground Water District, 128 p.

Hovorka, S.D., Mace, R. E., and Collins, E.W., 1998, Permeability structure of the Edwards aquifer, south Texas- Implications for aquifer management: Austin, Texas, Bureau of Economic Geology, University of Texas at Austin, Report of Investigations No. 250, 55 p.

Hovorka, S.D., Ruppel, S.C., Dutton, A.R., and Yeh, J., 1993, Edwards aquifer storage assessment, Kinney County to Hays County, Texas: Austin, Texas, Bureau of Economic Geology, University of Texas at Austin, report prepared for the Edwards Underground Water District, 101 p.

Hubbert, M.K., 1956, Darcy's law and the field equations of the flow of underground fluids: Transactions of the American Institute of Mining, Metallurgical, and Petroleum Engineers, v. 207, p. 222-239.

Jensen, J.L., Lake, L.W., Corbett, P.W.M., and Goggin, D.J., 1997, Statistics for Petroleum Engineers and Geoscientists: Upper Saddle River, New Jersey, Prentice Hall, 390 p.

Kabala, Z.J., 1993, The dipole flow test: a new single-borehole test for aquifer characterization: Water Resources Research, v. 29, no. 1, p. 99-107.

Kabala, Z.J., and Xiang, J., 1992, Skin effect and its elimination for single-borehole aquifer tests, in Computational Methods in Water Resources IX, Volume 1, Numerical Methods in Water Resources: New York, Elsevier Scientific, p. 467-474.

Kiraly, L., 1975, Rapport sur l'état actuel des connaissances dans le domaine des caractères physiques des roches karstiques, in Burger, A., and Dubertret, L., eds., Hydrogeology of Karstic Terrains: Paris, International Association of Hydrogeologists, p. 53-67.

Klemt, W.B., Knowles, T.R., Elder G.R., and Sieh, T.W., 1979, Ground-water resources and model applications for the Edwards (Balcones fault zone) aquifer in the San Antonio region, Texas: Austin, Texas, Texas Water Development Board, Report 239, 88 p.

Kohl, T., and Hopkirk, R.J., 1995, "FRACTure" - A simulation code for forced fluid flow and transport in fractured, porous rock: Geothermics, v. 24, no. 3, p. 333-343.

Lamb, 1932, Hydrodynamics, 6th edition: New York, Dover, 738 p.

Lapointe, P.R. and Hudson, J.A., 1985, Characterization and interpretation of rock mass joint patterns: GSA, Special Paper 199, 37p.

Leonards, G.A., 1962, Foundation Engineering: New York, McGraw-Hill, 1136 p.

Lindquist, E., 1933, On the flow of water through porous soil: Stockholm, Premier Congres des grands barrages, p. 81-101.

Long, J.C.S., Remer, J.S., Wilson, C.R., and Witherspoon, P.A., 1982, Porous media equivalents for networks of discontinuous fractures: Water Resources Research, v. 18, p. 645-658.

Longley, G., 1981, The Edwards aquifer: Earth's most diverse ground-water ecosystem: International Journal of Speleology, v. 11, p. 123-128.

Love, A.J., Cook, P.G., Halihan, T., and Simmons, C.T., 1999, Estimating groundwater flow rates in a fractured rock aquifer, Clare Valley, South Australia: Water 99 Joint Congress, Brisbane, Australia, 6-8 July, 1999, p. 1070-1075.

Mace, R.E., 1997, Determination of transmissivity from specific capacity tests in a karst aquifer: Ground Water, v. 35, no. 5, p. 738-742.

Mace, R.E., 1998, Regional distribution, spatial correlation, and scaling of permeability in a karstic aquifer, Edwards Group, south-central Texas: Ground Water, (in press).

Maclay, R.W., and Land, L.F., 1988, Simulation of Flow in the Edwards Aquifer, San Antonio Region, Texas, and Refinement of Storage and Flow Concepts: U.S. Geological Survey Water-Supply Paper 2336-A, 48 p.

Maclay, R.W., and Small, T.A., 1986, Carbonate geology and hydrology of the Edwards aquifer in the San Antonio area, Texas: Austin, Texas, Texas Water Development Board, Report 296, 121 p.

Marine, I.W., 1980, Determination of the location and connectivity of fractures in metamorphic rock with in-hole tracers: Ground Water, v. 18, n. 3, p. 252-261.

Marrett, R, 1996, Aggregate properties of fracture populations: Journal of Structural Geology, v. 18, no. 2/3, p. 169-178.

McKinney, D.C., and Watkins, D.W., Jr., 1993, Management of the Edwards Aquifer: A Critical Assessment: Austin, Texas, Center for Research in Water Resources, Technical Report CRWR 244, 94 p.

Miller, I., and Kleine, T., 1994, MAFIC Fracture/Matrix Flow and Transport Code Draft Verification Report: Seattle, WA, Golder Associates, Inc.

Molz, F.J., Güven, O., Melville, J.G., and Cardone, C., 1990, Hydraulic conductivity measurement at different scales and contaminant transport modelling, in Cushman, J.H., ed., Dynamics of Fluids in Hierarchical Porous Media: London, Academic Press, p. 37-59.

Morton, D., Love, A.J., Clarke, D., Martin, R., Cook, P.G., and McEwan, K., 1998, Clare Valley Groundwater Resources, Progress Report 1: Department of Primary Industries and Resources South Australia, Report Book 98/00015, 70 p.

Muldoon, M. A., and Bradbury, K. R., 1996, Hydrogeology of the fractured Silurian dolomite aquifer, Door County, Wisconsin, in The Silurian Dolomite Aquifer of the Door Peninsula: Facies, Sequence Stratigraphy, Porosity and Hydrogeology: Fieldtrip guidebook for 1996 Fall Field Conference of the Great Lakes Section of the SEPM, p. 26-124.

Muldoon, M.A., and Bradbury, K. R., 1998, Tracer study for characterization of groundwater movement and contaminant transport in fractured dolomite: Wisconsin Geological and Natural History Survey, Final Report WOFR 98-2.

Neuzil, C.E., 1994, How permeable are clays and shales?: Water Resources Research, v. 30, no. 2, p. 145-150.

Odling, N.E., 1997, Scaling and connectivity of joint systems in sandstones from western Norway: Journal of Structural Geology, v. 19, no. 10, p. 1257-1271.

Pavlicek, D.L., Small, T.A., and Rettman, P.L., 1987, Hydrogeologic data from a study of the freshwater zone/saline water zone interface in the Edwards aquifer, San Antonio region, Texas: U.S. Geological Survey Open-File Report 87-389, 108 p.

Poteet, D., Collier, H., and Maclay, R., 1992, Investigation of the fresh/saline-water interface in the Edwards aquifer in New Braunfels and San Marcos, Texas: San Antonio, Texas, Edwards Underground Water District, Report 92-02, 176 p.

Quinlan, J.F., Davies, G.J., and Worthington, S.R.H., 1992, Rationale for the design of cost-effective groundwater monitoring systems in limestone and dolomite terranes: cost-effective as conceived is not cost-effective as built if the system design and sampling frequency inadequately consider site hydrogeology, in Symposium on Waste Testing and Quality Assurance (8th, Washington, D.C., July 1992), Washington, D.C., US Environmental Protection Agency, p. 552-570.

Quinlan, J.F., and Ewers, R.O., 1985, Ground water flow in limestone terranes: strategy rationale and procedure for reliable, efficient monitoring of ground water quality in karst areas, in Proceedings of the Fifth National Symposium and Exposition on Aquifer Restoration and Ground Water Monitoring: Worthington, Ohio, National Water Well Association, p. 197-234.

Rasband, W., 1994, NIH Image, Version 1.50: U.S. National Institutes of Health.

Rehfeldt, K.R., Hufschmied, P., Gelhar, L.W., and Schaefer, M.E., 1989, Measuring hydraulic conductivity with the borehole flowmeter: Research Report EPRI EN-6511, Project 2485-5, Palo Alto, CA, Electric Power Research Institute, 209 p.

Renshaw, C. E., 1999, Connectivity of joint networks with power law length distributions: Water Resources Research, v. 35, no. 9, p. 2661-2670.

Rose, P.R., 1972, Edwards group, surface and subsurface, central Texas: Austin, Texas, Bureau of Economic Geology, The University of Texas at Austin, Report of Investigations 74, 198 p.

Rovey, C.W., II., 1994, Assessing flow systems in carbonate aquifers using scale effects in hydraulic conductivity: Environmental Geology, v. 24, p. 244-253.

Scheidegger, A.E., 1974, The physics of flow through porous media, 3rd edition: Toronto, University of Toronto Press, 353 p.

Sharp, J.M., Jr., and Banner, J.L., 1997, The Edwards aquifer: A resource in conflict: GSA Today, v. 7, no. 8, p. 1-9.

Sharp, J.M., Jr., Banner, J.L., and Halihan, T., 1998, Edwards aquifer: fracture control of regional groundwater flow.: 1998 SEPM Carbonate Research Conference, Door County, Wisconsin.

Snow, D.T., 1969, Anisotropic permeability of fractured media: Water Resources Research, v. 5, no. 6, p. 1273-1289.

Streeter, V.L., 1948, Fluid Dynamics: New York, McGraw-Hill, 480 p.

Streltsova, T.D., 1976, Hydrodynamics of groundwater flow in a fractured formation: Water Resources Research, v. 12, no. 4, p. 405-414.

Swanson, G.J., 1991, Super well is deep in the heart of Texas: Water Well Journal, no. 7, p. 56-58.

Taylor, K., Wheatcraft, S., Hess, J., Hayworth, J., and Molz, F., 1990, Evaluation of methods for determining the vertical distribution of hydraulic conductivity: Ground Water, v. 28, no. 1, p. 88-98.

Theis, C.V., 1935, The relation between the lowering of the piezometric surface and the rate and duration of discharge of a well using groundwater storage: Transactions of the AGU, v. 16, p. 519-524.

Therrien, R., and Sudicky, E.A., 1996, Three-dimensional analysis of variably-saturated flow and solute transport in discretely-fractured porous media: Journal of Contaminant Hydrology, v. 23, no. 1-2, p. 1-44.

Thiem, G., 1906, Hydrologische methoden: Leipzig, Gebhardt, 56 p.

Thorkildsen, D., and McElhaney, P.D., 1992, Model refinement and applications for the Edwards (Balcones fault zone) aquifer in the San Antonio region, Texas: Austin, Texas, Texas Water Development Board, Report 340, 33 p.

Thornhill, P.D., Harden, R.W., and Nevola, R., 1988, The Edwards aquifer, underground river of Texas: Seguin, Texas, Guadalupe-Blanco River Authority Publication, 63 p.

Tsoflias, G.P., Halihan, T., and Sharp, J.M., Jr., in review, Monitoring pumping test response in a fractured aquifer using ground penetrating radar: submitted to Water Resources Research.

Tsoflias, G.P. and Sharp, J. M., Jr., 1998, Three-dimensional hydrogeologic characterization of fractured carbonate aquifers using ground-penetrating radar: Gulf Coast Association of Geological Societies Transactions XL, VIII, p.439-447.

Tsoflias, S.R., in preparation, Investigation of the relationship between fracture surface roughness and fracture inducing stress [Masters Thesis]: Austin, The University of Texas at Austin.

Turcotte, D.L., and Schubert, G., 1982, Geodynamics: Applications of continuum physics to geological problems: New York, Wiley, 450 p.

Veni, G., 1988, The Caves of Bexar County, 2nd edition: Austin, Texas Memorial Museum, The University of Texas at Austin, 300 p.

Voss, C.I., 1984, SUTRA: A finite-element simulation model for saturated-unsaturated fluid density-dependent groundwater flow with energy transport or chemically reactive single-species solute transport: US Geological Survey Water Resource Investigations, Report 84-4369, 409 p.

Wermund, E.G., Cepeda, J.C., and Luttrell, P.E., 1978, Regional distribution of fractures in the southern edwards plateau and their relationship to tectonics and caves: Austin, Texas, Bureau of Economic Geology, The University of Texas at Austin, Geological Circular 78-2, 14 p.

Williams, R.E., 1985, Comment on "Double-porosity models for a fissured groundwater reservoir with fracture skin" by Allen F. Moench: Water Resources Research, v. 21, no. 6, p. 889-891.

Wilson, T., Heinson, G.S., Endres, A.L., and Halihan, T., 2000a, Fractured rock geophysical studies in the Clare Valley, South Australia: SAGEEP 2000, Annual meeting of The Environmental and Engineering Geophysical Society, poster.

Wilson, T., Heinson, G.S., Endres, A.L., and Halihan, T., 2000b, Fractured rock hydrogeophysics at Clare Valley, South Australia: ASEG 2000, 14th International Conference and Exhibition.

Wiltschko, D.V., Corbett, K. P., Friedman, M., and Hung, ., 1991, Predicting fracture connectivity and intensity within the Austin Chalk from outcrop fracture maps and scanline data: Transactions – Gulf Coast Association of Geological Societies, v. 41, p. 702-718.

Zahm, C.K., 1998, Use of outcrop fracture measurements to estimate regional groundwater flow, Barton Springs segment of Edwards aquifer, central Texas [Masters Thesis]: Austin, The University of Texas at Austin, 154 p.

Zhang, Q. and Sudicky, E., 1997, Editorial: Advances in Water Resources, v. 20, no. 5-6, p 251.

Zlotnik, V.A., and Ledder, G., 1994, Effect of boundary conditions on dipole flow, in Computational Methods in Water Resources X, Volume 2: Dordrecht, Kluwer Academic, p. 907-914.

Zlotnik, V.A., and Ledder, G., 1996, Theory of dipole flow in uniform anisotropic aquifers: Water Resources Research, v. 32, no. 4, p. 1119-1128.

Zlotnik, V.A., and Zurbuchen, B.R., 1998, Dipole probe: design and field applications of a single-borehole device for measurements of vertical variations of hydraulic conductivity: Ground Water, v. 36, no. 6, p.884-893.

The vita has been removed from the digitized version of this document.